Novel Phthalocyanines as n-Type Semiconductors for Organic Field-Effect Transistors

Weiyi Zhou

A Thesis Submitted in Partial Fulfillment of the Requirements for the

Master of Science Degree in Chemistry

Department of Chemistry and Biomolecular Sciences

Faculty of Science

University of Ottawa

Candidate **Supervisor**

Weiyi Zhou Jaclyn Brusso

Abstract

Over the past few decades, metal phthalocyanines (MPcs) have been thoroughly investigated as active materials in organic field-effect transistors (OFETs) towards the commercialization of flexible integrated circuits and displays. One of several advantages to MPcs as building blocks for OFETs is the high degree of functionality, from which the choice of metal ion, substituents along with the phthalocyanine framework and axially bound ligands can synergistically tune the physical and self-assembly properties of the material. Recent interest has been directed to the introduction of main-group elements as the central ion of MPcs as an avenue to install both hole and electron transport properties and improve device performance.

To prepare materials that are suitable to be employed as the semiconducting active layer in organic field-effect transistors, a family of novel silicon phthalocyanine derivatives was prepared. The synthesis and optoelectronic properties of those new axially disubstituted silicon phthalocyanines are detailed in this work. Axial ligand variation mainly includes alkylsiloxy derivatives. The emphasis of the current thesis, however, is on tailoring the Pc backbone, which includes replacing the four benzene units with pyrazine moieties, extending the degree of conjugation with naphthalene, and introducing substituents on their peripheral positions. Several metal-containing tetra-2,3-pyrazinoporphyrazines are also described, but their applications are limited due to the difficulty of purification.

Specifically, **Chapter 1** serves as a comprehensive review of main-group phthalocyanines and their use as active materials in organic field-effect transistors. In **Chapter 2**, silicon tetra-2,3-pyrazinoporphyrazine complexes are explored. The isosteric substitution of CH groups in Pc macrocycle for nitrogen atoms leads to an obvious hypsochromic shift in their main absorption band, and their relatively low energy levels make them promising air-stable *n*-type organic

semiconducting materials for OFETs. The synthesis and characterization of silicon tetra(*tert*-butyl)-2,3-naphthalocyanine complexes are described in **Chapter 3**. The extension of π-conjugation leads to obvious bathochromic shifts in the main absorption band. In addition, the introduction of *tert*-butyl groups on the periphery of the molecule reduces the tendency of the naphthalocyanine molecules to aggregate, thereby increase their solubility. **Chapter 4** covers the synthesis and characterization of zinc tetra-2,3-pyrazinoporphyrazine and cobalt tetra-2,3-pyrazinoporphyrazine, whereas more future works are expected. The fifth chapter provides a conclusion to this work, and possible future directions of the research conducted herein.

Contributions

Chapter 1 reference: **Zhou, W.**, Yutronkie, N.J., Lessard, B.H. and Brusso, J.L. "From chemical curiosity to versatile building blocks: unmasking the hidden potential of main-group phthalocyanines in organic field-effect transistors" ***Mater. Adv.***, 2021, **2**, 165-185.

Contributions: The first draft of the entire manuscript was written by Weiyi Zhou with relevant corrections and additions by Dr. Nathan J. Yutronkie and Prof. Jaclyn L. Brusso. All figures in this manuscript were either reprinted by permission from the respective journals, or prepared by Weiyi Zhou and Dr. Nathan J. Yutronkie. All schemes and tables were prepared by Weiyi Zhou, with relevant corrections and additions by Dr. Nathan J. Yutronkie and Prof. Jaclyn L. Brusso.

Thesis contributions: The research presented in **Chapter 2**, **3** and **4** has not yet been published. The synthesis of all compounds was performed by Weiyi Zhou. The DFT calculations presented in **Chapter 2** were carried out by Dr. Nathan J. Yutronkie. The synthesis of 6-(*tert*-butyl)-1*H*-benzo[*f*]isoindole-1,3(2*H*)-diimine (**^{t}BuNp-DIII**) and silicon tetra(*tert*-butyl)-2,3-naphthalocyanine dichloride (**(^{t}Bu)$_4$SiNPcCl$_2$**) was performed with the help of Dr. Pierre Josse. The NMR, FT-IR, UV-vis and CV characterization for all compounds presented in the thesis were performed by Weiyi Zhou. The MS data were collected by Dr. Sharon Curtis from the University of Ottawa (John L. Holmes Mass Spectrometry Facility) or by Dr. Matthew W. Forbes from the University of Toronto. This thesis was written by Weiyi Zhou. Relevant corrections and additions to the thesis were done by Dr. Jaclyn L. Brusso. All figures in this manuscript were prepared by Weiyi Zhou unless otherwise stated (i.e., reprinted by permission from the respective journals).

Acknowledgments

Studying abroad is a challenge, but also an amazing experience in my life. Without the support and help of my family and friends, I do not think I could reach this stage.

First, I am truly grateful to my supervisor, Dr. Jaclyn Brusso. I must thank Jaclyn for giving me this opportunity to join the group. Jaclyn has provided a lot of guidance and support during the past two years for research. When I first came here, my English was bad, but she is very patient and gave me a lot of help. Thank you for being such a nice and inspiring mentor! I am also truly grateful to Dr. Benoit Lessard, thank you for your guidance and support!

I am also particularly grateful to my committee members (Dr. Benoit Lessard and Dr. Muralee Murugesu) for taking the time to read my thesis and to sit on its oral defense. I appreciate all the feedback and comments.

Also, I would like to thank all my colleagues in the Brusso lab. Pierre, you are the person who helped me with starting a project from zero. Without your help, the first year would have been very tough. Nathan, you are an inspiration in the lab. Thank you so much for giving me help even after graduating from here. Raúl, you are the first person that I met in the Brusso lab. Thanks for showing me the lab when I first came here and teaching me how to use some software. Anindya, we joined the group at the same time, and I would thank you for all your help. Your fried noodles taste really good! Sumit, despite you just joining the group this summer, you still helped me a lot. I would also thank Mario, for helping me with Mass Spectrometry and sublimation. I also want to thank all the Chinese friends in the department for your support and company. It is my great honor to make friends with all of you.

I also need to thank the most excellent personnel and supporting staff from the University of Ottawa. Dr. Wendy Pell and Patrick, who helped me with IR data collecting; Dr. Peter Pallister and Dr. Sharon Curtis, who helped me with NMR and MS, respectively.

Finally, I am eternally grateful to my family, particularly my parents, Hongxia Kan and Shaoshan Zhou, who supported me throughout the years. Without your unconditional support and love, I wouldn’t be who I am today.

To my family and my beloved country, China.

Table of Contents

List of Figures

Chapter 1 Introduction

Chapter 2 Silicon Tetra-2,3-pyrazinoporphyrazine Complexes (SiPz)

Chapter 4 Metal-containing Tetra-2,3-pyrazinoporphyrazine (MPz)

List of Schemes

Chapter 4 Metal-containing Tetra-2,3-pyrazinoporphyrazine (MPz)

List of Tables

List of Abbreviations

AMF	Atomic force microscope
BC/BG	Bottom contact/bottom gate
BCP	Bathocuproine
BC/TG	Bottom contact/top gate
C_{60}	Buckminsterfullerene
$CDCl_3$	Deuterated chloroform
CV	Cyclic voltammetry
DBU	1,8-Diazabicyclo[5.4.0]undec-7-enes
o-DCB	*o*-Dichlorobenzene
DCM	Dichloromethane
DFT	Density functional theory
DIII	Diiminoisoindoline
DMF	Dimethylformamide
DMSO	Dimethyl sulfoxide
$E_{1/2}$	Quasi-reversible wave
E_g	Energy gap
EI	Electron ionization

ESI	Electrospray ionisation
EtOAc	Ethyl acetate
EtOH	Ethanol
Fc	Ferrocene
FOTS	(1H,1H,2H,2H-Perfluorooctyl) trichlorosilane
FTIR	Fourier transform infrared
HCl	Hydrochloric acid
HOMO	Highest occupied molecular orbital
HRMS	High-resolution mass spectrometry
I_D	Current flow
I_{on}/I_{off}	On/off current ratio
IR	Infrared spectroscopy
ITO	Indium-tin oxide
$LiN(TMS)_2 \cdot Et_2O$	Lithium bis(trimethylsilyl)amide etherate
LUMO	Lowest unoccupied molecular orbital
M	mol/L
MALDI-TOF	Matrix-assisted laser desorption ionization time-of-flight
MeOH	Methanol

MO	Molecular orbital
MPc	Metal phthalocyanine
MS	Mass spectrometry
NBu_4PF_6	Tetrabutylammonium hexafluorophosphate
NHE	Normal hydrogen electrode
nm	Nanometers
NMP	N-Methyl-2-pyrrolidone
NMR	Nuclear magnetic resonance
NPc	Naphthalocyanine
ODTS	Octadecyltrichlorosilane
OFET	Organic field-effect transistor
OLED	Organic light-emitting diode
OPV	Organic photovoltaic
OTFT	Organic thin-film transistor
OTS	Octyltrichlorosilane
p-6p	Parasexiphenyl
Pc	Phthalocyanine
PET	Poly(ethylene terephthalate)

PMMA	Polymethyl methacrylate
Pz	Tetra-2,3-pyrazinoporphyrazines
RT	Room temperature
S/D	Source and drain
SiOTf	Silyl trifluoromethanesulfonate
SubPc	Subphthalocyanine
Tbpc	Tetra-*tert*-butylphthalocyaninate
TC/BG	Top contact/bottom gate
TC/TG	Top contact/top gate
TMSCl	Chlorotrimethylsilane
UV-vis	Ultraviolet−visible
V_{DS}	Bais
V_G	Gate voltage
V_T	Threshold voltage
ε	Molar Absorption Coefficient
μ	Charge transfer mobility
λ_{max}	Wavelength of maximum absorbance

List of Compound Abbreviations

^{t}BuNp-DIII	6-(*tert*-Butyl)-1*H*-benzo[*f*]isoindole-1,3(2*H*)-diimine
(^{t}Bu)$_4$SiNPc	Silicon tetra(*tert*-butyl)-2,3-naphthalocyanine
(^{t}Bu)$_4$SiNPcCl$_2$	Silicon tetra(*tert*-butyl)-2,3-naphthalocyanine dichloride
(^{t}Bu)$_4$SiNPc(OH)$_2$	Bis(hydroxy) silicon tetra(*tert*-butyl)-2,3-naphthalocyanine
(^{t}Bu)$_4$SiNPc(Pr$_3$OSi)$_2$	Bis(tri-*n*-propylsiloxy) silicon tetra(*tert*-butyl)-2,3-naphthalocyanine
CoPz	Cobalt tetra-2,3-pyrazinoporphyrazines
Pz-DIII	5-Imino-5*H*-pyrrolo[3,4-*b*]pyrazin-7-amine
SiPz(^{t}BuMe$_2$OSi)$_2$	Bis(*tert*-butyldimethylsiloxy) silicon tetra-2,3-pyrazinoporphyrazine
SiPz	Silicon tetra-2,3-pyrazinoporphyrazine
SiPzCl$_2$	Silicon tetra-2,3-pyrazinoporphyrazine dichloride
SiPz(Et$_3$OSi)$_2$	Bis(tri-*n*-ethylsiloxy) silicon tetra-2,3-pyrazinoporphyrazine
SiPz(OH)$_2$	Bis(hydroxy) silicon tetra-2,3-pyrazinoporphyrazine
ZnPz	Zinc tetra-2,3-pyrazinoporphyrazines

Chapter 1 Introduction

Authorship disclosure: A version of this chapter was published in *Materials Advances* as "From chemical curiosity to versatile building blocks: unmasking the hidden potential of main-group phthalocyanines in organic field-effect transistors" **Zhou, W.**, Yutronkie, N.J., Lessard, B.H. and Brusso, J.L., ***Mater. Adv.***, 2021, **2**, 165-185. See page **iv** for details of contributions.

1.1 Background

Since their discovery in the early 20th century,[1–3] metal phthalocyanines (MPcs) have played a pivotal role in paving research efforts across many scientific disciplines. The extensive delocalization of π-electrons in the phthalocyanine framework affords the foundation for a molecular architecture in possession of impeccable stability and rich electronic behavior.[4–7] While MPcs were initially used as dyes and pigments due to their green-blue optical appearances,[1] this class of molecules has since been exploited for widespread applications in catalysis,[8] liquid crystals,[9] fluorescent probes and photosensitizers,[10] optoelectronic and redox-active materials,[11–14] magnetic materials,[15] sensors,[16] nonlinear optics,[17] and molecular electronics,[18–22] to name a select few.

Regarding molecular electronics, MPcs have gained tremendous traction towards the development of active materials in organic photovoltaics (OPVs),[23–26] light-emitting diodes (OLEDs),[27–30] and field-effect transistors (OFETs).[31–34] Given the monumental role of FETs in modern-day devices, the implementation of MPcs as intrinsic organic semiconductors within these devices offers several advantages over their traditional inorganic counterparts. For one, synthetic procedures of MPcs are relatively facile, inexpensive, and ideal for mass-production on an industrial scale. These materials can also be processed with ease through conventional wet-based

or vapor deposition methods on a range of compatible can be fabricated for flexible integrated circuits and displays. When juxtaposed to most organic molecules, the MPc building block itself is thermally and chemically robust in comparison, which reinforces the feasibility of their application in these molecular devices. Perhaps the greatest appeal of MPcs, especially for those aiming to enhance the performance of organic thin-film transistors (OTFTs), originates in the structural versatility of the molecule. Synthetic handles can be used to manipulate the properties of the material with control for the application at hand, thereby providing a means to rationally design MPc-based building blocks from a bottom-up approach.

With that said, the molecular infrastructure of MPcs, comprised of four aza-bridged isoindoline subunits coordinated to a central metal inclusion, possesses four regions where the properties can be tailored accordingly by chemical modifications (Figure 1.1).[21] Functionalities can be enabled through the choice of the central ion (M), the substituents along with the peripheral and bay positions (R^1 and R^2, respectively) of the phthalocyanine backbone (Pc), and the ligands bound at the axial positions of the metal center (X).[21] For sake of clarity and consistency, we herein refer to functionalized MPcs through the notation $M(R^1_mR^2_n)Pc\text{-}X^1X^2$, where 4-, 5- and 6-coordinate metal complexes are implied by the absence or inclusion of axial ligands X^1 and X^2, respectively. Furthermore, the degree and type of substitution along the Pc framework is denoted by R^1_m and R^2_n in parentheses, where m and n = 0–8.

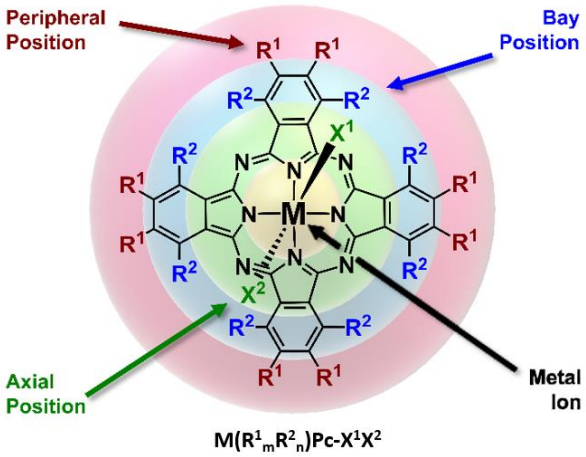

Figure 1.1 Chemical structure of metal phthalocyanines highlighting the regions for chemical functionalization. Reproduced from Ref. 35 with permission from the Royal Society of Chemistry.

To further elaborate on the influences imposed by functionalization, solubility is a key property that can be controlled through chemical moieties appending from the Pc framework and/or central ion. In general, MPcs are not inherently soluble in most common solvents as a consequence of aggregation via non-covalent interactions. Nonetheless, the attachment of flexible chains can aid in the disruption of these interactions or, in the case of polar and ionic groups, can enhance interactions with solvent molecules. On the other hand, judicious choice of these substituents can be used to rationalize favorable interactions (e.g., π–π, C–H···X, where X = heteroatoms, π, etc.) towards the preferential alignment and self-assembly of molecules in a condensed state.[18,36,37] Moreover, these same interactions can ultimately be used to strengthen intermolecular interactions in order to enhance the charge-transport properties.[38]

Functionalization can also alter the electronic structure of MPcs (e.g., influence the highest occupied and lowest unoccupied molecular orbitals; HOMO and LUMO, respectively), which are derived from the extensive π-system of phthalocyanine. Considering metal-free Pcs, large

coefficients of both the HOMO and LUMO reside on the phenyl α-carbon atoms (*i.e.*, bay positions) and chelating nitrogen atoms, respectively.[6,39,40] Hence, the orbital energies can be tailored by the direct implementation of electron-donating groups to destabilize molecular orbitals (MOs) and electron-withdrawing groups which favor stabilization.[41,42] With the appropriate choice of substituents and central ion attached to the Pc framework, the energy levels can be synergistically perturbed. As for axial substituents, which are not directly attached to the Pc framework, electronic effects imparted by these groups are minimal in comparison. To date, MPcs studied in OTFTs have, in general, fallen into the category of *p*-type semiconductive materials, while reports of those leaning towards *n*-type are much scarcer.[31] Presumably, this may reflect the large collection of easily accessible divalent transition metal complexes, which intrinsically favor *p*-type behavior. Additionally, the lack of precursors available to construct electron-deficient Pc macrocycles capable of stabilizing the LUMO energy levels for the injection of electrons may contribute to their slower progression.

A key objective for this thesis is the design and synthesis of a family of novel phthalocyanine derivatives to be employed as the semiconducting active layer in organic field-effect transistors. In particular, the aim is to tailor the Pc backbone such that electron mobility is favored; in other words, *n*-type organic semiconductors were targeted. As such, this chapter will outline the basics of OFET devices, and then a comprehensive overview of the synthesis of main-group phthalocyanines, along with their application in OFETs.

1.2 General introduction to organic field-effect transistors (OFETs)

From their outstanding properties to their chemical stability, MPcs have been sought out as tuneable active materials in OPVs,[23–26] OLEDs,[27–30] and, of particular importance to this thesis, in OFETs. The charge transport properties of MPcs make them ideal organic semiconductors in

OFETs. While a great deal of research is focused on various aspects of device optimisation,[43–49] attention will be placed on the employment of Pcs in the active layer and their configurations into devices. As well, a brief introduction to the basics of OFET devices will be provided in this section.

1.2.1 Device structure, operation and materials.

FETs are three-electrode devices that generally consist of five components: the substrate, which acts as a solid support for the device; the gate electrode, which modulates the conductivity of the active layer; the source and drain (S/D) electrodes where charge enters and leaves the active layer, respectively;[50] the insulating layer that prevents current flow between the gate and the S/D electrodes; and finally the active layer, which facilitates charge transport from the source to the drain electrodes. In the case of OFETs, the active material consists of an organic semiconductor that can be switched between on (*i.e.*, conductive) and off (*i.e.*, non-conductive) states remotely through an electric gate by the gate electrode. Due to the inherent properties of organic semiconductors, the active layer in OFETs can be deposited by various techniques, including vapor deposition[38,51–53] or solution processing[11,12,26] methods. While the S/D electrodes are directly connected to the semiconductor and the gate electrode is separated by an insulating layer in all OFETs, various device configurations are commonly employed based on the relative position of the electrodes. The four most common include top contact/bottom gate (TC/BG, Figure 1.2-i), bottom contact/bottom gate (BC/BG, Figure 1.2-ii), bottom contact/top gate (BC/TG, Figure 1.2-iii), and top contact/top gate (TC/TG, Figure 1.2-iv) structures.

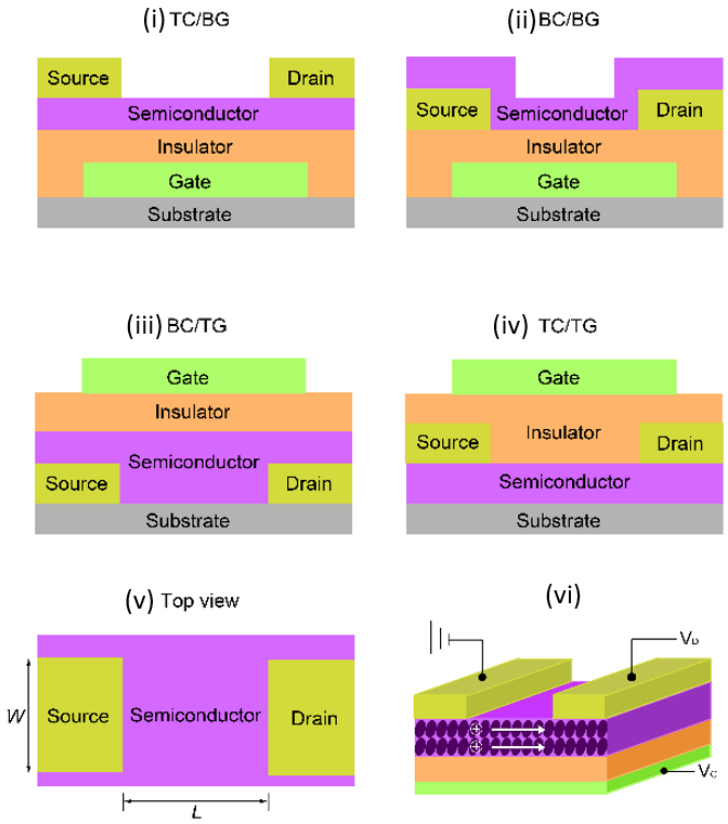

Figure 1.2 Four typical OFET configurations: (i) top contact, bottom gate (TC/BG); (ii) bottom contact, bottom gate (BC/BG); (iii) bottom contact, top gate (BC/TG); (iv) top contact, top gate (TC/TG). (v) The top view of source-and-drain electrodes and the semiconductor layer. (vi) A thin-film transistor with a flat film as the charge-transporting layer. Reproduced from Ref. 35 with permission from the Royal Society of Chemistry.

The basic principle behind OFETs involves modulation of the current between the S/D electrodes by application of a voltage to the gate electrode. A bias (V_{DS}) is applied between the S/D electrodes, and depending on the gate voltage (V_G), current flows through the semiconductor layer. When no V_G or a small V_G is applied, only negligible current flows across the semiconductor due to a lack of mobile charge carriers. This state is called the device's “off” state. If the applied V_G is larger than the threshold voltage (V_T) of the device, charge carriers can be electrostatically induced and the current flow (I_D) between the S/D electrodes increases, thus the device is “turned

on". During this process, specific charge carriers will transfer between the S/D electrodes, which is oriented parallel to the substrate surface. In order to achieve this, molecules in the semiconductor layer are required to "stand" on the substrate to ensure the π-π stacking direction is parallel to the substrate.[54] An OFET-device based on the film with vertical channels with respect to the substrate for charge transport is shown in Figure 1.2-vi. When a negative gate voltage is applied, positive charges (*i.e.*, holes) act as charge carriers; such transistors are defined as *p*-channel (or *p*-type) OFETs and the corresponding semiconductor in the active layer is a *p*-type semiconductor. Conversely, an *n*-channel (or *n*-type) OFET occurs when a positive gate voltage is applied and negative charge carriers (*i.e.*, electrons) flow through the active material. In this case, the organic semiconductor is defined as *n*-type. In some cases, ambipolar charge transport in single component OFETs can be realized by reducing the injection barrier of holes and electrons.

Related to MPc-based OFETs, some common features are noted. For example, the substrate is often treated with octyltrichlorosilane (OTS)[38,55,56] or parasexiphenyl (*p*-6p)[56] as it has been demonstrated that Pc molecules tend to grow larger domains on OTS or *p*-6p modified substrates. This leads to reduced grain boundaries, thereby enhancing charge transfer mobility (μ) and thus better device performance.[57–59] With respect to the insulating layer, to ensure sufficient charge carriers are present at the interface when a gate voltage is applied, a high dielectric strength material is necessary. While some polymers such as polymethyl methacrylate (PMMA)[60] have been reported, silicon dioxide (SiO_2) is by far the most commonly employed insulator. Given MPcs can act as either *p*-type or *n*-type semiconductors (depending on the choice of the central atom and functionalization of the Pc backbone, *vide infra*), variation in S/D electrodes is common. For the purpose of achieving sufficient injection efficiency, the work function of electrodes should be compatible with the energy levels of the frontier molecular orbitals of the semiconductor (Figure

1.3), and is therefore highly dependent on the active material. For OFETs with *p*-type organic semiconductors as the active channel material, high work function metals such as silver (~−4.7 eV), gold (~−5.1 eV), and platinum (~−5.6 eV) are often employed as the S/D electrodes, as their work functions are comparable to the HOMO of most of *p*-type channel materials (usually from −4.9 to −5.5 eV).[61] On the other hand, in order to match the LUMO of *n*-type channel materials (usually from −3 to −4.5 eV) and achieve efficient charge injection, low work function metals such as calcium (~−2.87 eV)[62] are also used in OFET devices. In some cases, using asymmetric electrodes, e.g., Au electrode for hole injection and a Ca electrode[63] for electron injection in the same device, leads to ambipolar behavior for semiconductors.

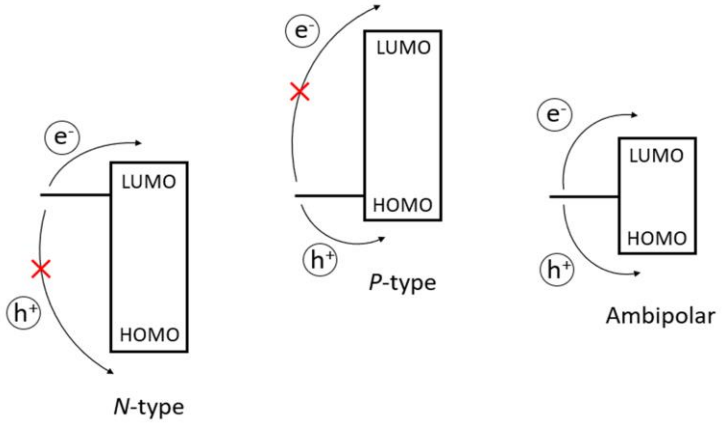

Figure 1.3 The compatible relationship between the work function of S/D electrodes and the HOMO/LUMO of the semiconductor material. Reproduced from Ref. 35 with permission from the Royal Society of Chemistry.

1.2.2 OFET performance and characterization.

The following three parameters are integral to the evaluation of active materials in OFETs. Perhaps most significant is the charge transfer mobility (μ, $cm^2/V \cdot s$), which quantifies the average charge carrier drift velocity per unit electric field.[50] Another key parameter is the threshold voltage

(V_T, V) that represents the minimum gate-to-source voltage required to induce current between the S/D terminals. And finally, the on/off current ratio (I_{on}/I_{off}), which is the ratio of the drain current in the on-state compared to that in the off-state and is typically reported as 10^x (x = 1, 2, 3,…).[44] In general, high μ, low V_T and large on/off current ratio are favorable for high-performing OFETs. Typical output curves of *p*-type, *n*-type and ambipolar OFETs are shown in Figure 1.4. The relationship between drain-source current (I_D) and the voltage in the linear (**1-1**) and saturated (**1-2**) regions can be described by the equations below:

$$I_D = \frac{W}{L}\mu C_i(V_G - V_T)V_{DS} \qquad (\mathbf{1-1})$$

$$I_D = \frac{W}{2L}\mu C_i(V_G - V_T)^2 \qquad (\mathbf{1-2})$$

where W and L are the channel width and length, respectively (Figure 1.2-v), and C_i is the capacitance per unit area of the insulating layer.

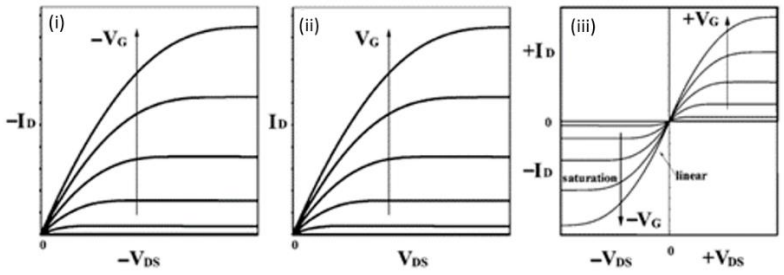

Figure 1.4 Schematic diagram of current-voltage characteristics of (i) *p*-type, (ii) *n*-type, and (iii) ambipolar OFET device. Reproduced from Ref. 35 with permission from the Royal Society of Chemistry.

Apart from μ, V_T, and I_{on}/I_{off}, stability is also an important aspect while evaluating the performance of OFET devices. To obtain air-stable and high-performing OFETs, appropriate HOMO or LUMO energy levels of the active material are required. The energy of the HOMO (E_{HOMO}) for *p*-type organic semiconductors is usually in the range of −4.9 to −5.5 eV, which should

be high enough with respect to the work function of the electrode to achieve a low hole injection barrier thereby a low V_T , but not too large to avoid being oxidized by air (below −4.0 eV). Compared to *p*-channel counterparts, it is well known that *n*-channel OFET devices are much more air-sensitive due to the intrinsic instability of organic radical anions under ambient conditions.[64] As such, most *n*-type OFETs can only operate under a vacuum or an inert atmosphere. Such unacceptable instability towards air, however, can be improved by lowering the energy level of the semiconductor LUMO below −4.0eV.[65] This can be achieved by functionalizing *p*-type materials with electron-withdrawing groups such as halogen atoms[31,66–69] or cyano groups,[70–73] thereby efficiently converting them into *n*-type semiconductors. Alternatively, introducing pyrazine into the framework of conjugated molecules not only maintains molecular planarity but also decreases the E_{HOMO} and $E_{LUMO,}$ thereby increasing air stability and electron injection affording *n*-channel materials.[74] Inclusion of a six-membered imide ring into aromatic diimides can also lead to potential *n*-type semiconducting materials with promising air stability.[64] Interestingly, in some reports of metal phthalocyanines as the active layer in OFETs, the transition from unipolar *n*-type to ambipolar[38] or even to *p*-type semiconductor[62] was observed, with the *p*-type conduction increasing after exposing the device to air for several minutes. That behavior is potentially due to oxygen in air acting as an electron acceptor from the central ion, thereby creating holes in some molecules.[38] Apart from that, a series of processing parameters including the processing technique (e.g., solution processing, thermal vapor deposition), substrate temperature, annealing, etc. can also influence OFET performance by affecting thin film morphology. Studies of the impact of these parameters on the performance of MPc-based OTFTs have been summarised by Bender, Lessard and co-workers in detail in their review article.[21]

1.3 General synthesis of metal phthalocyanines

Highlighting the ubiquity of MPcs, over 95 metals and metalloids of the periodic table have been chelated to the indole nitrogen atoms of phthalocyanine.[75] Of all these examples, two general preparative routes are typically employed as outlined in Scheme 1.1.[8,39,76] The most common synthetic approach involves the template method, which entails the cyclotetramerization of phthalonitrile (**1a**) guided by a metal/metalloid precursor. While halide salts (MX_n where X = Cl, Br, I) are most prevalently used as the template, the use of elemental metals or alloys, which are subsequently reduced in the process, have also been reported. These reactions are often carried out at elevated temperatures in non-aqueous high boiling solvents (e.g., nitrobenzene, quinoline, chlorinated benzenes and naphthalenes) and, depending on the nature of the reagents, several conditions can be altered to optimize MPc formation. For example, metal centers possessing strong Lewis acidity can activate the external nitrile groups, enabling nucleophilic addition of disassociated halide ions and anionic intermediates during the initiation and propagation steps of the macrocyclisation. Additives such as bases (e.g., 1,8-diazabicyclo(5.4.0)undec-7-ene, DBU) and initiators (e.g., alkoxides) have also been shown to be effective at promoting ring formation. In addition to phthalonitrile, other 1,2-disubstituted benzenes have been employed as synthons for the template method, including 1,3-diiminoisoindolines (DIII; **1b**), phthalamides (**1c**), phthalimides (**1d**), phthalic acids (**1e**), and phthalic anhydrides (**1f**). Depending on the reagents chosen, additional sources of nitrogen may also be required for phthalocyanine formation such as urea in the presence of a catalyst (e.g., $(NH_4)_2MoO_4$). While the template method is by far the most employed preparative route for MPcs, direct metalation is also commonplace. The latter involves the incorporation of the central ion following macrocycle formation, typically involving the reaction between a metal/metalloid halide salt and metal-free phthalocyanine.

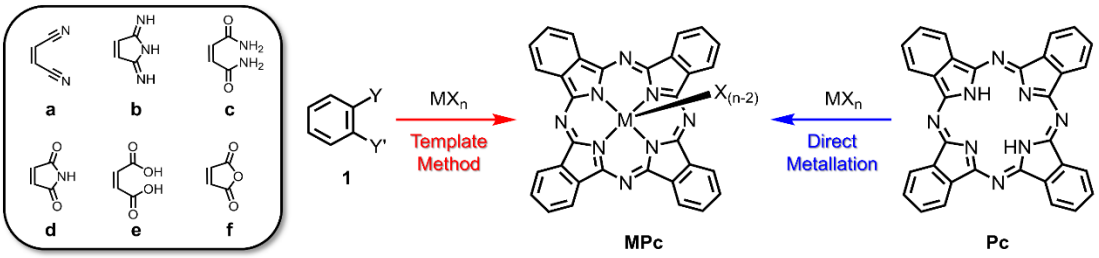

Scheme 1.1 General synthesis towards MPcs using phthalonitrile and related synthons (**1a–f**) via the template method (red) or direct metallation of metal-free Pcs (blue). Reproduced from Ref. 35 with permission from the Royal Society of Chemistry.

In view of tailoring the properties of MPcs, functionalization at the peripheral, bay and axial positions has been extensively explored.[21] To that end, functionalization can occur post MPc synthesis or via incorporation of functional groups to precursors prior to macrocycle formation.[8,39,76] The latter is most common for targeting the bay and peripheral positions, whereas the former is most appealing for axial substitution. For modifications about the Pc framework, the generation of MPcs with symmetrically substituted phthalonitriles or related precursors (e.g., **1a–f**) is preferred as predictable substitution patterns, specifically with D_{4h} symmetry, can be achieved rather than tediously modifying up to 16 positions post-cyclization.[8] Axial functionalization on the other hand is best achieved through nucleophilic substitutions of an axial leaving group, such as chlorine and bromine atoms, bound to the central atom of preformed MPcs; however, the valency of the central ion must be considered as neutral divalent complexes are not generally capable of such functionalization, whereas trivalent and tetravalent atoms offer one and two substituents, respectively.

As highlighted here, there are two main synthetic routes to generate MPcs, the template method and direct metalation. In moving towards main-group phthalocyanines, their preparation

takes inspiration from this but some changes are necessary due to differences related to their reactivity, Lewis acidity, etc.

1.4 Synthesis of main-group phthalocyanines

While there is some focus on the preparation of transition metal phthalocyanines in **Chapter 4**, developing main-group phthalocyanines, especially silicon phthalocyanines, is the key to the objectives of this thesis. As such, an overview of the synthetic routes to afford main-group phthalocyanines is presented here.

1.4.1 Group 13 phthalocyanines

1.4.1.1 Boron subphthalocyanines (metalloid Pcs).

Contrary to the majority of metal precursors, boron-centered Lewis acids facilitate the macrocyclization of phthalonitriles to yield an exceptional case of subphthalocyanines (BsubPc-X), which are composed of three isoindoline subunits oppose to four.[77] Such truncation of the phthalocyanine is to be expected given the smaller atomic size of boron, coupled to its trivalent oxidative state.[78] Interestingly, the 14 π-electron macroaromatic framework adopts a conical topography amending to the geometric constraints of the sp^3-hybridized boron center (Figure 1.5). An axially bound substituent protrudes from the central boron atom on the convex side of the macrocycle thereby affording C_{3v} symmetry. This unique structural feature of BsubPc-X derives their physicochemical properties, which has garnered considerable attraction towards their candidacy as active materials in organic optoelectronics applications. In particular, for OPVs, these building blocks act as electron acceptors and have shown great promise in replacing fullerene in these devices.[26,79–83] To date, SubPcs have not been isolated without the presence of boron at the center and attempts to exchange boron for other coordinating atoms have remained unsuccessful.

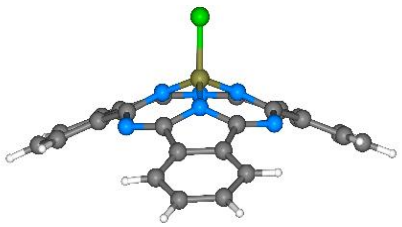

Figure 1.5 Molecular structure of BsubPc-Cl.[84] Reproduced using reported cif. Reproduced from Ref. 35 with permission from the Royal Society of Chemistry.

Since the synthesis, reactivity and reaction mechanism of a series of BsubPc-X derivatives have been well described in other review articles,[77,85] herein we only briefly present some key aspects of their preparation. First synthesized serendipitously by Meller and Ossko in 1972,[86] BsubPc-Cl was prepared via the reaction of phthalonitrile with gaseous boron trichloride (BCl_3) in chloronaphthalene at 200 °C, which afforded a cyclotrimerized product with an axially bound chlorine atom in 40% yield (Scheme 1.2). Since then, the reaction has been modified over the years to address issues with yield, purity and practicality, as it is the most common approach to generate BsubPc-Xs. For example, Giribabu *et al.* utilized microwave irradiation for this cyclization, increasing the yield of BsubPc-Cl up to 90% and reducing the reaction time to only 4–6 minutes.[87] Torres and co-workers described a highly efficient method for the synthesis of BsubPc-Cls, refluxing a 1 M BCl_3 solution in *p*-xylene with phthalonitrile, resulting in a yield of 82%.[88] Through this approach, the boron reagent can be easily handled in solution oppose to gas, which allows for greater control over its stoichiometry and thus minimizing unwanted reactivity from excess Lewis acid. Additionally, the generation Cl_2 as a side product is less pronounced through this method and significantly reduces the potential for halogenation along SubPc.

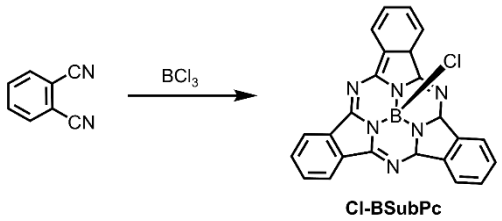

Scheme 1.2 Cyclotrimerization of phthalonitrile with BCl_3 affording BsubPc-Cl. Reproduced from Ref. 35 with permission from the Royal Society of Chemistry.

The cyclotrimerization reaction has been adapted for the derivatization of BsubPc-Xs using pre-functionalized phthalonitriles. Meticulous attention must be given to the compatibility of the functional groups with the boron Lewis acid. Substituents such as alkanes, halogens, nitrates, thioethers and sulfones are typically unaffected in the synthesis, whereas limitations are seen with alcohols, amines, ethers, carbonyls and related unsaturated functional groups among others, due to their proclivity to react with acidic substrates. As such, these functionalities are best introduced with protecting groups or post-cyclization.[77] Recently, modifications to the π-conjugated framework of phthalonitrile have provided an alternative avenue to optimize the optoelectronic properties of BsubPc-Xs. For instance, the frontier MOs can be stabilized from the replacement of the benzo moiety for electron-deficient heterocycles, such as pyrazine,[89] thiophene,[90] and 1,2,5-chalcadiazoles.[91–93] On the other hand, when aromatic hydrocarbons[94–96] and heterocycles[97–101] are instead annulated to benzene, or even used to bridge other porphyrinoids,[102–105] the extension of π-conjugation leads to bathochromic shifts in the main absorption band (Q-band).

Although less common, the boron reagent can be modified in these reactions in order to install non-halogen groups to the axial positions of BsubPc-X. For instance, treatment of phthalonitriles with BPh_3 in the presence of base has led to both substituted and unsubstituted BsubPc-Ph.[106–108] An advantage to utilizing boron precursors with carbon-based groups is the

tuning of the Lewis acidity (e.g., $BPh_nCl_{(3-n)}$; n = 1–3), which subsequently suppresses undesirable reactivity with sensitive functionalities.[92,109] As a trade-off, the stronger B–C bonds noticeably hinder product yields, due to the difficulties with eliminating the excess groups attached to the boron atom. In one instance, DIII was used as an alternative to phthalonitrile for these reactions. Regarding (^{t}Bu)$_3$BsubPc-Ph, the reaction of BPh_3 with either the corresponding DIII or phthalonitrile led to small differences in their yields (*i.e.*, 3% and 5%, respectively). While the use of this precursor did not prove to be advantageous in the synthesis, DIII has found tremendous success in the preparation of silicon phthalocyanines, which will be discussed in detail in the following section.

Due to the lability of the B–Cl bond, various axially substituted BsubPcs can be easily prepared by displacing the halide with different nucleophiles. Such functionalization thereby introduces an additional molecular fragment, which can be used to enhance structure-property relationships. For example, the substitution of the axial halide by a hydroxide group can be achieved by refluxing a suspension of BsubPc-X (X = Cl or Br) in water,[110] or toluene/SiO_2.[111] Torres' group devised an optimized method to synthesize phenol derivatives from BsubPc-Cl by heating the appropriate phenols in toluene.[88,112] In their following research, fullerene (C_{60}) was introduced in the axial position of BsubPcs by 1,3 dipolar cycloaddition reaction between formyl-substituted BsubPcs and C_{60} in the presence of *N*-methylglycine.[112] Besides water and phenol[111], other nucleophiles such as carboxylic acids,[113] alkyl alcohols,[94,114,115] and even some cholesterols[115] can also yield corresponding axial-substituted derivatives. A ferrocene-based derivative, BsubPc-$FcCO_2$, was obtained by refluxing a mixture of ferrocene carboxylic acid and BsubPc-Cl in *o*-dichlorobenzene (*o*-DCB), resulting in new donor-acceptor dyads that are potentially useful in light-harvesting elements.[113] In order to synthesize trialkylsiloxy derivatives

BsubPc-(R_3SiO) (R = alkyl), Zyskowski and Kennedy first heated a mixture of sodium metal and trihexylsilanol in anhydrous chlorobenzene to form the sodium salt, then added BsubPc-Cl and subsequently refluxed the reaction mixture for 1.5 hours.[94] Alternatively, BsubPc-(R_3SiO) can also be obtained through a two-step reaction, first preparing the BsubPc-OH, then functionalizing it with trihexylchlorosilane via nucleophilic substitution, as reported by Martínez-Díaz *et al*.[110] In 2011, Bender and co-workers discovered that phthalimides can also function as suitable nucleophiles in the displacement of the chloride in BsubPc-Cl to form phthalimido-boron subphthalocyanines.[116] Interestingly, ~10% of μ-oxo-$(BsubPc)_2$ was also obtained as a by-product suggesting hydrolyzation of BsubPc-Cl to BsubPc-OH occurs in the presence of trace amounts of water, which subsequently reacts with another equivalent of BsubPc-Cl or condenses with another BsubPc-OH.[116]

1.4.1.2 Aluminum, gallium and indium phthalocyanines (metal Pcs).

The remaining elements of Group 13 can all be introduced into the Pc framework. Within this section, we direct our attention to their syntheses, specifically for aluminum, gallium and indium, from which this family of molecules has been previously studied in OTFTs. Out of the three, aluminum was among a series of elements in the initial studies of metal phthalocyanines pioneered by Linstead in 1934.[117] In his report, the reaction between phthalonitrile and aluminum trichloride ($AlCl_3$) in heated quinoline led to the formation of AlPc-Cl. He also noted AlPc-Cl can be generated through the direct insertion of $AlCl_3$ to metal-free Pc with the subsequent release of HCl. Years later, Colaïtis applied the template method to phthalonitrile using trivalent metal halides of gallium and indium to afford GaPc-Cl and InPc-Cl, respectively.[118] Single crystals have been grown of axial-halide substituted complexes, from which each trivalent metal ion puckers

out-of-plane to the phthalocyanine framework, presumably as a consequence of their larger ionic radii (Figure 1.6).[119,120]

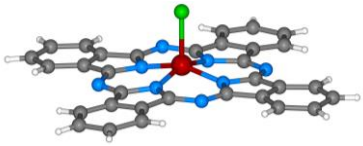

Figure 1.6 Molecular structure of AlPc-Cl.[121] Reproduced using reported cif. Reproduced from Ref. 35 with permission from the Royal Society of Chemistry.

Additionally, DBU has been shown to be effective at catalyzing the cyclotetramerization of phthalonitrile in solution. [122–128] As a result, a range of peripherally-functionalized Cl-MPc derivatives have been obtained that bear, for example, alkyl, [125,127] thioethers,[122] phenoxy,[124,129] and pyridyloxy.[130] Extended π-conjugated naphthalocyanines of each trivalent metal ion (MNPcs) have also been reported using similar preparative methods as their MPc-X counterparts. More specifically, the synthesis of InNPc-Xs usually starts from the appropriate naphthalonitriles or DIIIs, which can be prepared from *o*-xylenes as reported previously.[127,128,131] It has been demonstrated that the use of DIII affords a preformed naphthalocyanine core, which is much more reactive than the corresponding dicyanonaphthalenes.[131] Apart from that, AlPc-OH[132,133] and GaPc-OH[126] derivatives can be directly synthesized based on dicarboxylic acid or dianhydride, with the presence of urea and catalyzed by ammonium molybdate.

Axial replacement of MPc-Cl (M = Al, Ga, In) can be facilitated by nucleophilic addition. Hydroxy derivatives are commonly obtained by hydrolyzing the corresponding MPc-Cl under acidic or basic conditions. For instance, AlPc-OH can be synthesized from the reaction of AlPc-Cl in the presence of NH_4OH in a refluxing pyridine solution.[134] GaPc-OH can be prepared by casting a concentrated sulfuric acid solution of GaPc-Cl into the water followed by neutralization

with NH_4OH.[135] Based on the hydroxy derivatives, more axial substituted complexes can be prepared. For example, the conversion of AlPc-OH to AlPc-F can be achieved by treating the former with hydrofluoric acid (~48 wt. %).[134,136,137] Similar conversion was achieved in the case of GaPc-Cl.[136] In addition, Grant *et al.* reported a more straightforward and safer one-step synthetic route to obtain MPc-F from MPc-Cl (M = Al, Ga) directly, using cesium fluoride as the fluoride source in high boiling polar solvents.[138] Phenol complexes are also commonly used nucleophiles that can introduce phenoxy groups onto the center of MPcs, such as *p*-methoxyphenol,[139] pentafluoro phenol,[140] *p*-nitrophenol,[140] *p*-chlorophenol,[125] etc. The introduction of aryl groups to the axial position of Pcs can be achieved by using appropriate Grignard reagents,[125,127,129] or lithium salts for the introduction of aryl substituents[127] upon nucleophilic substitutions of MPc-Cls. Chen *et al.*[141] even introduced InPcs into a polymer backbone by reacting InPc-Cl with polystyrene$(MgBr)_n$. Apart from that, Sakai *et al.*[142] synthesized poly(hydroxyimide)-AlPcs copolymer by the reaction of poly(hydroxyimide) with aluminium phthalocyanine triflate, which was obtained from AlPc-Cl and silver triflate. MPcs were also demonstrated to play an important role in the field of graphite materials, in which the first soluble graphite oxide (GO) axially substituted GaPc hybrid material was prepared by Li *et al.*[143] in 2011. This was achieved via the reaction of GaPc-Cl with GO in DMSO at 110 °C in the presence of K_2CO_3.

1.4.2 Group 14 phthalocyanines

1.4.2.1 Silicon and germanium phthalocyanines (metalloid Pcs).

Incorporation of Group 14 atoms into MPcs offers the potential for stable hexacoordinate complexes given the accessibility to tetravalent oxidation states. Advantageously, this provides an

additional synthetic handle to fine-tune the properties of the material, specifically solubility and the solid-state arrangement, as two axial substituents are present (Figure 1.7).

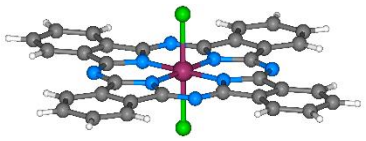

Figure 1.7 Molecular structure of $SiPcCl_2$.[144] Reproduced using reported cif. Reproduced from Ref. 35 with permission from the Royal Society of Chemistry.

The first attempts to generate silicon phthalocyanines were focused on the direct metalation of Pc by Linstead.[145] Although unsuccessful, these involved pressure tube reactions comprised of disodium phthalocyanine and silicon tetrachloride ($SiCl_4$).[146] Several decades later, Kenney and co-workers described the formation of what they proposed to be dichlorosilicon phthalocyanine ($SiPcCl_2$) via the template method in 1960,[147] which was later supported by elemental analysis.[148] While reacting phthalonitrile with silicon $SiCl_4$ in refluxing quinoline affords $SiPcCl_2$, only 7% of the desired product was isolated using this approach. In the same report, various silicon sources were explored including trichloromethylsilane, trichloromethylsilane, and hexachlorodisiloxane to varying levels of success. Product formation was not observed for the former two reagents; however, the synthetic route employing hexachlorodisiloxane provided a yield of approximately 43%. Alternatives to phthalonitrile were reviewed in a study by Kenney in 1964, which demonstrated that both *o*-cyanobenzamide and DIII could be converted to $SiPcCl_2$ in 35% and 71% yields, respectively.[149] The yield of this reaction has been enhanced by Marks and co-workers through their modified procedure that introduces DIII once the reaction temperature reached 200 °C, which afforded yields reaching 80%.[150] Additionally, Noboru *et al*. synthesized $SiPcCl_2$

in a 90% yield by replacing quinoline with tetrahydronapthalene and tri-*n*-butylamine,[151] yet the authors note that the crude product contains as much as 30─50% impurities.

The vast majority of derivatization with respect to silicon phthalocyanines is directed to axial functionalization (*vide infra*), while peripherally substituted complexes are few and far between. This may be attributed to the lack of commercially available DIIIs, along with their less-than-ideal preparative routes, which require the use of sodium metal and a constant flow of ammonia gas in a refluxing methanolic solution of phthalonitrile for several hours.[149] However, an alternative approach to the classical preparative route for DIII was recently reported by Brusso and co-workers (Scheme 1.3) that employs $LiN(TMS)_2 \cdot Et_2O$ as a nucleophilic source of nitrogen.[152] This new route eliminates the undesired expenses attributed to the strenuous reaction conditions required and the hazardous reagents employed in the preparation of DIII, thus it is anticipated that other derivatives with modified molecular frameworks can now be explored.

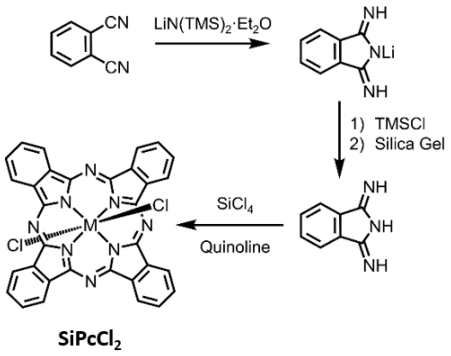

Scheme 1.3 Synthetic routes in the preparation of $SiPcCl_2$, including the preparation of DIII.[152] Reproduced from Ref. 35 with permission from the Royal Society of Chemistry.

In contrast to X_2-SiPcs, tetravalent germanium complexes are readily prepared by the template reaction of phthalonitrile and germanium tetrachloride ($GeCl_4$) to afford dichlorogermanium phthalocyanine ($GePcCl_2$).[150,153] Alternatively, $GePcCl_2$ can also be prepared

by mixing powdered germanium metal with phthalonitrile under a stream of ICl vapor at ~160°C. The latter route affords isomorphous triclinic crystals of $GePcCl_2$, whereas monoclinic crystals of $GePcCl_2$ can be prepared *via* the same reaction at ~180 °C.[154] At these temperatures, melted phthalonitrile undergoes catalytic tetramerization while two-electron transfer occurs from the Ge atom to the Pc ring simultaneously and two other electrons are transferred from the Ge atom to ICl forming I^- and Cl^- ions.[154] In 2017, Slodek *et al*. reported a less common synthetic route for $GePcCl_2$ in which the product was obtained by reacting 4-nitrophthalic anhydride with $GeCl_4$ using urea as a source of ammonia and ammonium molybdate as the catalyst.[155]

In 1970, Joyner and co-workers[156] reduced $GePcCl_2$ with sodium borohydride ($NaBH_4$) or tin dichloride ($SnCl_2$) to obtain divalent germanium phthalocyanine (GePc), which is a very light-sensitive compound. The authors also noted that a large excess of $NaBH_4$ led to complete decomposition of the ring system. Interestingly, GePc is surprisingly resistant to oxidation back to form $GePcX_2$, while a similar oxidation process is much easier for divalent SnPc (vide infra).[145] In the case of GePc, phthalocyanine oxidation and decomposition usually occur before the oxidation of Ge^{II} to Ge^{IV}, potentially due to the smaller covalent radius of Ge^{II} (compared to Sn^{II}), which could allow it to fit tightly within the Pc plane thereby enhancing its stability.[157]

The synthesis of dihydroxysilicon phthtalocyanine ($SiPc(OH)_2$) and dihydroxygermanium phthalocyanine ($GePc(OH)_2$)[150,153] have been extensively reported with the most common preparative method achieved via hydrolysis of their dichloride counterparts. In these processes, both strongly acidic (typically involving concentrated sulfuric acid)[148] and basic (employing, for example, sodium hydroxide,[150,158] cesium hydroxide,[159] concentrated aqueous ammonia,[148] sodium methoxide,[149] etc.) conditions can be used to hydrolyze the $MPcCl_2$ complexes. In the case of $SiPc(OH)_2$, it can also be prepared directly from DIII. As well, the two axial positions of the

tetravalent metal centers can be displaced by various substituents such as phenyl,[160] phenoxy,[25,153,155,159] siloxy,[148,153,159,161] alkynyl,[162] diethylaminophenoxyethoxy,[163] 1-benzylpiperidin-4-oxy,[164] and even graphene[165] or benzyl ester dendrimers.[166] For this reason, a number of symmetrically and asymmetrically substituted $SiPcX_2$ and $GePcX_2$ derivatives have been developed over the years. The majority of axially substituted systems can be prepared via nucleophilic substitution of $MPcCl_2$[25,155,160,164,166] or $MPc(OH)_2$,[147,148,153,159] while there are also examples starting from DIII for silicon-based derivatives. For example, Barker *et al.*[160] first synthesized chloro phenyl silicon phthalocyanine chloride (SiPc(Cl)(Ph)) by the reaction between DIII and phenyltrichlorosilane. They then synthesized a series of axial-substituted esters and bis-ether through nucleophilic displacement of one or two Cl substituents from either SiPc(Cl)(Ph) or $SiPcCl_2$, respectively.[160] The introduction of various substituents can not only enhance the solubility of MPcs, but also suppress aggregation by introducing steric hindrance.[167,168]

1.4.2.2 Tin and lead phthalocyanines (metals Pcs)

It is well known that tin is stable in both the +2 and +4 oxidation states,[169] thus in Pc based complexes it can exist in either divalent or tetravalent form. Lead on the other hand only exhibits bivalency, which limits the functionalization of PbPcs to the phthalocyanine framework. Template cyclisation of phthalonitrile using MCl_n (where M = Sn and Pb; n = 2 or 4) in a refluxing high boiling point solvent is an effective preparative method, giving rise to dichlorotin phthalocyanine ($SnPcCl_2$)[150,170] and lead phthalocyanine (PbPc).[171] $SnPcCl_2$ was first synthesized by Linstead and co-workers in which the reaction between phthalonitrile and $SnCl_2$ was violently exothermic, affording $SnPcCl_2$ in a 90% yield.[146] Subsequent work by Kroenke and Kenney investigated the same reaction in 1-chloronaphthalene,[170] which Dirk *et al.*[150] then modified to obtain $SnPcCl_2$ in an excellent yield of 96%. The synthesis of isomorphous triclinic and monoclinic crystals of

$SnPcCl_2$ was accomplished in the identical fashion to that of $GePcCl_2$ (*vide supra*), except metallic Sn was used instead of Ge.[154] Another synthetic procedure involving metal-free phthalocyanine (H_2Pc) as carried out using commercially available dilithium phthalocyanine,[172] where Sn was introduced into the Pc ring by boiling a mixture of H_2Pc and $SnCl_2$ in dry quinoline. This reaction requires high energy, due to the relatively large size of Sn atoms for coordination with Pc ligand. Here, the high boiling point solvent was used for the coordination of both ions and the reactions were performed by preheating of the starting compound to allow the high yielded coordination reactions.[172] Additionally, the preparation of MNPcs can be achieved by reaction between 2,3-naphthalenedicarbonitrile with $SnCl_2$ or $SnCl_4$ gives rise to SnNPc[173] and $SnNPcCl_2$,[173] respectively.

Divalent tin phthalocyanine (SnPc) can be obtained by mixing metallic tin and phthalonitrile and heating to 300 °C without solvent.[146] In addition, SnPc can also be prepared by the reduction of its tetravalent counterpart (e.g., $SnPcCl_2$). For instance, Kroenke and Kenney[170] reduced $SnPCl_2$ with anhydrous $SnCl_2$ in refluxing quinoline.[170] Linstead and co-workers[145] passed hydrogen through a solution of $SnPcCl_2$ in boiling quinoline to obtain SnPc. They also showed oxidation of solid SnPc with dry chlorine gas afforded the tetravalent dichlorotin chlorophthalocyanines, where chlorination was observed along the phthalocyanine framework. All the records suggest that interchange between stannous and stannic phthalocyanines can be readily affected (Scheme 1.4).

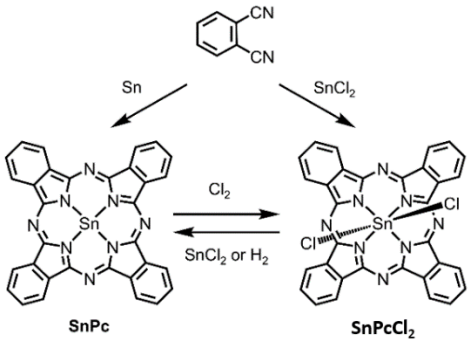

Scheme 1.4 Synthetic routes to divalent SnPc and tetravalent $SnPcCl_2$. Reproduced from Ref. 35 with permission from the Royal Society of Chemistry.

It is noteworthy that lead phthalocyanine (PbPc) is kind of abnormal compared with other phthalocyanines in which the central elements belong to Group 14. Since the central Pb ion only exhibits bivalency, axial substituents cannot be attached to the central atom, thereby limiting functionalization (Figure 1.8). In general, PbPcs can be prepared by the violently exothermic reaction between litharge (PbO) and phthalonitrile,[146,174] or by the more common reaction between phthalonitrile and $PbCl_2$.[171] Moreover, extended PbNPcs have been achieved through similar reactions by treating 2,3-naphthalenedicarbonitrile with $PbCl_2$.[175]

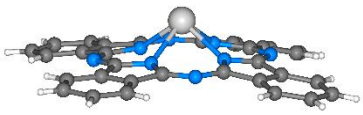

Figure 1.8 Molecular structure of PbPc.[176] Reproduced using reported cif. Reproduced from Ref. 35 with permission from the Royal Society of Chemistry.

So far, the literature of axially substituted $SnPcX_2$ is not well established, especially compared to $SiPcX_2$. Similar to $SiPc(OH)_2$ and $GePc(OH)_2$, $SnPc(OH)_2$[150,170] can also be prepared via the hydrolysis of $SnPcCl_2$ in the presence of strong acid or base. Axial substituted reactions for SnPcs[177] have been achieved via nucleophilic substitution of either $SnPc(OH)_2$ or $SnPcX_2$. For

example, Rafaeloff *et al.*[178] prepared $SnPc(OCPh_3)_2$ and $SnPc(OSiPh_3)_2$ by reacting $SnPcI_2$ or $SnPc(OH)_2$ with triphenylcarbinol or triphenyisilanol, respectively. Then in 2002 Maree *et al.* synthesized diestronetin phthalocyanine by modifying their method used for substitution with silanols.[177] In 2019, Lessard and co-workers reported the synthesis of two soluble axially functionalized tin phthalocyanines with silyl ethers, $SiPc(OSi(n\text{-}Bu)_3)_2$ and $SiPc(OSi(n\text{-}Hx)_3)_2$ (Bu = butyl; Hx = hexyl), by the reaction between $SnPcCl_2$ and corresponding tri-*n*-alkylchlorosilanes in the presence of NaOH and Aliquat HTA-1, a phase transfer catalyst, in boiling chlorobenzene.[179] In early 2020, Lessard's group extended their research to the synthesis and the OTFT application of complexes with electron-deficient polyfluorinated aryl substituents at the axial positions, including $SnPc(F_5Ph)_2$ and $SnPc(2,4,6\text{-}F_3Ph)_2$.[34] The reaction of $SnPcCl_2$ with fluorophenol in refluxing chlorobenzene resulted in bis(fluorophenoxy) substituted SnPcs in good yields of ~ 80%.

1.4.3 Group 15 phthalocyanines

1.4.3.1 Phosphorus phthalocyanines (non-metal Pcs).

Elements from Group 15 have also been incorporated into phthalocyanines, thereby Pcs will exist in different oxidation states (radical anions/cations, *etc*).

Phosphorus can exist in two different oxidation states, P^{III} and P^{V}, while in phthalocyanine rings it usually tends to be pentavalent. It has a large electronegativity so that it can withdraw electrons strongly.[41] Introducing a phosphorus atom into the core of free-base Pcs is the most widely used synthetic route to prepare phosphorus phthalocyanine (PPc) derivatives. Gouterman *et al.*[180] first synthesized PPc species by the reaction of metal-free Pcs and a reactive pyridine PBr_3 intermediate (py-PBr_3) in 1981. Compared to PCl_3 and PI_3, only PBr_3 can form a new, highly reactive species in pyridine (Scheme 1.5). The final product includes a mixture of fluorescent P^{III}Pc species and nonfluorescent P^{V}Pc

species, which can be separated by column chromatography on Al_2O_3. However, Tomilova's group[181] only obtained triazatetrabenzocorrole, a product of the phthalocyanine nature, based on the same reaction that Gouterman *et al.* reported. Then they modified the reaction by replacing PBr_3 with phosphorus oxyhalides (POX_3, X = Cl, Br). The mixture was quenched with water after the reaction was complete, which provided axial hydroxy ligands for the central phosphorus atom. The final product, dihydroxo(phthalocyaninato) phosphorus(v) hydroxide was isolated by chromatography.[181] In 2011, Kobayashi *et al.*[41] also selected $POBr_3$ for the purpose of introducing a phosphorus atom into the center of the Pc ring. In their work, the product was quenched with methanol to obtain axial methoxide ligands. And the potassium hexafluorophosphate (KPF_6) was used to achieve the counteranion exchange in order to give a stable Pc as the hexafluorophosphate salt.[41] In their later work, they synthesized the same P^VPc complexes according to a similar procedure except for the reaction temperature.[42] Here, the introduction of P^V ion proceeded at room temperature for hours instead of keeping it refluxing.[41,42] This suggested that electron-rich group 16 elements (e.g., S and Se) on the Pc periphery can stabilize the electron-deficient P^V complex by increasing the bond order between the pyrrole nitrogen and P^V ion.[42]

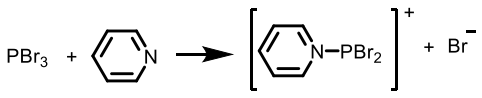

Scheme 1.5 The synthesis of pyridine PBr_3 intermediate.

There is only one related report which focused on phosphorus phthalocyanine so far: Nyokong *et al.*[182] expanded their research to phenyl axial substitution based on

$[P^{V}Pc(OH)_2](OH)$. The axial ligand exchange of OH in $[P^{V}Pc(OH)_2]^+$ for a phenyl group was obtained by employing the Grignard reaction with C_6H_5MgBr to form $[(P^{V}Pc(Ph)_2]^+$.[182]

1.4.3.2 Arsenic and Antimony phthalocyanines (metalloid Pcs)

Both arsenic and antimony can exhibit trivalence or pentavalence in phthalocyanines. The synthesis of $[As^{III}Pc]^+$ and $[Sb^{III}Pc]^+$ has been reported by several works. Most of them were prepared by the template method, starting from the reaction of phthalonitrile with MX_3[183–185] or pure metal powder[186–188] (M = As, Sb, X = Cl or I) at a high temperature. The $Sb^{V}Pc$ complex $[Sb^{V}(Pc)Cl_2]^+$ was synthesized in 1994 for the first time by fusing a mixture of phthalonitrile and $SbCl_3$.[189] Apart from this typical route, it has been demonstrated that $Sb^{III}Pc$ can readily be converted to the corresponding $Sb^{V}Pc$.[185,190] For example, Isago *et al.*[185] synthesized $[Sb^{V}Pc(OH)_2]^+$ by oxidizing $[Sb^{III}Pc]I_3$ with tert-butyl perbenzoate. The final product was isolated as hexafluorophosphate and triflate salts. In Knör's work, 30% hydrogen peroxide was utilized as the oxidizing agent to convert $[Sb^{III}Pc]F$ into $[Sb^{V}Pc(OH)_2]F$.[190]

However, $As^{V}Pc$ was not obtained until 2012 by Isago's group[183], due to the instability and poor solubility in common organic solvents of $As^{III}Pc$ complexes, and the toxicity of arsenic. As reported, *tert*-butyl groups were introduced on the periphery of the macrocyclic ligand for the purpose of improving the solubility of $As^{III}Pcs$, which was $[As(tbpc)]^+$ in their work (tbpc denotes tetra-*tert*-butylphthalocyaninate, $C_{48}H_{48}N_8^{2-}$).[183] Therefore, the succeeding oxidation reactions of $As^{III}Pcs$ with XeF_2 can be easily achieved. The first reported stable $As^{V}Pc$ complex was thus obtained as $[As^{V}(tbpc)F_2]PF_6$.

As mentioned above, As^{V}[183] and Sb^{V}[185,190] Pcs can be obtained by oxidizing their trivalence complexes. There is another effective synthetic route: introducing As or Sb atom into the core of

metal-free Pcs. Kobayashi *et al.*[42] demonstrated that α-chalcogenyl Pcs are suitable ligands for inserting group 15 elements into the central core. Based on this consideration, As^{V} and Sb^{V} ions were introduced into the center of metal-free α-thioaryl Pcs. $AsCl_3$ and $SbBr_3$ were employed as the source of arsenic and antimony in the case of As^{V}Pcs and Sb^{V}Pcs, respectively. Unstable As^{III} specie was first obtained, and then it was oxidized to As^{V} by adding pyridinium tribromide. In terms of Sb^{V}Pcs, a stable unsymmetrically axial substituted complex was synthesized (X_1 = OMe, X_2 = OH).

1.4.3.3 Bismuth phthalocyanines (metal Pcs).

As reported, $[Bi^{III}Pc]^{+}$ can be prepared by the reaction of phthalonitrile and powdered bismuth[191]. Introducing Bi^{III} into the core of free-based Pcs (e.g., Li_2Pcs) also leads to a satisfying result,[192] while for the nitrile method pure product was hard to isolated from the solution.[192] It is noteworthy that those Pc macrocycle ions usually show a saucer shape rather than planar due to the interaction of the central trivalent ion with the oppositely charged counter-ion.[186] Bi^{V}Pc complexes are rarely investigated as pentavalent bismuth is unstable.

1.4.4 Group 16 phthalocyanines

As for group 16 phthalocyanines, no complexes have been reported in the literature to the best of our knowledge. Thus, there remains an untapped potential to explore the synthesis of MPcs bearing these elements; however, that is beyond the scope of the current thesis so will not be addressed further.

1.5 Applications of main-group phthalocyanines in organic field-effect transistors

To reap the benefits provided from axial functionalities, attention has been drawn towards main-group Pcs, as a range of stable oxidation states can be accessed from these elements.

Trivalent and tetravalent main-group Pcs are in possession of one and two chemical handles, respectively, that can be easily modified for tuning of the material properties. Moreover, higher valencies and greater electronegativities found for many of the *p*-block elements have been shown to intrinsically affect the nature of the organic semiconductor, from which unipolar *n*-type and ambipolar behaviors have been observed for unsubstituted Pc complexes. In this section, we provide a view of the OFET performances for devices fabricated with main-group Pcs of Groups 13 (B, Al, Ga and In) and 14 (Si, Ge, Sn, and Pb). Interestingly, there are currently no reports of main-group Pcs with thallium or Group 15 elements in the application of OFETs, to the best of our knowledge, despite their chemistry being established.

1.5.1 Group 13 phthalocyanines in OFETs

Key parameters from the performances of OTFTs fabricated from Group 13 main-group Pcs have been tabulated in Table A.1 (see Appendix A). Among this group, BsubPc-X derivatives have been widely employed as functional materials in OLEDs and OPVs,[20,22] however, there remains a paucity of research on their role in OFETs. In 2007, Yasuda and Tsutsui reported the fabrication of OTFT devices using BsubPc-Cl within the active layer.[62] Metal calcium was utilized for the S/D electrodes with an Ag overlayer, as its low work function reduces electron injection barriers. OFETs, with BsubPc-Cl deposited by vacuum sublimation, exhibited *n*-channel behavior with an electron μ of 5.4×10^{-5} $cm^2/V \cdot s$ and V_T of 11 V. For reference, devices were also constructed using Au for the S/D electrodes, which showed a drop in the mobility ($\mu = 1.2 \times 10^{-5}$ $cm^2/V \cdot s$) and rise in the threshold voltage ($V_T = 45$ V). At the time, the reference OFET with Au S/D electrodes showed a curious ambipolar behavior when expose to air for a few minutes with a field-effect hole μ reaching 7.5×10^{-7} $cm^2/V \cdot s$; however, since then, this type of charge carrier μ is well accepted in BsubPc-Xs, as shown in their fabrication into OPVs.[22]

Apart from this work, Bender and co-workers investigated the basic electron mobilities of a series of fluorinated phenoxy BsubPcs (*i.e.*, BsubPc-($OPhF_5$), $(F)_{16}$BsubPc-(OPh), and $(F)_{16}$BsubPc-($OPhF_5$)) using admittance spectroscopy.[193] At high electric fields, mobilities reached approximately 10^{-4} $cm^2/V{\cdot}s$, which are higher than that reported for BsubPc-Cl. Although these mobilities were not determined for OTFTs, rather sandwiched between two electrodes perpendicular to the substrate, investigations into the axial ligands in X-BsubPc warrants further attention to improve OTFT performances based on these systems.

AlPc-Cl, a nonplanar and pyramid-like trivalent phthalocyanine, has been used as in the semiconductor layer of OFET devices in many reports. Compared to the most commonly used planar divalent Pcs such as CuPc, AlPc-Cl forms a face-to-face π-stacked structure that leads to more efficient π-orbital overlap, facilitating charge carrier transport.[55] Recently, Boileau *et al.*[33] reported the impact of environmental pressure and operating temperature on charge transport and electrical stability of *p*-type BC/BG OTFTs based on AlPc-Cl semiconductor layer. The hole μ increased from 0.001 $cm^2/V{\cdot}s$ in vacuum to 0.04 $cm^2/V{\cdot}s$ in air, indicating that the oxygen present under ambient conditions coordinates to the surface AlPc-Cl metal centers, which will act as an electron acceptor/trap and increase positive charge carrier density in the bulk film as a result.[33,62] Figure 1.9 shows how hole μ changes with V_{GS} at different device testing temperatures under either vacuum (i, 25–150°C) or air (ii, 25–85°C) ambience. In general, the μ increases with increasing temperature in vacuum, while in air it shows a minimal change. Besides, under vacuum, the higher the temperature applied, the lower voltage (V_T) is required to turn the transistor on. However, this overall shift in curves with increasing temperature (ΔV_T) is less obvious in air. In the same paper, Boileau *et al.*[33] also investigated five other divalent transition-metal Pcs, including ZnPc, MgPc, FePc, CoPc and CuPc Figure 1.10 illustrates ΔV_T and percentage changes in μ of different MPcs.

The result indicates that divalent MPcs show generally greater changes in μ and V_T in performance with temperature by comparison with AlPc-Cl. In other words, AlPc-Cl film has more air-stable electrical properties. This is attributed to its distinct film morphologies with larger grain sizes and higher surface roughness, leading to the lower surface area to volume ratios and thus reducing the access of ambient gases to the overall volume, based on the Atomic Force Microscope (AFM) results (Figure 1.11).

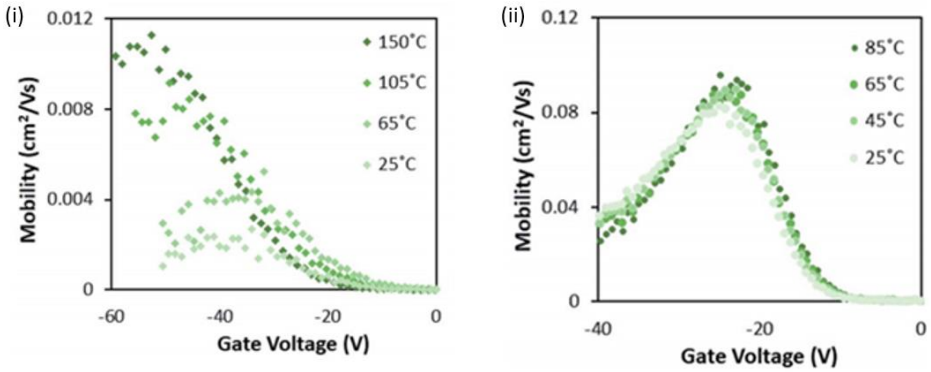

Figure 1.9 Characterization of AlPc-Cl OTFTs. (i). V_{GS} vs. μ curves at temperatures ranging from 25 °C to 150 °C in vacuum. (ii). V_{GS} vs. μ curves at temperatures ranging from 25 °C to 85 °C in air. Reproduced from Ref. 35 with permission from the Royal Society of Chemistry.

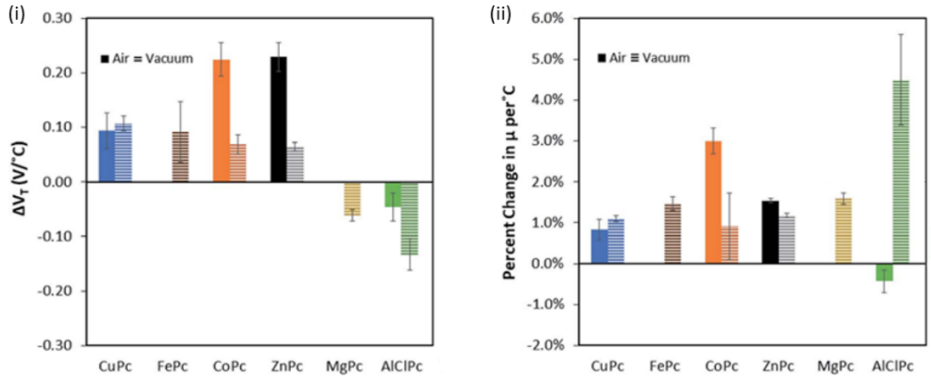

Figure 1.10 (i) Change in threshold voltage per degree celsius, (V_T/°C) within the characterized temperature range (25 °C to 85 °C for air and 25 °C to 150 °C for vacuum) for each phthalocyanine material (blue:

CuPc; brown: FePc; orange: CoPc; black: ZnPc; yellow: MgPc; green: AlPc-Cl) characterized in BC/BG OTFT under air (solid bars), and vacuum (horizontal line bars). (ii) % change in hole mobility, μ, compared to baseline at 25 °C per °C. Materials that did not function in air have no corresponding data (FePc, and MgPc). Reproduced from Ref. 35 with permission from the Royal Society of Chemistry.

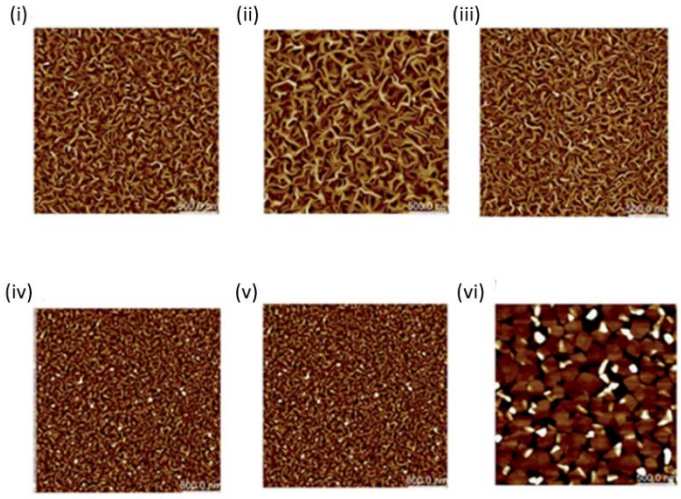

Figure 1.11 AFM images (2.5 mm × 2.5 mm) of (i) CuPc (ii) FePc (iii) CoPc (iv) ZnPc (v) MgPc (vi) AlPc-Cl deposited on heated silicon substrates. Reproduced from Ref. 35 with permission from the Royal Society of Chemistry.

As previously mentioned, the semiconductor layer can be deposited using different approaches. Since most MPcs have poor solubility, MPc based OFETs are commonly fabricated by vacuum evaporation. To develop a device using solution processing, Glezos and co-workers synthesized water-soluble aluminum complexes by sulfonating unsubstituted AlPc-OH with fuming sulfuric acid.[194,195] The crude product was a mixture of mono-, di-, tri- and tetra-sulfonated isomers of $(HO_3S)_m$ AlPc-OH (m = 1–4), which was separated by column liquid chromatography, and subsequently treated with NaOH to afford their fully deprotonated sodium salts. Thin films of $(NaO_3S)_m$ AlPc-OHs were analyzed by X-ray photoelectron spectroscopy, from which the atomic ratios of the elements detected on the surface of the spin-casted material indicated a chemical

composition reflecting that of $(NaO_3S)_{1.5}$AlPc-OH. This was believed to arise from the atmospheric exposure upon processing the material onto the substrate. *p*-Channel OFET devices based on $(NaO_3S)_{1.5}$ AlPc-OH exhibited field-effect mobilities of 0.02 $cm^2/V{\cdot}s$, V_T of −1.42 V and ~10^3 current on/off ratios.

In 2011, Chi and co-workers investigated the molecular packing mode and optoelectronic properties of AlPc-Cl which was utilized as the semiconductor layer in TC/BG OTFT devices fabricated on pure SiO_2 substrate at room temperature and 120 °C, and on an OTS-treated surface at 120 °C.[55] The output and transfer characteristics of these devices are illustrated in Figure 1.12, which reveal inferior hole mobilities for the devices fabricated on SiO_2 (10^{-4} $cm^2/V{\cdot}s$ for room temperature, and 10^{-6} $cm^2/V{\cdot}s$ for 120 °C) compared to that of devices employing OTS-modified substrates (0.06 $cm^2/V{\cdot}s$ for 120 °C). This difference in device performance is related to the molecular orientation of the molecules on the three substrates. As shown in Figure 1.13, when AlPc-Cl molecules are depositing on an OTS-modified surface, they align with an inclination angle of 18.2° with respect to the surface normal, resulting in continuous and flat films. Compared with random or face-on molecular orientations that were formed on the SiO_2 surface (Figure 1.13-i, ii), this edge-on orientation is much more favorable for in-plane charge transport due to the reduced grain boundary and the consistency between the charge-transport direction and the π-stacking direction.[55] It can therefore be concluded that high-performance OTFTs can be obtained by tuning the surface properties and substrate temperature to control the growth of the film with appropriate packing mode.

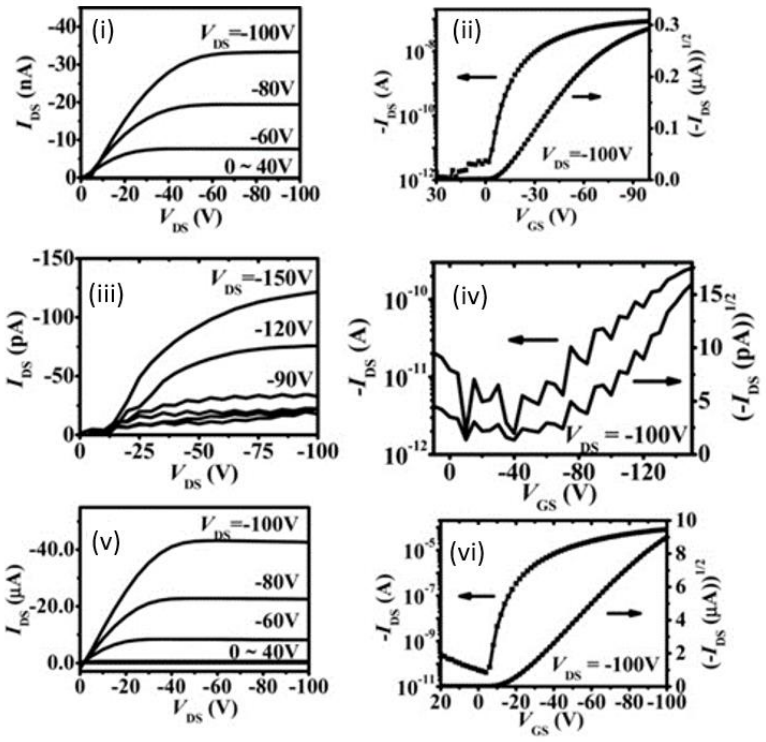

Figure 1.12 Output and transfer curves of devices with AlPc-Cl active layer fabricated under different conditions: (i, ii) pure SiO_2 surface at room temperature; (iii, iv) pure SiO_2 surface at 120 ° C; (v, vi) OTS-modified surface at 120 °C. Reproduced from Ref. 35 with permission from the Royal Society of Chemistry.

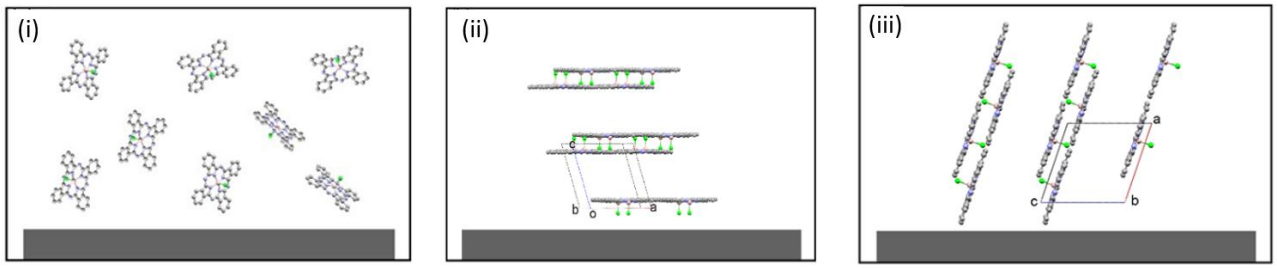

Figure 1.13 Schematic molecular packing of an AlPc-Cl (CCDC: 1134071) film fabricated on a pure SiO_2 substrate at room temperature (i) and 120 °C (ii), and on an OTS-modified surface at 120 °C (iii). Reproduced from Ref. 35 with permission from the Royal Society of Chemistry.

Hexadecafluoro- and hexadecachloro-substituted AlPc-Cls and InPc-Cls in OTFTs have also been reported.[56] Those derivatives exhibited *n*-type behavior with varied electron mobilities,

depending on the choice of central ion, S/D electrodes and surface modification layers (*p*-6p or OTS). In addition, the only data regarding GaPc-Cl as the semiconductor layer in OFETs was reported in the same article.[56] The electron μ was 0.01 $cm^2/V \cdot s$. Other properties such as types of the carriers, the carrier μ, and on/off current ratio of the thin-film transistor are listed in Table A.1 (see Appendix A). No more analysis was provided in this article.

Hamui and co-workers prepared a high-performance OFET with a μ of 36.2 $cm^2/V \cdot s$ and a V_T of 0.59 eV by employing InPc-Cl as a *p*-type semiconductor and including a bilayer gate dielectric consisting of poly(ethylene terephthalate) (PET) and indium-tin oxide (ITO).[196] Within a short potential window, the device quickly responded to an increase in the gate voltage to −5.6 V resulting in a minimum μ of 3.2 $cm^2/V \cdot s$. The gate voltage was further increased to −12 V, from which a second maximum μ of 5.9 $cm^2/V \cdot s$ was observed. The improved μ was attributed to the bilayer structure and the ability for Cl-InPc to be an effective hole carrier through the extensive π-system.

1.5.2 Group 14 phthalocyanines in OTFTs

For Group 14 main-group Pcs, their performances in OTFTs have been tabulated in Table A.2 (see Appendix A). Tetravalent MPcs with Group 14 elements are of increasing interest in the field of organic electronics due in part to the presence of two axial substituents that can be modified. Not only can these be tailored to enhance solubility, but they can also be functionalized to augment the solid-state arrangement and thin-film packing of the molecules. Furthermore, recent studies have demonstrated that $SiPcX_2$ exhibits promising *n*-type mobilities, offering an alternative to the widely employed fullerene base acceptors.[197,198]

In 2018, Melville *et al.* reported $SiPcX_2$ in OTFT application for the first time.[32] Specifically, they investigated the use of a series of $SiPcX_2$ axially functionalized with carboxylates attached to aromatic rings as active materials in OTFTs (Figure 1.14 i–iii). Encouragingly, all derivatives exhibited *n*-channel behavior and revealed the importance of the axial substituents on the thin film morphology. The authors noted that an increase in the steric bulk of the aromatic axial substituents was accompanied by a decrease in both the electron μ and I_{on}/I_{off} ratio. The same tendency was also observed with the V_T. The structures of the molecules as determined using single-crystal X-ray diffraction are shown in Figure 1.14. Notably, $SiPc(PhCOO)_2$ displays the 2D arrangement of π-π stacking pathways while $SiPc(1\text{-}NpCOO)_2$ does not, despite $SiPc(1\text{-}NpCOO)_2$ having the closest π-π distance. On the other hand, the structure of $SiPc(9\text{-}AnCOO)_2$ possesses little π-π overlap, which may explain why $SiPc(PhCOO)_2$ has the highest μ among those three derivatives. Furthermore, the performance of devices using $SiPc(PhCOO)_2$ was systematically probed through modifications to the dielectric surface treatments. It was observed when octyltrichlorosilane (OTS) and octadecyltrichlorosilane (ODTS) were employed, mobilities were enhanced, while the inverse was observed with trichloro(1H,1H,2H,2H-perfluorooctyl)silane (FOTS).

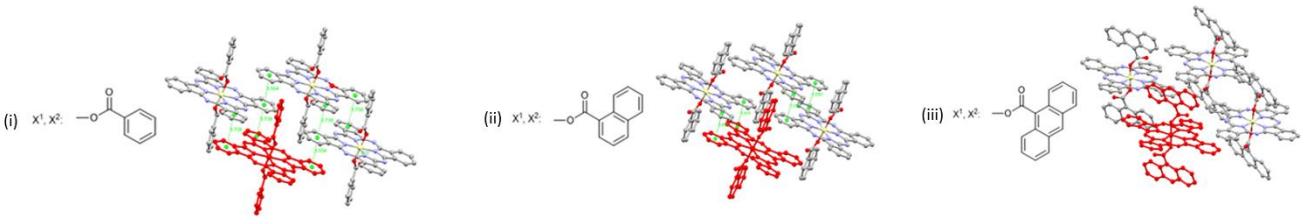

Figure 1.14 Chemical structures and solid-state arrangement of three X_2-SiPc axially substituted with carboxylates. Molecular overlap with a centroid–centroid distance <4 Å are indicated with dotted green lines. Reproduced from Ref. 35 with permission from the Royal Society of Chemistry.

Following that initial report, OTFTs were studied employing SiPcs axially functionalized with pentafluorophenoxy (SiPc$(F_5PhO)_2$), 2,4,6-trifluorophenoxy (SiPc(2,4,6-F_3PhO_2) and 3,4,5-trifluorophenoxy (SiPc(3,4,5-$F_3PhO)_2$) substituents further revealing the *n*-type behavior of SiPcs.[38] Devices based on SiPc$(F_5PhO)_2$ possessed the highest electron μ (up to 0.5 $cm^2/V{\cdot}s$), and currently holds the highest record for all *n*-type MPcs, along with the lowest V_T averaging around 12.0 V. Conversely, $SiPcCl_2$ based devices exhibited the highest V_T (up to 37 V) and relatively low μ_e. These results reveal the importance of the substituents and suggest the addition of the fluorinated phenoxy pendant groups induce π-π overlap. The authors also investigated the effect of characterization atmosphere on device performance, with all OTFTs characterized at both positive and negative V_{GS} and V_{DS} under vacuum and air conditions. As an example, Figure 1.15 shows a sample transfer curve under each condition for material SiPc$(F_5PhO)_2$. The results, listed in Table A.3 (See appendix A), reveal an interesting phenomenon of increased *p*-type charge transfer while transferring devices from vacuum to air, except $SiPcCl_2$, which did not show a significant field effect for holes under any condition. This change may be attributed to oxygen in air acting as an electron acceptor from the central metal atom, creating holes in some molecules.

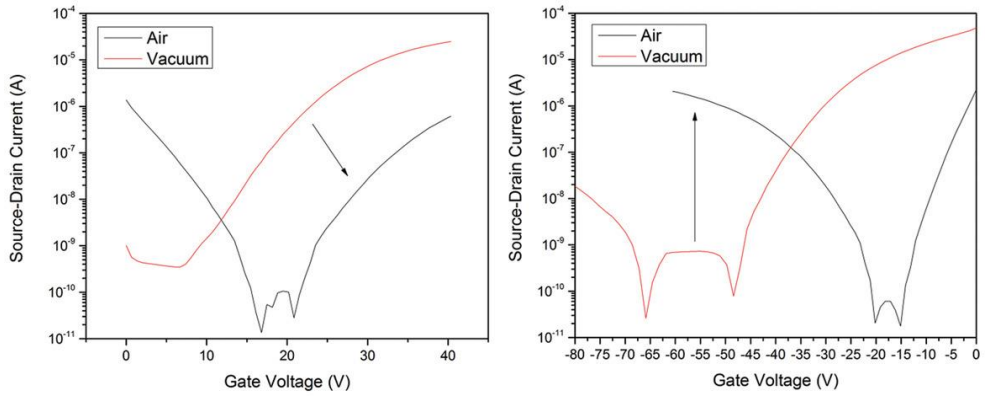

Figure 1.15 Sample transfer curves for OTFTs using SiPc$(F_5PhO)_2$ as the active layer when operated in the electron accumulation region (left) and hole accumulation region (right) and characterised either under vacuum or in air. Reproduced from Ref. 35 with permission from the Royal Society of Chemistry.

To enhance device performance and reduce the injection barrier between the organic semiconductor and contacts, Melville *et al.* have introduced either an electron dopant layer (bathocuproine, BCP) or low-work-function metals (Mn/Cr) between the high work-function electrodes (Au, Ag) and the SiPc(F_5PhO)$_2$ semiconductor layer.[34] The device structure is shown in Figure 1.16, and the saturation region properties are shown in Figure 1.17. This study reveals the presence of these interlayers reduces V_T, contact resistance and saturation region μ, while improving the linear region mobility (Table A.3, see Appendix A). The same treatment and characterization methods were also applied to their tin counterparts, namely SnPc(F_5PhO)$_2$ and SnPc(2,4,6-F_3PhO)$_2$.[34] The results of this study indicate that Mn and Cr interlayers do not strongly affect performance, while BCP can increase the off-current provided the entire organic semiconductor film is covered. These results were attributed to the larger Sn atom, which has a higher propensity for interaction with BCP than SiPc.

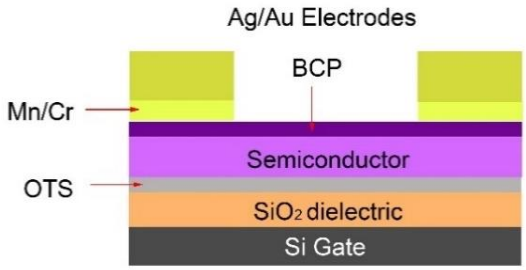

Figure 1.16 Device schematic for TC/BG OTFTs with either an electron transport (bathocuproine (BCP)) or low-work-function metal (Mn/Cr) interlayer between the main electrode (Ag/Au) and organic semiconductor. Reproduced from Ref. 35 with permission from the Royal Society of Chemistry.

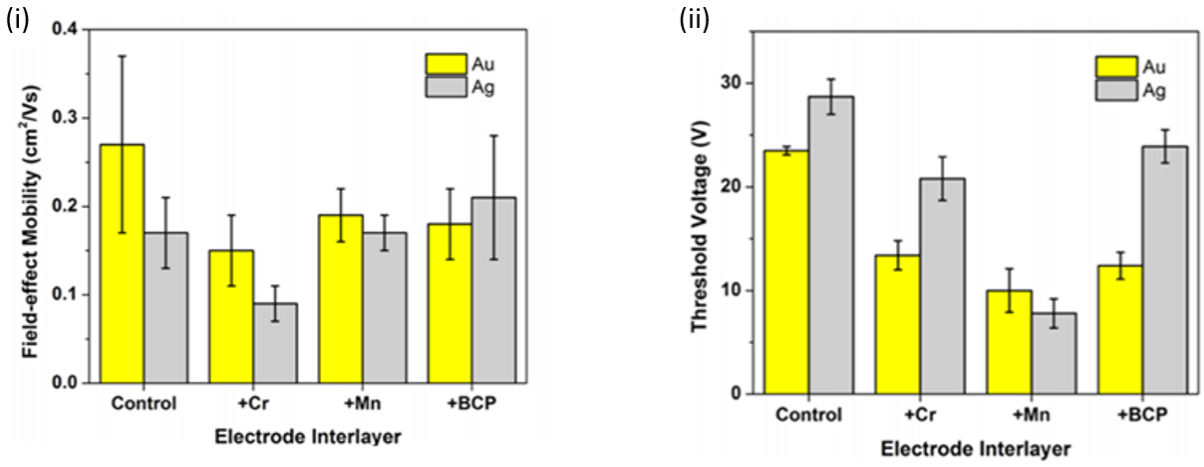

Figure 1.17 Saturation region properties for OTFTs using $SiPc(F_5PhO)_2$ as the semiconductor layer with Au and Ag electrodes and Cr, Mn, or BCP interlayers: (i) field-effect mobility and (ii) threshold voltage. Reproduced from Ref. 35 with permission from the Royal Society of Chemistry.

$SnPcX_2$s are widely used as *n*-type semiconductors due to the relatively high electronegativity of tetravalent tin,[57] and the closely π-stacked intermolecular motifs that they formed in crystals.[154] For example, Giri and co-workers reported that vacuum-deposited $SnPcCl_2$ OFETs exhibited good *n*-channel behavior with electron μ of 0.01 $cm^2/V{\cdot}s$, low V_T of 4 V, current on/off ratio of 10^4, and high operation stability with no hysteresis when tested in low vacuum condition.[52] Yan and co-workers reported a high-performance air-stable *n*-type OTFT device based on $SnPcCl_2$ deposited on a *para*-sexiphenyl modified substrate with the electron μ of 0.30 $cm^2/V{\cdot}s$ and the current on/off ratio of 10^6.[53] After storage in air for 45 days, this device still has a μ up to 0.12 $cm^2/V{\cdot}s$ which indicated its excellent stability. Song's group also fabricated another air-stable OTFT based on tin phthalocyanine oxide (SnPc=O).[57] An electron μ of 0.44 $cm^2/V{\cdot}s$ has been achieved, and it did not obviously change after storage in air for 32 days. The results reveal that incorporating appropriate electron-withdrawing groups such as chloride and oxygen into π-conjugated systems is an effective approach to design air-stable *n*-type semiconductors. The

electron mobilities of OTFT devices based on $(F)_{16}SnPcCl_2$ and $(Cl)_{16}SnPcCl_2$ were reported as well.[56] The OTFTs using *p*-6P modified substrate exhibited approximately 10 times larger μ_e than that of OTFTs using OTS modified substrate.

Transistor behavior has also been studied in divalent tin complexes, specifically SnPc. Bao and Lovinger studied the performance of devices with thin films of SnPc vacuum deposited at three temperatures (*i.e.*, 30, 125, 200°C), from which the material operated as a *p*-type semiconductor. Average electron mobilities were shown to increase from 30°C to 125°C ($7.3x10^{-5}$ to $3.4x10^{-3}$ $cm^2/V{\cdot}s$, respectively) and subsequently exhibited no field-effect when deposition temperatures reached 200 °C. Presumably, better morphological ordering and an enlargement in the size of crystals were attributed to the enhancements in mobilities up to 125°C, while the presence of large voids appears at higher temperatures.

Reports focusing on GePc derivatives in the application of OFET are less. The only report demonstrates that $GePcCl_2$ showed *p*-type results in OTFTs, achieving electron mobilities up to 0.06 and 0.09 $cm^2/V{\cdot}s$ on OTS or *p*-6P modified substrate, respectively.[56] As for PbPc, a series of devices have been explored. It is known that a parallel charge transport direction is favorable for high-performance OFETs. In the case of PbPc molecules, the highest conductivity is perpendicular to the molecular plane as shown in Figure 1.18.[54] Richter and co-workers indicated that an epitaxial-like growth mode of PbPc molecules on reconstructed GaAs(001) surfaces takes place by Raman spectroscopy, which is an important result for OFETs.[54] In addition, the relatively low bandgap of PbPc (1.2 eV) makes it a good candidate in the application of ambipolar OFETs. For instance, Yasuda *et al.*[51] fabricated OTFT devices based on PbPc semiconductor layer, and both devices with Au or Ca S/D electrodes showed typical ambipolar characteristics. In the case of Au, the field-effect electron μ was calculated to be 8.3×10^{-4} $cm^2/V{\cdot}s$ when the V_T was 31 V, while the

hole μ was calculated to be 7.1×10^{-4} $cm^2/V\cdot s$ when the V_T was −58 V. In the case of Ca, an electron μ of 1.3×10^{-3} $cm^2/V\cdot s$ (V_T = 36 V) and a hole μ of 4.7×10^{-4} $cm^2/V\cdot s$ (V_T = −60 V) were estimated from saturation currents. After annealing in the glove box for 12 h at 100 °C, the field-effect mobilities of all the devices increased for both carriers. In addition, Peng *et al.*[199] discovered the photo-induced balanced ambipolar transports in PbPc-based OFETs. As reported, PbPc semiconductor initially behaves *p*-channel unipolar in the dark due to the significantly lower energy barrier for hole injection (0.1 eV) compared to the energy barrier for electron injection (1.2 eV). However, the electron μ increased to 1.8×10^{-5} $cm^2/V\cdot s$ under illumination at 655 nm, 100 mW/cm^2, which is very close to the value of the hole μ (3.0×10^{-5} $cm^2/V\cdot s$), as the high electron injection barrier was reduced by light illumination. They attribute this to the reduction in electron potential energy from the downward bend of the HOMO and LUMO of PbPc as a consequence of photo-generated holes accumulated near the source electrode. Subsequently, this reduces the electron injection barrier at the S/D interface.[199]

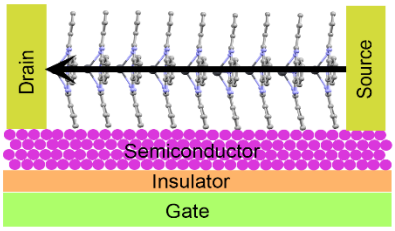

Figure 1.18 The favorable molecular orientation of PbPc in OFETs. The arrows indicate the direction of the highest electrical conductivity. Reproduced from Ref. 35 with permission from the Royal Society of Chemistry.

OFETs based on PbPc derivatives were also reported to be used as non-volatile organic memory device with continuous write-read-erase-read switching performance by Mukherjee *et al.*[200] The device exhibited *p*-channel behavior. The introduction of hexyl- substituents in bay

positions, as in (n-C_6H_{13})$_8$PbPc, efficiently improved the solubility of the material, enabling its ready formulation as thin film by spin-coating. Reports focusing on GePc derivatives in the application of OFET are less. The only report demonstrates that $GePcCl_2$ showed *p*-type results in OTFTs, achieving electron mobilities up to 0.06 and 0.09 $cm^2/V{\cdot}s$ on OTS or *p*-6P modified substrate, respectively.[56]

1.5.3 Group 15 and 16 phthalocyanines in OTFTs

The fabrication of OTFTs utilizing Group 15 phthalocyanines as organic semiconductors has not been explored. As for Group 16 phthalocyanines, no complexes have been reported in the literature to the best of our knowledge. Thus, there remains an untapped potential to explore the synthesis of MPcs bearing these elements and their integration.

1.6 Transition metal phthalocyanines

There is a wealth of literature involving Pcs containing transition metals including scandium,[201–204] yttrium,[205–214] lutetium,[207] lanthanoid,[206,207] titanium,[215–222] zirconium,[223–231] hafrium,[225–230] vanadium,[183,232–236] niobium,[11,237–239] tantalum,[240,241] chromium,[242–245] molybdenum,[231,246–251] tungsten,[246,247] manganese,[222,252–257] technetium,[258] rhenium,[246,247,258–260] iron,[220,242,257,261–263] ruthenium,[264–267] osmium,[268–270] cobalt,[220,242,255,257,271–274] rhhodium,[275] iridium,[275–277] nickel,[257,262,278] palladium,[275,279,280] platium,[275,281–284] copper,[220,285–287] silver,[288,289] gold,[290] zinc,[242,257,281,291–295] cadmium,[291,296–298] and mercury.[291,299] However, as this thesis mostly concerns main-group Pcs (especially SiPcs), an exhaustive review of the literature on transition metal Pcs will not be included here, only key contributions related to this thesis will be discussed.

The synergistic effects between many transition metal ions and the unsubstituted Pc framework have led to high hole mobilities observed for MPcs, thereby rendering these ideal

building blocks as intrinsic *p*-type organic semiconductors in OFETs. Notably, field-effect mobilities for divalent copper[300] and zinc[301] complexes (MPc; M = Cu and Zn) have been achieved with values around 10^{-1} $cm^2/V \cdot s$, while those for tetravalent titanium[302] and vanadium oxides[303] (MPc=O; M = V and Ti) have been reported in the range of 1–10 $cm^2/V \cdot s$; some of the highest for *p*-type organic semiconductors within this class of molecules. As for *n*-type organic semiconductors, which are of particular importance to the objectives of this thesis, the portfolio of MPcs exhibiting this type of behavior with transition metal ions is substantially less. In order to activate charge injection, transition metal complexes generally require the introduction of strong electron-withdrawing groups along the Pc framework to drop the energy level of the LUMO.[31] For example, the perfluorination of copper phthalocyanine (*i.e.*, F_{16}CuPc) reverts the nature of the unsubstituted hole carrier to afford the best *n*-type field-effect mobility reported for transition metal Pcs of 0.11 $cm^2/V \cdot s$.[301]

While these field-effect mobilities are comparable to devices utilizing benchmark organic semiconductors like pentacene, improvements on overall device performance for these systems are limited from a molecular design approach. A caveat amongst many MPcs with divalent transition metal centers is, for the most part, the lack of tuneable substituents bound to the central ion, which can be used to manipulate the solid-state packing in particular. In general, divalent MPcs tend to assemble in edge-to-face herringbone motifs, reducing π-orbital overlap and consequentially leading to moderate charge mobilities. Conversely, when these substituents are present, the axial ligands can direct MPcs into face-to-face π-stacking assemblies, which in turn can strengthen pathways for charge transport.[31,32,53,304,305]

1.7 Outline of the thesis

The underlying motivation for this work was to design and synthesize a family of novel phthalocyanine derivatives to be employed as the semiconducting active layer in organic field-effect transistors. In particular, the phthalocyanine backbone was tailored to favor *n*-channel property, as predicted by DFT calculations (See **Chapter 2**). As such, the first chapter provided an overview of the synthesis of main-group phthalocyanines, with emphasis on their applications in organic field-effect transistors. The subsequent chapters of this thesis will describe the work we have carried out on specifically functionalized derivatives of phthalocyanine macrocycles.

The second chapter covers the synthesis and characterization of a series of silicon tetra-2,3-pyrazinoporphyrazine complexes (**SiPzs**, Figure 1.19). In this structure, the four benzene units of the phthalocyanine framework are substituted by pyrazine units. These rarely reported azaphthalocyanines were functionalized with different functional groups in the axial positions, and the influence of the pyrazine rings and the axial substituents on the optoelectronic properties of silicon tetra-2,3-pyrazinoporphyrazines (**SiPzs**) was investigated.

The third chapter focuses on the preparation of silicon tetra(*tert*-butyl)-2,3-naphthalocyanine complexes (**(^{t}Bu)$_4$SiNPc**, Figure 1.19). The optical and electrochemical properties of axially substituted **(^{t}Bu)$_4$SiNPc**, and the influence of the peripheral substitution and extended degree of conjugation were investigated. Although the fourth chapter introduces the synthesis and characterization of selected metal-containing tetra-2,3-pyrazinoporphyrazines (**MPzs**, Figure 1.19), challenges faced during purification limited further exploration of this series of complexes. Finally, the last chapter of the thesis outlines the conclusions drawn from this work and future directions for furthering this research.

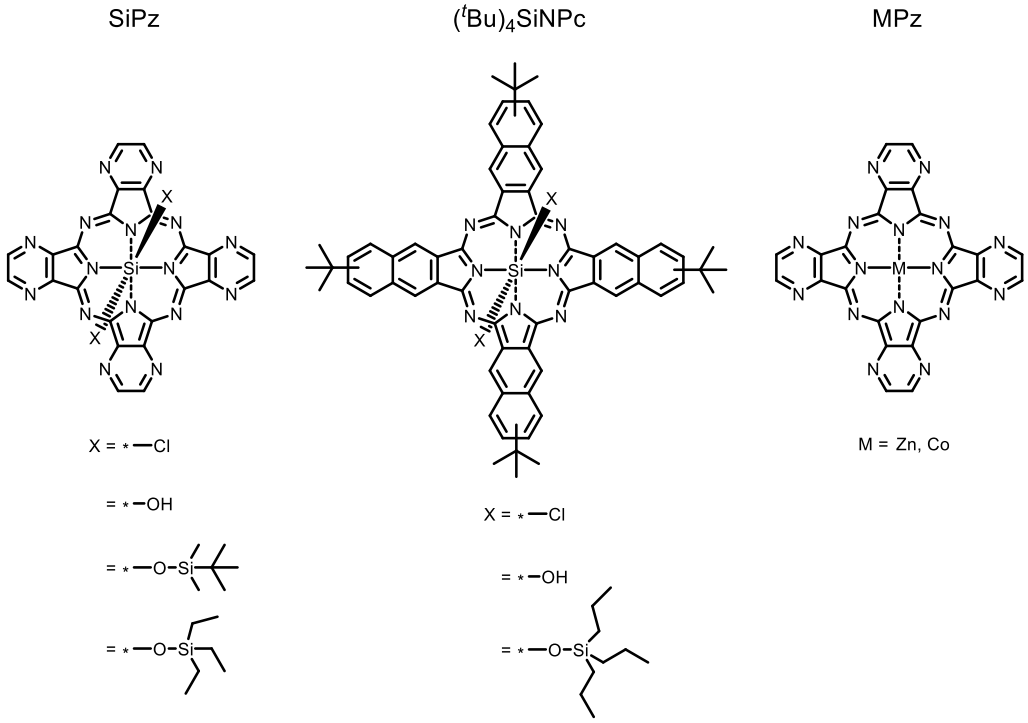

Figure 1.19 Chemical structures of **SiPz**, **(^{t}Bu)$_4$SiNPc** and **MPz** which were involved in this thesis.

Chapter 2 Silicon Tetra-2,3-pyrazinoporphyrazine Complexes (SiPz)

2.1 Introduction

Azaphthalocyanines, the heterocyclic aza-analogs of the phthalocyanine macrocycle, have been known since 1937 and were intensively studied especially in the last fifteen years.[306] The growing interest in azaphthalocyanines is connected with their potential practical applications in different fields such as photodynamic therapy,[307–310] plurimodal cancer therapy[311–314] and as active catalysts in redox processes.[315–317] Similar to phthalocyanines, the structure of azaphthalocyanines can be achieved by substitution of CH groups within the four benzene units of the phthalocyanine (Pc) framework with nitrogen atoms. The introduction of two nitrogen atoms into the equivalent 1,4-positions of the Pc benzene moieties leads to tetra-2,3-pyrazinoporphyrazine (Pz; Figure 2.1). In comparison to phthalocyanines, the eight additional nitrogen atoms in Pzs induce large electronic effects on the structure. Orbitals with large orbital coefficients at the positions of the nitrogen atoms are lower in energy compared to the corresponding phthalocyanine orbitals; thus, tetrapyrazinoporphyrazines are less 'electron-rich' than their phthalocyanine counterparts.[318]

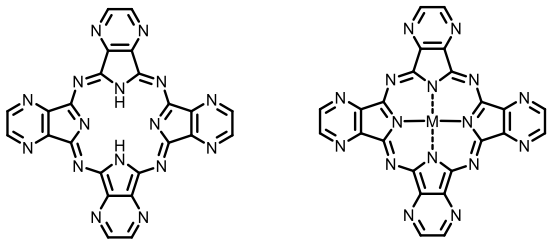

Figure 2.1 Structure of metal-free tetra-2,3-pyrazinoporphyrazine (H_2Pz) and metal-containing tetra-2,3-pyrazinoporphyrazine (MPz).

While unsubstituted Pzs exhibit very low solubility in organic solvents due to their strong π-π interactions (*i.e.*, molecular stacking), this gives rise to strong intermolecular interactions

between neighboring macrocycles.[319] As such, Pzs tend to aggregate in solution, which is usually depicted as a coplanar association of rings progressing from monomer to dimer and higher-order complexes.[182] An efficient method to improve solubility relies on the use of tri- or tetravalent metal or metalloid ions incorporated into the core of the Pz macrocycle, which provides one or two additional synthetic handles on the axial positions of the molecules to fine-tune the properties of the material. The attachment of different functional groups helps to reduce the aggregation of the molecule, thereby enhance their solubility.

In this chapter, silicon was selected as the central atom of the Pzs. Silicon phthalocyanines are of interest due to the unusual hexacoordinated silicon^{IV} core and robust chemical stability of the Si–N bonds. The first silicon-centered Pc was reported by Kenney and co-workers in 1960.[147] In their work, dichlorosilicon phthalocyanine ($SiPcCl_2$) was synthesized *via* the template reaction of phthalonitrile with either $SiCl_4$ or hexachlorodisiloxane. In the following years, more convenient approaches to $SiPcCl_2$ were rapidly developed, utilizing both *o*-cyanobenzamide and 1,3-diiminoisoindoline in place of the phthalonitrile.[149] The labile Si–Cl bond in $SiPcCl_2$ allows easy ligand substitution at the central metal atom. For example, the two Cl groups can be hydrolyzed under strongly acidic or basic conditions, resulting in $SiPc(OH)_2$.[150,158,159] As well, a series of symmetrically and asymmetrically axially substituted SiPc derivatives have been developed by nucleophilic substitution over the years. [25,148,153,155,159,161] A key advantage to employing **SiPzs** over divalent MPzs is the ability to modify the axial substituents, which provides a facile avenue for functionalization.[152] Incorporating bulky axial substituents will not only enhance molecular solubility by preventing the aggregation of Pc molecules in solutions, but will also augment the solid-state arrangement and thin-film packing of the molecules. The HOMO/LUMO energy levels for 4 silicon tetra-2,3-pyrazinoporphyrazine derivatives were computed by our group *via* DFT

calculations. The results are shown in Table 2.1, which suggest that tailoring the Pc backbone *via* the inclusion of electron-withdrawing substituents may lead to semiconductors that favor *n*-type transport for the application of organic field-effect transistors.

Table 2.1 Predicted HOMO/LUMO energy levels of $SiPzF_2$, $SiPzCl_2$, F_8SiPzF_2 and $F_8SiPzCl_2$. All calculations were performed at the DFT level using the B3LYP functional, as contained in the Gaussian 09W suite of programs.[320] Molecular geometries were optimized using the 6-311+G(2d, p) basis set with D_{4h} symmetry constraints.

Compound	Molecular structure	HOMO (eV)	LUMO (eV)
Silicon tetra-2,3-pyrazinoporphyrazine difluoride ($SiPzF_2$)	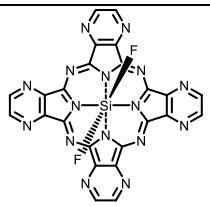	−6.301	−3.956
Silicon tetra-2,3-pyrazinoporphyrazine dichloride ($SiPzCl_2$)	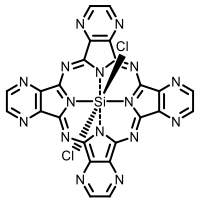	−6.382	−4.067
Octafluorotetra-2,3-pyrazinoporphyrazine difluoride (F_8SiPzF_2)	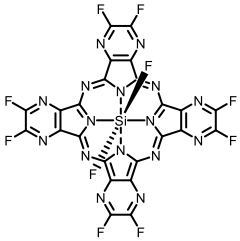	−6.973	−4.564
Octafluorotetra-2,3-pyrazinoporphyrazine dichloride ($F_8SiPzCl_2$)	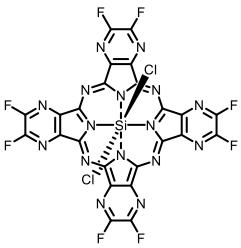	−7.046	−4.067

In this chapter, a series of silicon tetra-2,3-pyrazinoporphyrazine complexes were investigated. The synthetic avenues were explored to prepare silicon tetra-2,3-pyrazinoporphyrazine dichloride (**SiPzCl$_2$**), bis(hydroxy) silicon tetra-2,3-pyrazinoporphyrazine (**SiPz(OH)$_2$**), bis(*tert*-butyldimethylsiloxy) silicon tetra-2,3-pyrazinoporphyrazine (**SiPz(^{t}BuMe$_2$OSi)$_2$**), and bis(tri-*n*-ethylsiloxy) silicon tetra-2,3-pyrazinoporphyrazine (**SiPz(Et$_3$OSi)$_2$**). Nuclear magnetic resonance spectroscopy (NMR), Infrared spectroscopy (IR), UV-vis Spectroscopy (UV-vis), Mass Spectroscopy (MS), and Cyclic Voltammetry (CV) were employed to characterize the compounds.

2.2 Results and discussion

2.2.1 Synthesis of silicon tetra-2,3-pyrazinoporphyrazine dichloride (SiPzCl$_2$).

Preparation of **SiPzCl$_2$** was attempted *via* various synthetic routes as outlined in Scheme 2.1. As reported previously, silicon phthalocyanines can be effectively prepared starting from diiminoisoindolines.[151,321,322] Therefore, the synthesis of 5-imino-5*H*-pyrrolo[3,4-*b*]pyrazin-7-amine (**Pz-DIII**) was first attempted (**Route A**).[152] The traditional synthetic route to isolate DIII involves a constant flow of ammonia gas bubbling through a refluxing phthalonitrile solution in sodium methoxide.[323,324] In order to avoid these harsh reaction conditions, an alternative preparative approach that employs lithium bis(trimethylsilyl)amide etherate (LiN(TMS)$_2$·Et$_2$O) as a nucleophilic source of nitrogen to generate the DIII precursor was applied in this work.[152] To be more specific, a solution of 2,3-dicyanopyrazine in anhydrous toluene was added to LiN(TMS)$_2$·Et$_2$O, resulting in a color change of the reaction mixture from clear to black. This treatment led to the formation of the anionic intermediate **2-1**,[152] as shown in Scheme 2.1. After 3 hours, chlorotrimethylsilane (TMSCl) was added, and the reaction mixture was kept refluxing for 24 hours. Quenching the intermediate **2-1** with TMSCl afforded the silylated **Pz-DIII** intermediate,

while the LiCl by-product precipitated out of solution, which was removed through hot filtration of the mixture. The solvent of the filtrate was then concentrated by rotary evaporation before passing through a silica plug to remove the TMS protecting groups, replacing them with hydrogen atoms. Further purification was achieved *via* trituration of the resulting solution with ether, affording **Pz-DIII** as a brown powder. The NMR, FT-IR and EI-MS characterizations of **Pz-DIII** are consistent with literature data, as shown in Figure 2.2.[323] As shown in Figure 2.2-i, the two H atoms on the pyrazino ring are shown as a singlet at 8.77 ppm, while the NH signal was missing due to the NH exchange with trace amounts of water in the sample. The EI-MS data also confirmed the mass peak at *m*/*z* 147.1. Subsequently, attempted synthesis of **SiPzCl$_2$** starting from **Pz-DIII** in the presence of $SiCl_4$, using quinoline as solvent only resulted in a highly insoluble black solid, which was completely insoluble in common organic solvents. As such, none of the characterization technique employed were successful in identifying the dark solid isolated. Further reaction of this crude material with CsOH, followed by treatment with trialkylsilyl triflate in an attempt to effect axial substitution, was unsuccessful. Thus, this route to isolate **SiPzCl$_2$** was no longer pursued.

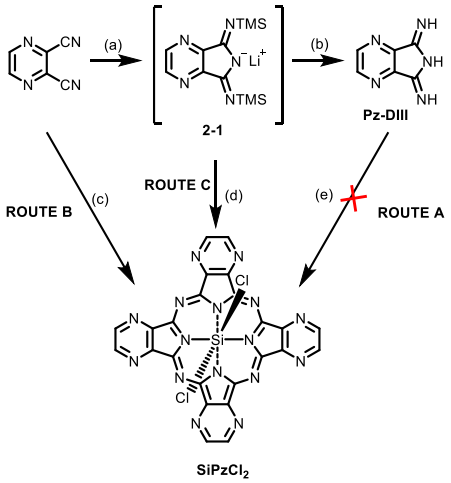

Scheme 2.1 Attempted synthetic routes toward the preparation of **SiPzCl$_2$**. Reagents and conditions: (a) $LiN(TMS)_2 \cdot Et_2O$, Toluene or Tetralin, RT, 2 − 3 h; (b) (i) TMSCl, Reflux, 24 h, (ii) Silica gel; (c) $SiCl_4$, Urea, Tri-*n*-butylamine, Quinoline, 160 °C, 3 h; (d) $SiCl_4$, 170 °C, 4 h; (e) $SiCl_4$, Quinoline, 200 °C, 2 h.

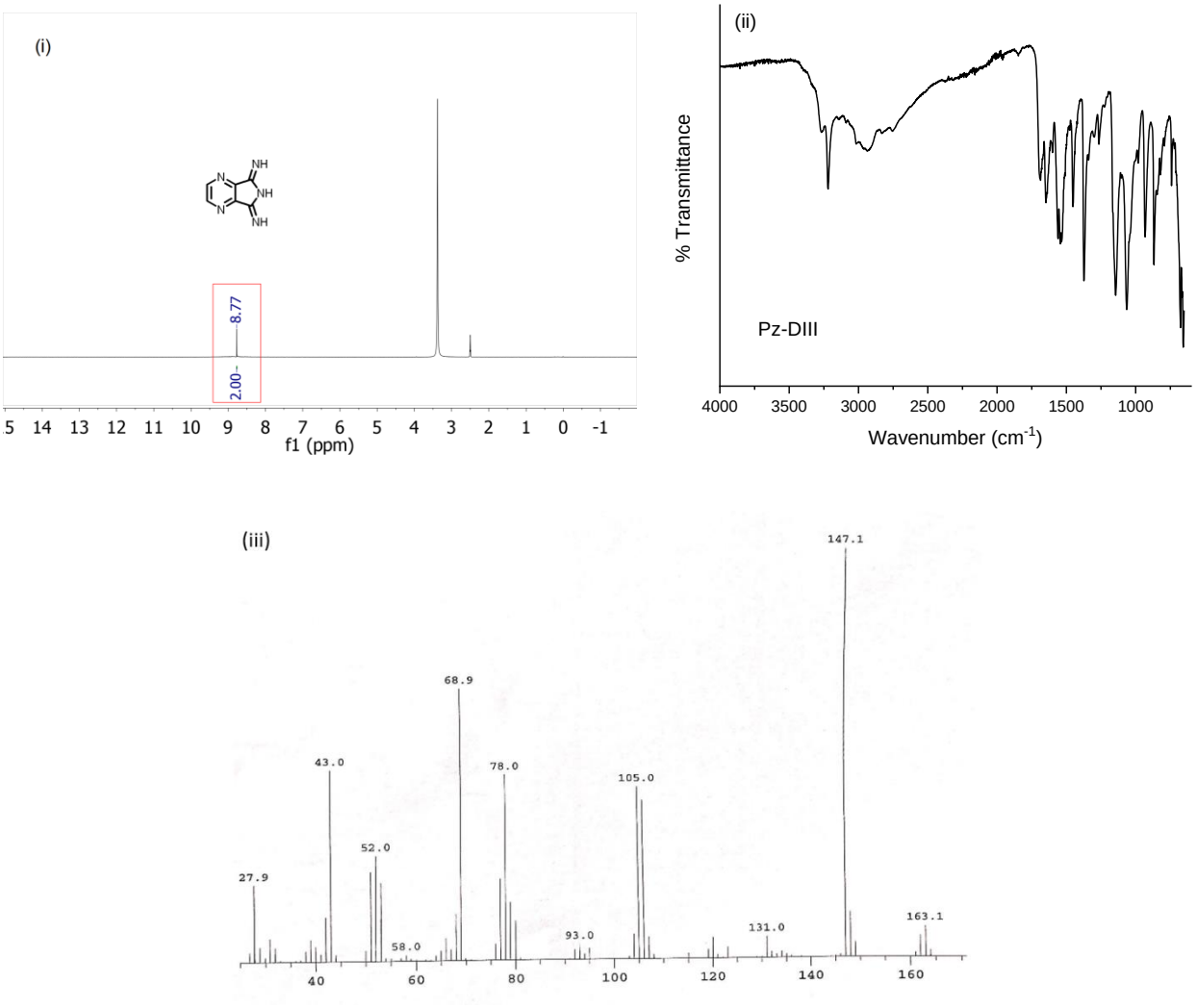

Figure 2.2 NMR (i, DMSO-d_6, 8.77 (s, 2H-pyrazino),) FTIR (ii) and EI-MS (iii, *m*/*z* 147.1) spectra of **Pz-DIII**.

Since repeated attempts to generate **SiPzCl$_2$** were unsuccessful when starting with **Pz-DIII**, focus was shifted towards *o*-dinitriles, which have been shown to be effective starting materials for the synthesis of **SiPzCl$_2$.**[325] To that end, 2,3-dicyanopyrazine was condensed with $SiCl_4$ in the presence of urea using quinoline as a solvent and twofold excess of tri-*n*-butylamine to account for HCl that evolves during the reaction (**Route B**). In comparison with 1,2-benzenedicarbonitrile, the additional N atoms on 2,3-dicyanopyrazine increase the donating ability of the molecule,

allowing it to compensate for the weaker acceptor Si, thereby making the reaction feasible. The identity of the resulting blue **SiPzCl$_2$** was confirmed by Mass Spectroscopy and Infrared Spectroscopy (Figure 2.3). IR spectra of **SiPzCl$_2$** features a characteristic band at ~460 cm^{-1} (Si–Cl stretch). EI-MS data also confirmed the mass peak at *m*/*z* 619.63. Given the low solubility of this compound, ^{1}H and ^{13}C NMR spectroscopic analyses were not possible. Recrystallization was impossible due to its poor solubility in most organic solvents and, unfortunately, sublimation attempts were also unsuccessful in purifying the crude material. More specifically, sublimation either at a pressure of 10^{-5} torr or with carbon dioxide as the carrier gas was insufficient to sublime the material even at temperatures up to 400 °C. Based on IR of the residue after sublimation attempts, the crude **SiPzCl$_2$** decomposed under these conditions. Nonetheless, the crude material was of sufficient purity to be used as an intermediate for the preparation of the dihydroxysilicon complexes **SiPz(OH)$_2$** (See Section 2.2.2).

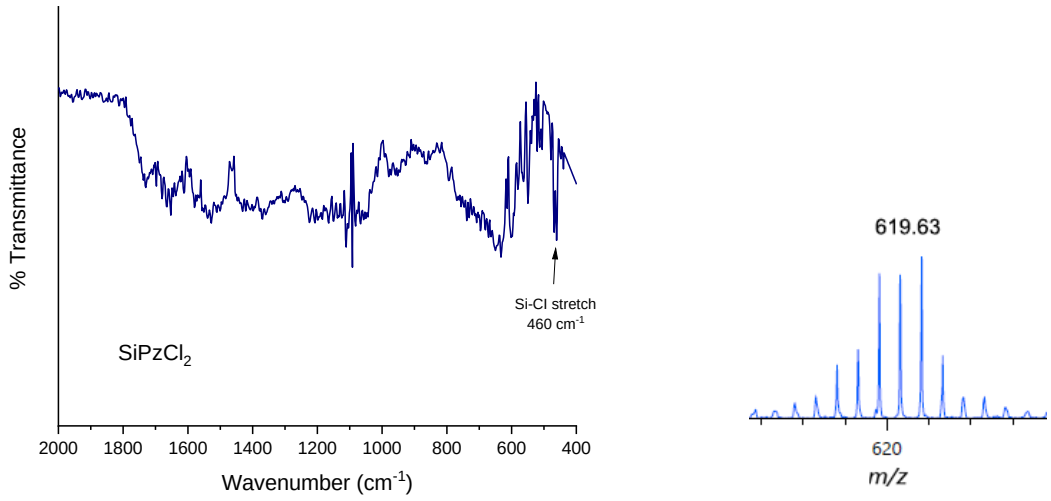

Figure 2.3 FTIR spectrum and EI-MS (*m*/*z* 619.63) spectrum of **SiPzCl$_2$**.

Another synthetic route to isolate **SiPzCl$_2$** (**Route C**) was explored by adding LiN(TMS)$_2$·Et$_2$O into the solution of 2,3-dicyanopyrazine in tetralin at room temperature to afford

the anionic intermediate **2-1**. Silicon tetrachloride was subsequently added dropwise to the reaction mixture, then left to stir at 170 °C for 4 hours. This route also resulted in the dark blue insoluble powder, with a yield of up to 90%. Both the MS and IR results indicated that the product is **$SiPzCl_2$**. Attempts at purification include washing the product with toluene, acetone and EtOH. The crude material was of sufficient purity for the synthesis of **$SiPz(OH)_2$** (See section 2.2.2). The reaction is quantitative within a few hours.

2.2.2 Synthesis of bis(trialkylsiloxy) silicon tetra-2,3-pyrazinoporphyrazine ($SiPz(^tBuMe_2OSi)_2$, $SiPz(Et_3OSi)_2$).

Given **$SiPzCl_2$** tends to aggregate in solution, it is fairly insoluble in most common organic solvents. This lack of solubility can be avoided *via* silylation of the axial positions (*i.e.*, replacement of -Cl with $-OSiR_3$). In general, silylated SiPcs tend to be quite soluble in most common organic solvents, and they can be purified easily by column chromatography and characterized spectroscopically. Here, the bulky siloxy groups were specifically introduced to prevent the formation of H-aggregates. Furthermore, bulky substituents could reduce interfacial recombination.[326] The synthesis of silyl substituted SiPcs usually follows a two-step route: first, the dichloro SiPc is hydrolyzed under an acidic or basic condition; following this, the precursor dihydroxy SiPc is functionalized by silyl groups *via* nucleophilic substitution. A commonly used synthetic route for silylation of the $SiPc(OH)_2$ is its reaction with chlorosilane,[159] or silyl triflates,[318] both of which are commercially available.

To that end, the synthetic route to isolate bis(trialkylsiloxy) silicon tetra-2,3-pyrazinoporphyrazine is shown in Scheme 2.2. Initially, **$SiPzCl_2$** was hydrolyzed under basic conditions *via* cesium hydroxide,[159] resulting in a black insoluble powder. Note that the solubility of **$SiPz(OH)_2$** in organic solvents is much lower than the corresponding dichloro analogs making

characterization difficult. For example **SiPz(OH)$_2$** is barely soluble in DMSO, thereby NMR spectroscopic analysis was not possible and characterization was achieved through IR spectroscopy. The IR spectra of **SiPz(OH)$_2$** features absorption bands at 3455 cm^{-1} (O–H) and 862 cm^{-1} (Si–O).

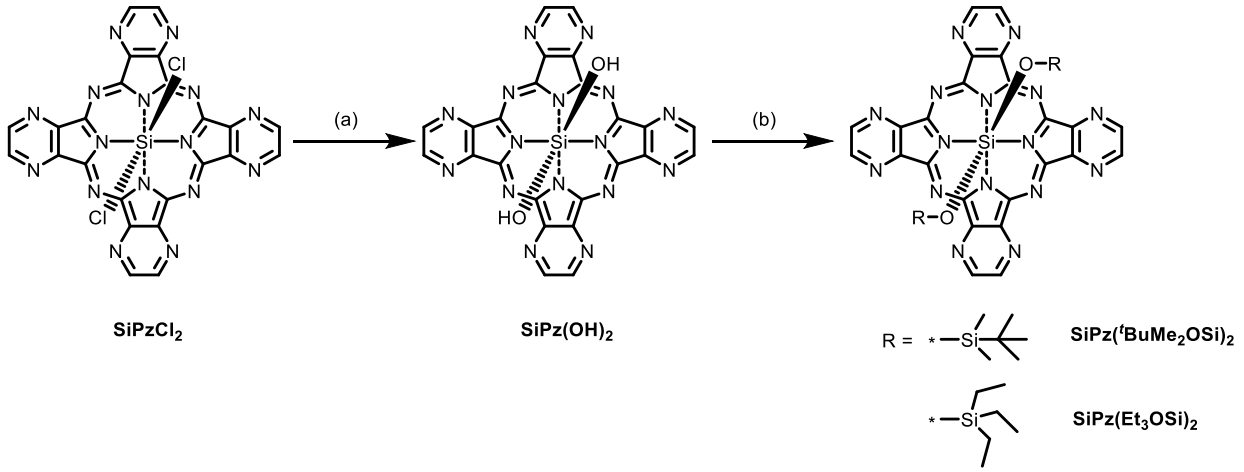

Scheme 2.2 Synthetic routes toward the preparation of **SiPz(*t*BuMe$_2$OSi)$_2$** and **SiPz(Et$_3$OSi)$_2$**. (a) CsOH (50 wt% in water), DMF, 120 °C, 4 h; (b) *tert*-butyldimethylsilyl trifluoromethanesulfonate or triethylsilyl trifluoromethanesulfonate, Pyridine, DCM, RT, 48 h.

Although hydroxy-substituted silicon tetrapyrazinoporphyrazine is fairly insoluble, it is quite reactive at the axial hydroxy positions, thus silylation of **SiPz(OH)$_2$** was performed following the methodology of Hanack *et al*.[318] The reaction of **SiPz(OH)$_2$** with commercially available silyl triflates R$_3$SiOTf in dichloromethane in the presence of pyridine at room temperature afforded the bis-silyloxy derivatives bis(*tert*-butyldimethylsiloxy) silicon tetra-2,3-pyrazinoporphyrazine (**SiPz(*t*BuMe$_2$OSi)$_2$**) and bis(tri-*n*-ethylsiloxy) silicon tetra-2,3-pyrazinoporphyrazine (**SiPz(Et$_3$OSi)$_2$**), which are soluble in most common organic solvents. The improved solubility is attributed to the substitution of the central silicon by two alkylsiloxy substituents, which inhibits aggregation. The compounds were purified by column chromatography on silica gel using

MeOH/chloroform as the eluent. Attempted sublimation was tried either at a pressure of 10^{-5} torr, or with carbon dioxide as the carrier gas. Unfortunately, sublimation was not observed even as the temperature was increased up to 400 °C and, upon the investigation of the resulting residue following sublimation attempts, the crude material decomposed at these temperatures. Note that this reaction works better in the silylation of Pzs compared to the conventional silylation procedure using chlorosilanes in refluxing pyridine. That is because the silyl triflate is more reactive since triflate is a better leaving group compared to Cl.[327] The reaction of **SiPz(OH)$_2$** with chlorosilane in pyridine only led to a faint color change of the liquid of the reaction mixture from colorless (most of the reagent did not dissolve in pyridine) to light blue, and the yield is to low to collect the product.

The NMR results of **SiPz(^{t}BuMe$_2$OSi)$_2$** and **SiPz(Et$_3$OSi)$_2$** are shown in Figure 2.4. Although the material is not pure, the NMR indicated that they were successfully synthesized. The positions of the ^{1}H-NMR resonances of **SiPz(^{t}BuMe$_2$OSi)$_2$** and **SiPz(Et$_3$OSi)$_2$** in $CDCl_3$ solution are clearly influenced by the strong ring current of the macrocycle. Due to the magnetic anisotropy of the aromatic macrocycle, protons in the axial positions are strongly shielded and therefore shifted upfield, while the aromatic protons (8H-pyrazino) situated in the plane of the macrocycle are shifted downfield.[328] Protons of the aliphatic chains are significantly shifted to lower field, depending on their distance from the macrocycle, and appear well separated from each other in the spectra. MALDI-TOF data also confirmed the mass peak at *m*/*z* 811 as well as containing minor peaks from loss of one (*m*/*z* 679) or two (*m*/*z* 548) axial alkylsiloxy groups (Figure 2.5).

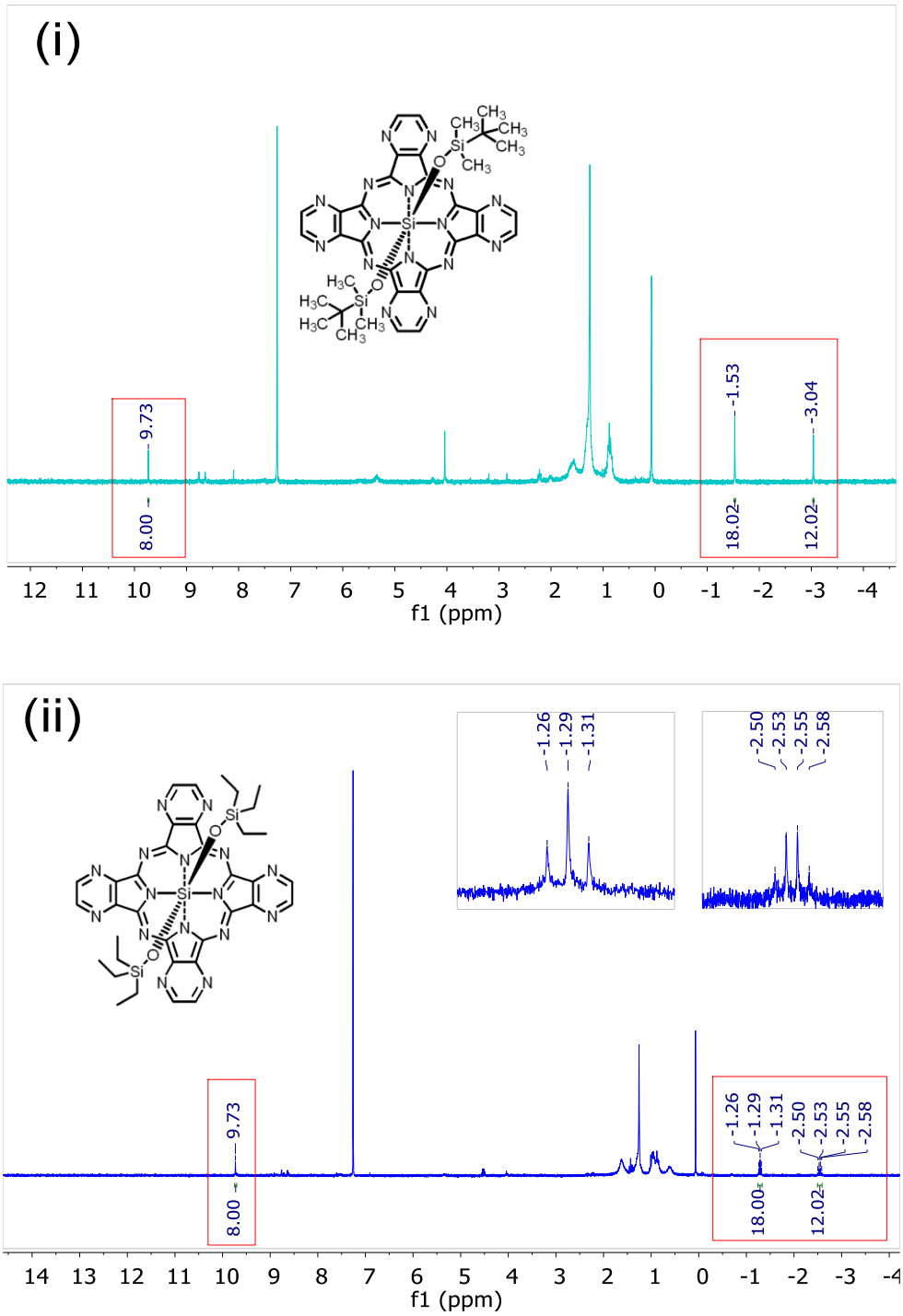

Figure 2.4 ^{1}H NMR spectrum of (i) **SiPz(^{t}BuMe$_2$OSi)$_2$** and (ii) **SiPz(Et$_3$OSi)$_2$** in $CDCl_3$. (i) 9.73 (s. 8H-pyrazino), -1.53 (s, 18H-^{t}Bu), -3.04 (s, 12H-dimethyl). (ii) 9.73 (s. 8H-pyrazino), -1.29 (t, 18H-CH_3), -2.54 (q, 12H-α-CH_2).

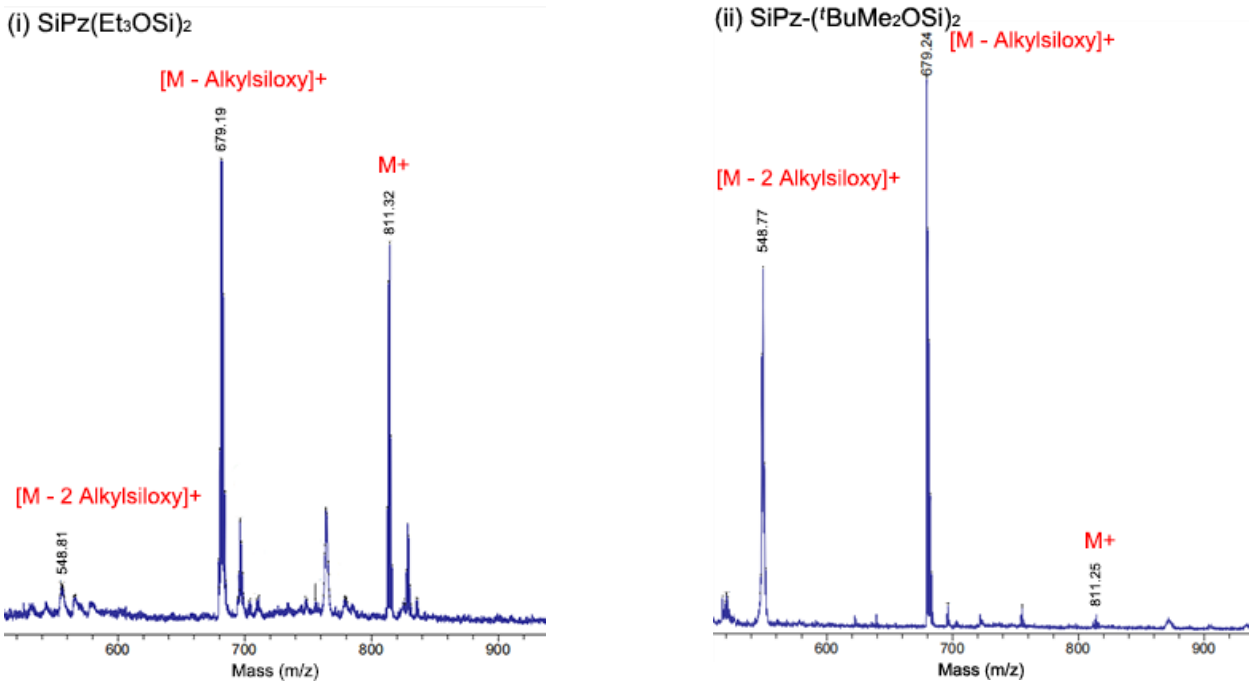

Figure 2.5 MALDI-MS spectrum of (i) **SiPz(Et$_3$OSi)$_2$** (*m/z* 811.32) and (ii) **SiPz(^{t}BuMe$_2$OSi)$_2$** (*m/z* 811.25).

2.2.3 Optical and electrochemical studies

UV-vis absorption is a key technique in probing the properties of Pc derivatives, as the spectral shape of an absorption spectrum is determined by the molecular and electronic structures of the compounds.[329] Due to the special shape of the absorption curve of Pc complexes, UV-vis spectroscopy has become a useful characterization technique that can effectively identify the formation of Pc skeletons. In general, Pc frameworks possess two types of energy bands attributed to a few allowed π-π* transitions: the *B*-band (γ or Soret band) near 300 − 400 nm and *Q*-band (α band in porphyrin) at ca. 600 − 800 nm. In metal-centered Pcs, typically one sharp intense absorption peak in the *Q*-band is observed, which can be assigned to the first π-π* transition of the phthalocyanine macrocycle.[330] In contrast, in the absorption spectra of free center phthalocyanines, this band becomes split into two distinct peaks, denoted Q_x and Q_y, as shown by the example

presented in Figure 2.6.[331] This splitting can be attributed to the removal of the metal ion and its subsequent replacement by two central hydrogen atoms, causing a change in the overall symmetry of the molecule from D_{4h} to D_{2h}.[332] The shoulders at the *Q*-band are likely of vibronic origin.[150]

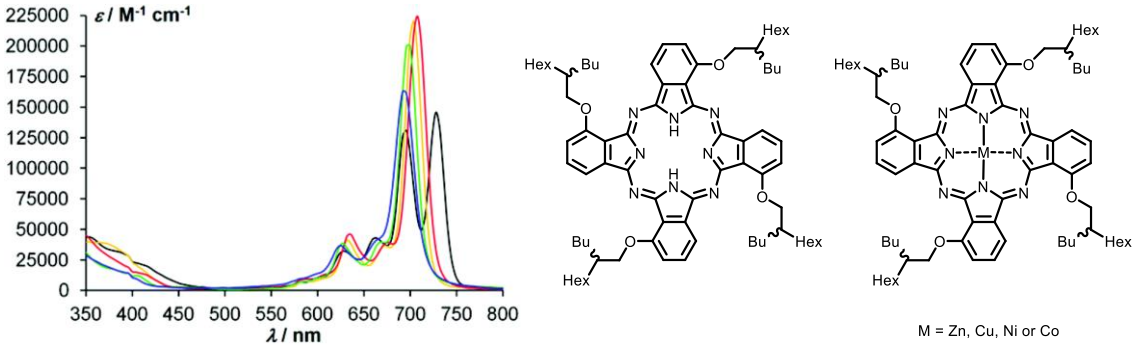

Figure 2.6 Absorption spectra (5 μM in $CHCl_3$) of metal-free 1,8,15,22-tetraalkoxy-phthalocyanine (black) and of the corresponding metal(II) phthalocyaninates (Zn-yellow, Cu-red, Ni-green and Co-blue). The molecular structures are shown on the right. Reproduced from Ref. 333 with permission from the Royal Society of Chemistry.

Apart from the solvatochromic effect that causes the redshift of Pc and similar macrocycles independence on increasing refractive index of the solvent and can be easily characterized by "polarization redshift", the *Q*-band position may be influenced by several structural factors.[334] For example, the central atom/ion may influence the *Q*-band position. As the electronegativity of the central atom/ion decreases, the *Q*-band usually shifts bathochromically (*i.e.*, redshift). Lower electronegativity causes a shift of charge on the metal onto the Pc ring, which results in an increase in energy of the $a_{2u}(\pi)$ orbital.[329] The *Q*-band position also depends on the atom(s) by which the peripheral chain is attached to the core of the Pc. Aliphatic carbon as the first atom of a chain almost does not contribute to a shift and Pc derivatives modified with such substitutions absorb at the same wavelength as unsubstituted Pcs. Heteroatoms tend to only influence the *Q*-band when directly attached to the macrocycle since only then can they contribute to the conjugation with

their free electron pairs (*i.e.*, auxochromes). For example, oxygen causes a blue shift of the *Q*-band compared to the unsubstituted or carbon substituted Pcs. In contrast, both sulfur and nitrogen directly bound to the Pc framework shift the absorption spectrum bathochromically. Carbonyl groups of, for example, an ester may participate in a conjugated system and shift the spectrum significantly to higher wavelengths. Peripheral aryl substituents may also partially conjugate with the aromatic π-system of the Pc, even if they are partially rotated out of the plane of the macrocycle.[335] On the other hand, axial substitution shows little to no influence on the optoelectronic properties of Pcs.

In tetrapyrazinoporphyrazines, the isosteric substitution of CH groups in the Pc macrocycle for nitrogen atoms does not change the molecular symmetry. In other words, the orbital scheme of the SiPcs in principle should not be changed. MOs with large orbital coefficients at the positions of the electronegative nitrogen atoms will be lowered energetically; thus, Pzs are less 'electron-rich' than the corresponding Pcs, thereby causing a significant hypsochromic shift of the *Q*-band position in the range of 40 − 60 nm.[318, 334] For this reason, **SiPz** derivatives usually show an intense red fluorescence after irradiation with light (Figure 2.7).

Figure 2.7 Solution of **SiPz(Et$_3$OSi)$_2$** in DCM under visible light (left) and irradiation with 254 nm UV light (right).

As shown in Figure 2.8, the absorption profile of **SiPzCl$_2$** and the two axially substituted derivatives show intense absorption peaks near 620 − 635 nm and 337 nm, which can be assigned as *Q*-band and *B*-band π-π* transitions of the macrocycle, respectively. Based on the UV-vis spectra, the bandgap of **SiPz(**^{t}**BuMe$_2$OSi)$_2$** and **SiPz(Et$_3$OSi)$_2$** can be calculated by the following equation:

$$E_{gap} = \frac{hc}{\lambda} \quad \textbf{(2-1)}$$

where h = planks constant, c = speed of light, and λ = the onset wavelength of absorption. Both **SiPz(**^{t}**BuMe$_2$OSi)$_2$** and **SiPz(Et$_3$OSi)$_2$** show a bandgap of 1.96 eV.

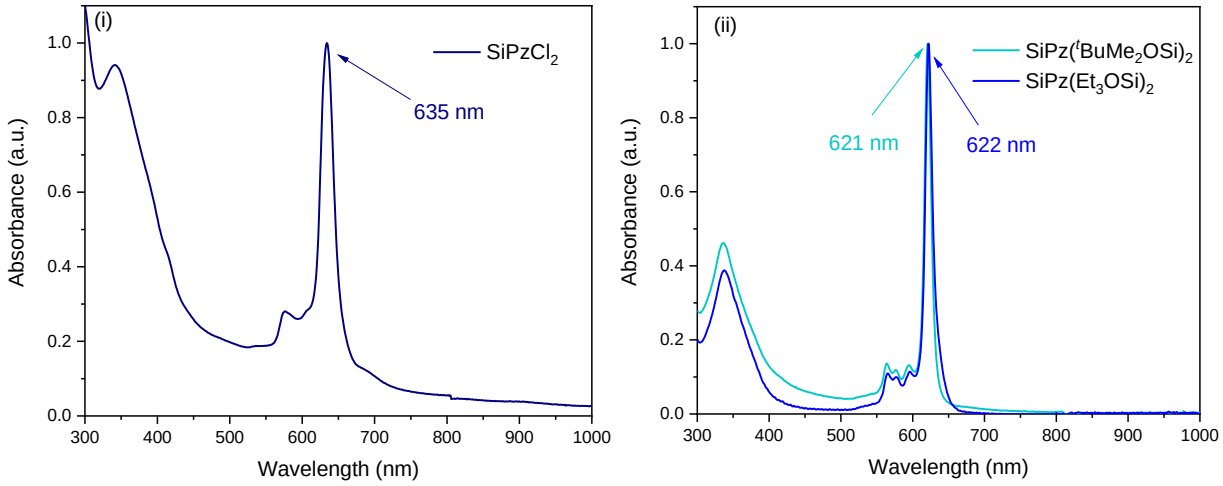

Figure 2.8 (i) Normalized UV-vis spectra of **SiPzCl$_2$** in DMSO. λ_{max} **SiPzCl$_2$** = 635 nm; (ii) Normalized UV-vis spectra of **SiPz(**^{t}**BuMe$_2$OSi)$_2$** and **SiPz(Et$_3$OSi)$_2$** in DCM. λ_{max} **SiPz(**^{t}**BuMe$_2$OSi)$_2$** = 621 nm, λ_{max} **SiPz(Et$_3$OSi)$_2$** = 622 nm.

For organic field-effect transistors, charge injection from the electrode to the organic semiconductor is a critically important process and is governed by the frontier molecular orbitals of the organic semiconductor. The energy of the HOMO and the LUMO represent the energy required to remove an electron (oxidize) and inject an electron (reduce) from the semiconducting

material, respectively. Besides charge injection, the HOMO/LUMO energy levels determine if a molecule would be suitable for electron or hole transport, or if it is capable of ambipolar charge transport. A crude approximation of the HOMO/LUMO levels of a compound can be obtained from the onset of reduction/oxidation from the cyclic voltammogram, which has become a traditional method of characterization in the field of organic electronics. Therefore, cyclic voltammetry (CV) is a crucial and commonly employed technique in this field.

In this chapter, CV was used to determine the LUMO levels of **SiPz(^{t}BuMe$_2$OSi)$_2$** and **SiPz(Et$_3$OSi)$_2$**, and the reduction process of these two derivatives are shown in Figure 2.9. Experiments were carried out in DCM solutions with tetrabutylammonium hexafluorophosphate (NBu_4PF_6) as the supporting electrolyte. Platinum wires were used for all three electrodes and the potentials were referenced internally to the Fc/Fc^+ redox couple. Compound **SiPz(Et$_3$OSi)$_2$** displayed a quasi-reversible reduction wave at $E_{1/2}$ = −1.02 V versus Fc/Fc^+. Compound **SiPz(^{t}BuMe$_2$OSi)$_2$** shows similar voltammetric behaviour to **SiPz(Et$_3$OSi)$_2$**. It also exhibited a quasi-reversible reduction wave at $E_{1/2}$ = −0.98 V versus Fc/Fc^+. The LUMO levels of **SiPz(Et$_3$OSi)$_2$** and **SiPz(^{t}BuMe$_2$OSi)$_2$** were then calculated to be −4.15 eV and −4.20 eV (versus vacuum) respectively from the reduction potentials using the following equation:[336]

$$E_{\mathrm{LUMO}} = -\left(E_{[\text{onset, red vs. Fc+/Fc}]} + 5.1\right)\ \mathrm{eV} \qquad \textbf{(2-2)}$$

where E_{LUMO} is the energy level of the LUMO; $E_{[\text{onset, red vs. Fc+/Fc}]}$ is the potential at which the corresponding reduction process is occurring after calibration of the ferrocene signal.

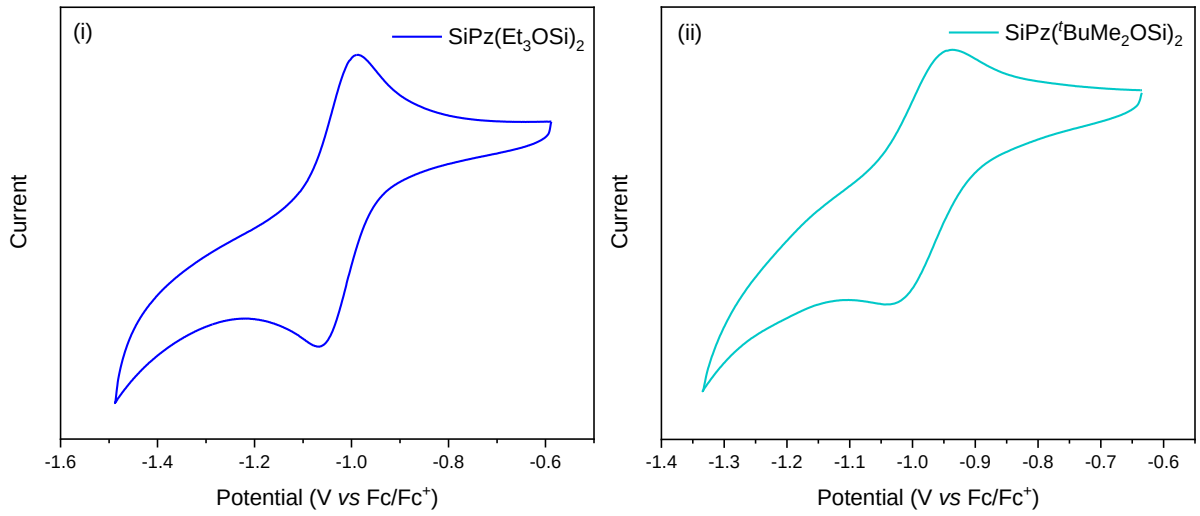

Figure 2.9 Cyclic Voltammagram (reduction behaviour) of (i) **SiPz(Et$_3$OSi)$_2$** and (ii) **SiPz(^{t}BuMe$_2$OSi)$_2$**.

Using the energy gap (E_g) which was obtained from the optical study, and the LUMO energy (E_{LUMO}) from the electrochemical study, we can then calculate the E_{HOMO} using the following equation:

$$E_{HOMO} = (E_{LUMO} - E_g)\ \text{eV} \qquad \textbf{(2-3)}$$

The results are summarized in Table 2.2, and shown in Figure 2.10. The similar electrochemical results of **SiPz(^{t}BuMe$_2$OSi)$_2$** and **SiPz(Et$_3$OSi)$_2$** indicate that axial substitution shows little to no change to the optoelectronic properties of the complexes presented here, since the axial substituents are not part of the conjugated framework and therefore will not significantly influence the energy of the frontier molecular orbitals. It is also important to mention that the LUMO values of silicon tetra-2,3-pyrazinoporphyrazine complexes are below −4.0 eV, which makes them promising *n*-type materials in the application of air-stable OTEFs. To be more specific, introducing pyrazine into the framework of conjugated molecules not only maintains molecular planarity but also decreases the E_{HOMO} and $E_{LUMO,}$ thereby suggesting that these complexes should exhibit

increased air stability and electron injection as *n*-channel materials;[74] however, device studies are necessary to confirm this.

Table 2.2 Electrochemical results of **SiPz(^{t}BuMe$_2$OSi)$_2$** and **SiPz(Et$_3$OSi)$_2$**.

Compound	$E_{onset,\ red}$ (V)	$E_{1/2}$ (V)	[a]LUMO (eV)	[b]HOMO (eV)	E_g (V)
SiPz(Et$_3$OSi)$_2$	−0.95	−1.02	−4.15	−6.11	1.96
SiPz(^{t}BuMe$_2$OSi)$_2$	−0.90	−0.98	−4.20	−6.16	1.96

a: $E_{LUMO} = -(E_{onset,\ red} + 5.1)$ eV;[336] *b*: $E_{HOMO} = (E_{LUMO} - E_g)$ eV.

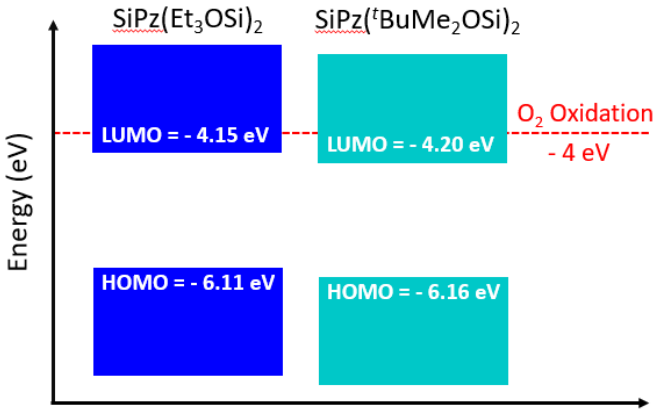

Figure 2.10 HOMO and LUMO of **SiPz(Et$_3$OSi)$_2$** and **SiPz(^{t}BuMe$_2$OSi)$_2$**.

2.3 Conclusion

In this chapter, two different routes to prepare silicon tetra-2,3-pyrazinoporphyrazine dichloride were developed. From this, it was found that the phthalonitrile is a better starting material in the synthesis of **SiPzCl$_2$**, compared to the corresponding diiminoisoindoline. While the poor solubility and failure of sublimation result in the difficulty of purifying of **SiPzCl$_2$**, this challenge can be solved by introducing alkylsiloxy chains to the axial position of Pzs. The synthesized bis-silyloxy derivatives **SiPz(^{t}BuMe$_2$OSi)$_2$** and **SiPz(Et$_3$OSi)$_2$** are soluble in most

common organic solvents since the two alkylsiloxy substituents bring very good inhibition of aggregation, thereby purification *via* column chromatography becomes feasible.

The optical and electrochemical properties of **SiPzs** were also studied. The isosteric substitution of CH groups in Pc macrocycle for nitrogen atoms leads to an obvious hypsochromic shift in their main absorption band (*Q*-band), compared to normal SiPcs. In addition, the relatively lower energy levels of **SiPzs** make them a potential air-stable *n*-type semiconducting material candidate.

2.4 Future work

While the characterization results indicate that SiPz derivatives probably be promising air-stable *n*-type semiconducting material, device testing studies are significantly necessary to confirm this. Therefore, further investigation for this project may focus on obtaining analytical pure **SiPz(^{t}BuMe$_2$OSi)$_2$** and **SiPz(Et$_3$OSi)$_2$** samples, which are suitable to be used in devices. For example, **SiPz(Et$_3$OSi)$_2$** crystals were tried to grown by slow vapor diffusion in a series of solvents and anti-solvents, as summarized in Table 2.3. After 3 weeks, red crystals were found only in number 13 and 15 trials. Other crystallization techniques should also be explored in the future. It is also necessary to develop various axial substituted derivatives, such as phenoxy substituted derivatives, and difluoro substituted derivatives to explore their impact on the solid-state structure and thin film morphology to optimize device performance. Introducing peripheral substituents is also a promising area to explore to increase the solubility of tetra-2,3-pyrazinoporphyrazines.

Table 2.3 Vapor diffusion crystallization conditions and results for **SiPz(Et$_3$OSi)$_2$**.

Number	Solvent	Anti-solvent	Result
1	DMF	Ether	No crystal
2	DMF	Hexane	No crystal

3	DMF	Toluene	No crystal
4	NMP	Ether	No crystal
5	NMP	Hexane	No crystal
6	NMP	Toluene	No crystal
7	DMSO	Ether	No crystal
8	DMSO	Hexane	No crystal
9	DMSO	Toluene	No crystal
10	Pyridine	Ether	No crystal
11	Pyridine	Hexane	No crystal
12	Pyridine	Toluene	No crystal
13	DCM	Ether	Red crystals
14	DCM	Hexane	No crystal
15	DCM	Toluene	Red crystals

2.5 Experimental section

Materials and methods.

Chlorotrimethylsilane (Acros), silicon tetrachloride (Sigma-Aldrich), cesium hydroxide (50 wt% in water, Sigma-Aldrich), urea (Sigma-Aldrich), tri-*n*-butylamine (Sigma-Aldrich), *tert*-butyldimethylsilyl trifluoromethanesulfonate (Sigma-Aldrich), and triethylsilyl trifluoromethanesulfonate (Sigma-Aldrich) were obtained commercially and used as received. Tetralin (Sigma-Aldrich) was distilled over sodium dust. Lithium bis(trimethylsilylamide) etherate was prepared as outlined in the literature,[337] and 2,3-dicyanopyrazine was prepared according to published methods.[338] All solvents were ACS grade; dry solvents were obtained by passing through activated alumina on a J.C. Meyer solvent purification system. Quinoline (Oakwood) was distilled over zinc dust prior to use.

All reactions were performed under an atmosphere of dry nitrogen. NMR spectra were run in either DMSO-d_6 or $CDCl_3$ solutions at room temperature on a Bruker Avance 300 or 400 MHz spectrometers (Billerica, MA, USA). Spin multiplicities are designated by the following abbreviations: s (singlet), d (doublet), t (triplet), q (quartet), m (multiplet), and br (broad). Infrared spectra of solid samples were recorded either on an Agilent Technologies Cary 630 FT-IR spectrometer using Attenuated Total Reflection, or in KBr pellets on BOMEM MB100 FT-IR spectrometer. UV-vis absorption spectra were measured using an Agilent Cary 5000 UV-Vis-NIR spectrophotometer in the range 300─1000 nm. Solution absorption measurements were completed using DCM or DMSO solutions with standard 10 mm pathlength cuvettes. Mass spectroscopy was acquired on a AccuTOF GCx plus mass spectrometer (JEOL USA Inc., Peabody, Massachusetts, USA) equipped with an Electron Ionization (EI) ion source, or on a Bruker Autoflex Speed Matrix-assisted laser desorption ionization time-of-flight mass spectrometer (MALDI-TOF/MS) (Bruker Daltonics Inc., Billerica, Massachusetts, USA), or on a Kratos Concept - Magnetic sector Electron impact mass spectrometer. Cyclic voltammetry was carried out using a Bioanalytical Systems C3 electrochemical workstation. The working electrode, the counter electrode and the reference electrode were platinum wires. Spec-grade dichloromethane was purged with N_2 gas at room temperature prior to its use. Three cycles at a scan rate of 100 mV/s were measured for the sample. Tetrabutylammonium hexafluorophosphate (0.1 M) was used as the supporting electrolyte, and decamethylferrocene was used as an internal reference.

Synthesis of 5-imino-5*H*-pyrrolo[3,4-*b*]pyrazin-7-amine (Pz-DIII).[152] To a solution of 2,3-dicyanopyrazine (1.00 g, 7.69 mmol) in anhydrous toluene (10 mL) was added lithium bis(trimethylsilyl)amide etherate (2.23 g, 9.22 mmol) in one portion under a nitrogen atmosphere. After stirring the reaction mixture for 3 hours at room temperature, chlorotrimethylsilane (1.07

mL, 8.45 mmol) was added *via* syringe in one portion and the reaction mixture was kept refluxing for 24 hours. Lithium chloride was removed through hot filtration and the solvent of the filtrate was partially removed by rotary evaporation to about one-third of the initial volume then poured through a silica gel plug. The latter was flushed with DCM (2 x 100 mL), EtOAc (2 x 100 mL) and MeOH. The MeOH fraction was concentrated under vacuum and the product was isolated by precipitation from the ether. The solids are collected by filtration, washed with ether and dried to afford a brown powder. Yield: 0.41 g (36 %). MS (EI) calcd for 147.14, found 147.12. ^{1}H NMR (δ, DMSO-d_6, RT, 300 MHz): 8.77 (s, 2H-pyrazino), 8.90 (br, 3H-NH). IR ν_{max} (cm^{-1}): 3267, 3219, 3017, 2940, 2831, 2756, 1686, 1647, 1561, 1544, 1534, 1453, 1373, 1265, 1144, 1064, 932, 867, 741.

Synthesis of silicon tetra-2,3-pyrazinoporphyrazine dichloride ($SiPzCl_2$). Route B:[325] 2,3-Dicyanopyrazine (0.98 g, 7.50 mmol), urea (0.5 g), dry tri-*n*-butylamine (3.57 mL, 15.00 mmol), and freshly distilled quinoline (5 mL) were added into a flame-dried two-necked round-bottom flask. Then silicon tetrachloride (0.86 mL, 7.50 mmol) was added *via* a syringe, and the mixture was heated to 160 °C for 3 hours. Then the mixture was allowed to cool, the precipitate was collected, thoroughly washed with hot ethanol, and air-dried, resulting in a dark blue powder. The products contained some impurities but were suitable for use as intermediates for the preparation of axial substituted complexes without further purification. Crude yield: 0.70 g (60 %).

Route C: To an oven-dried two-necked round-bottom flask was added 2,3-dicyanopyrazine (1.00 g, 7.69 mmol), lithium bis(trimethylsilyl)amide etherate (2.04 g, 8.45 mmol) and freshly distilled tetralin (50 mL) in one portion under a nitrogen atmosphere. After stirring the reaction mixture for 2 hours at room temperature, silicon tetrachloride (0.97 mL, 8.45 mmol) was added *via* a syringe. Then the mixture was heated to 170 °C for 4 hours. The mixture was filtered before it cool, then

the precipitate was collected, thoroughly washed with toluene, acetone and EtOH until the coming out solvent was colorless. The resulting dark blue powder was then dried under a vacuum. Crude yield: 1.07 g (90 %). MS (EI) calcd for 619.43, found 619.63. IR ν_{max} (KBr, cm^{-1}): 1625, 1522, 1457, 1365, 1293, 1204, 1131, 1054, 960, 927, 848, 460.

Synthesis of bis(hydroxy) silicon tetra-2,3-pyrazinoporphyrazine (SiPz(OH)$_2$).[159] To an oven-dried two-necked round-bottom flask was added **SiPzCl$_2$** (2.00 g, 3.23 mmol), cesium hydroxide (50 wt% in water, 1.69 mL, 19.37 mmol), and DMF (70 mL) in one portion under a nitrogen atmosphere. The reaction mixture was heated to 120 °C for 4 hours. The crude product was precipitated into MeOH and filtered to give a black powder, which was used for the subsequent axial substitution reaction without further purification. Crude yield: 1.75 g (90 %). IR ν_{max} (cm^{-1}): 3455, 1616, 1522, 1456, 1364, 1292, 1201, 1133, 1018, 960, 927, 862.

Synthesis of bis(*tert*-butyldimethylsiloxy) silicon tetra-2,3-pyrazinoporphyrazine (SiPz(^{t}BuMe$_2$OSi)$_2$).[318] To a solution of **SiPz(OH)$_2$** (1.00 g, 1.72 mmol) in DCM (115 ml) and pyridine (17 ml) was added *tert*-butyldimethylsilyl trifluoromethanesulfonate (3.94 mL, 17.17 mmol), and the mixture was stirred at room temperature for 48 hours. The reaction mixture was poured into water (500 ml), the phases separated and the organic phase was washed with $NaHCO_3$ solution (2 x 200 mL) and water (2 x 200 mL). The solvent was removed from the organic phase, and the residue was chromatographed on a short column of silica gel (eluent MeOH/chloroform, 1 %). The product was a blue powder. Yield: 0.56 g (27 %). ^{1}H NMR (δ, $CDCl_3$, RT, 300 MHz): 9.73 (s. 8H-pyrazino), −1.53 (s, 18H-^{t}Bu), −3.04 (s, 12H-dimethyl). MS (MALDI) calcd for 811.06, found 811.25. IR ν_{max} (cm^{-1}): 2955, 2921, 2852, 1725, 1670, 1464, 1377, 1260, 1216, 1096, 1051, 927, 835, 802.

Synthesis of bis(tri-*n*-ethylsiloxy) silicon tetra-2,3-pyrazinoporphyrazine (SiPz($Et_3OSi)_2$).[318] The synthesis of **SiPz($Et_3OSi)_2$** was performed under similar conditions to that of **SiPz(^{t}BuMe$_2$OSi)$_2$**, except for using triethylsilyl trifluoromethanesulfonate. The product was a blue powder. Yield: 0.46 g (35 %). ^{1}H NMR (δ, $CDCl_3$, RT, 300 MHz): 9.73 (s. 8H-pyrazino), −1.29 (t, 18H-CH_3), −2.54 (q, 12H-α-CH_2). MS (MALDI) calcd for 811.06, found 811.32. IR ν_{max} (cm^{-1}): 2955, 2918, 2850, 1712, 1522, 1464, 1411, 1365, 1261, 1214, 1096, 1050, 1017, 926, 879, 803, 759.

Chapter 3 Silicon Tetra(*tert*-butyl)-2,3-naphthalocyanine Complexes ((^{t}Bu)$_4$SiNPc)

3.1 Introduction

Naphthalocyanines (NPcs) are structurally similar to phthalocyanines (Pcs) but have additional benzene rings fused to the periphery of the Pc framework, which extend the π-conjugated system. They possess an intense absorption band in the near IR region (λ_{max} at approximately 800 nm, ε at approximately 2×10^5, around 50% larger than the structurally related phthalocyanine, since the *Q*-band shifted with respect to the conjugation degree of the molecule) and excellent thermal and photochemical stability.[127,128,339,340] These facts render them attractive for photodynamic therapy,[341] photoacoustic imaging[342,283,343] and organic electronics. Naphthalocyanines are also of interest because of the extension of the π-electron system, compared to phthalocyanines, which can effectively modify the opto-electronic properties such as redox potentials, electrical conductivity, photoconductivity and catalytic activity.[344]

To date, the majority of NPc research has focused on 2,3-naphthalocyanine, where the naphthalene unit is incorporated into the macrocycle fused through the carbon atoms at the 2 and 3 positions of the naphthalene ring, as shown in Figure 3.1.[265] Compared to Pcs, NPcs have received less research attention, which may be attributed to their higher tendency to aggregate affecting their solubility and their sensitivity towards oxidization owing to the relatively high HOMO and LUMO energy levels.[125] To address the former challenge, substituents are usually introduced into peripheral sites of the NPc backbone in order to enhance steric hindrance, thereby inhibiting aggregation. In addition, peripheral substituents can also be used to fine-tune the ground

state absorption to help enhance the visible window by red shifting the long-wavelength *Q*-band absorption.[129]

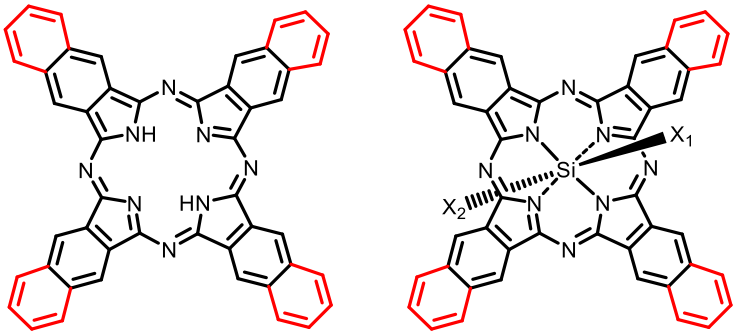

H_2NPc **SiNPcX_2**

Figure 3.1 The structure of metal-free 2,3-naphthalocyanine and silicon 2,3-naphthalocyanine.

In this chapter, silicon tetra(*tert*-butyl)-2,3-naphthalocyanine complexes were prepared and characterized. The synthetic avenues were explored to prepare silicon tetra(*tert*-butyl)-2,3-naphthalocyanine dichloride (**(^{t}Bu)$_4$SiNPcCl$_2$**), bis(hydroxy) silicon tetra(*tert*-butyl)-2,3-naphthalocyanine (**(^{t}Bu)$_4$SiNPc(OH)$_2$**), and bis(tri-*n*-propylsiloxy) silicon tetra(*tert*-butyl)-2,3-naphthalocyanine (**(^{t}Bu)$_4$SiNPc(Pr$_3$OSi)$_2$**). A key feature of these naphthalocyanine derivatives is the incorporation of four bulky *tert*-butyl substituents to the periphery of the molecule, which improves solubility in common organic solvents and reduces the likelihood of large-scale aggregation due to weaker intermolecular interactions between the conjugated naphthalocyanine cores of adjacent molecules.[345] As mentioned in **Chapter 2**, selecting Si as the Pc core provides the ability to modify the axial substituents, leading to a facile avenue for functionalization. Nuclear magnetic resonance spectroscopy (NMR), Infrared spectroscopy (IR), UV-vis Spectroscopy (UV-vis), Mass Spectroscopy (MS), and Cyclic Voltammetry (CV) were employed to characterize the compounds.

3.2 Result and discussion

The general synthetic method of NPcs is similar to that of the parent Pcs, with naphthanitriles possessing the necessary peripheral substituents typically employed as the starting materials.

3.2.1 Synthesis of 6-(*tert*-butyl)-1*H*-benzo[*f*]isoindole-1,3(2*H*)-diimine (ᵗBuNp-DIII).

As mentioned in **Chapter 1**, most silicon phthalocyanines can be effectively synthesized from the corresponding diiminoisoindolines (DIII). Following a similar route, 6-(*tert*-butyl)-1*H*-benzo[*f*]isoindole-1,3(2*H*)-diimine (**ᵗBuNp-DIII**) was synthesized from *tert*-butyl-2,3-naphthalenedicarbonitrile utilizing a nitrile ammonolysis, as outlined in Scheme 3.1. A solution of *tert*-butyl-2,3-naphthalenedicarbonitrile in anhydrous toluene was added to $LiN(TMS)_2 \cdot Et_2O$, forming the intermediate **3-1**.[152] After 3 hours, chlorotrimethylsilane (TMSCl) was added, and the reaction mixture was stirred overnight (15 − 20 hours) at room temperature. Quenching the intermediate **3-1** with chlorotrimethylsilane (TMSCl) afforded the silylated DIII intermediate, while the LiCl by-product precipitated out of solution and was removed by filtration. The reaction mixture was then concentrated by rotary evaporation before passing through a silica plug to remove the TMS groups and replace them with hydrogen atoms. Further purification was achieved by triturating the resulting brown solution with ether, affording **ᵗBuNp-DIII** as a greenish-yellow fine powder. Both NMR and MS results indicate the presence of the desired DIII product. For example, as shown in Figure 3.2, the NH groups are shown as a broad signal at 10.32 ppm, while multiple signals in the aromatic region reveal the five protons in the naphthalene ring and the singlet at 1.41 ppm integrates to the nine protons of the *tert*-butyl group. Using EI-MS analysis, the parent signature $[M]^+$ for **ᵗBuNp-DIII** was observed at 251.15 m/z (Figure 3.3).

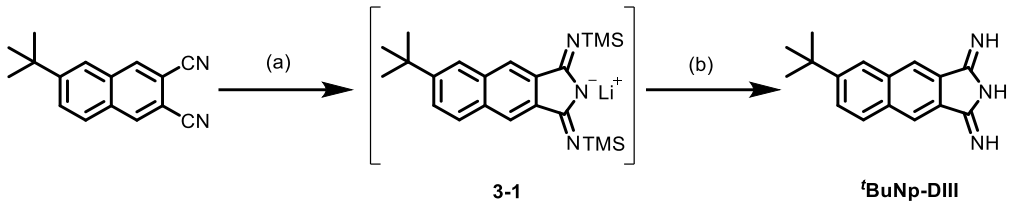

Scheme 3.1 Synthetic route toward the preparation of 6-(*tert*-butyl)-1*H*-benzo[*f*]isoindole-1,3(2*H*)-diimine (**^{t}BuNp-DIII**). Reagents and conditions: (a) $LiN(TMS)_2 \cdot Et_2O$, Toluene, RT, 3 h; (b) (i) TMSCl, RT, Overnight, (ii) silica gel.

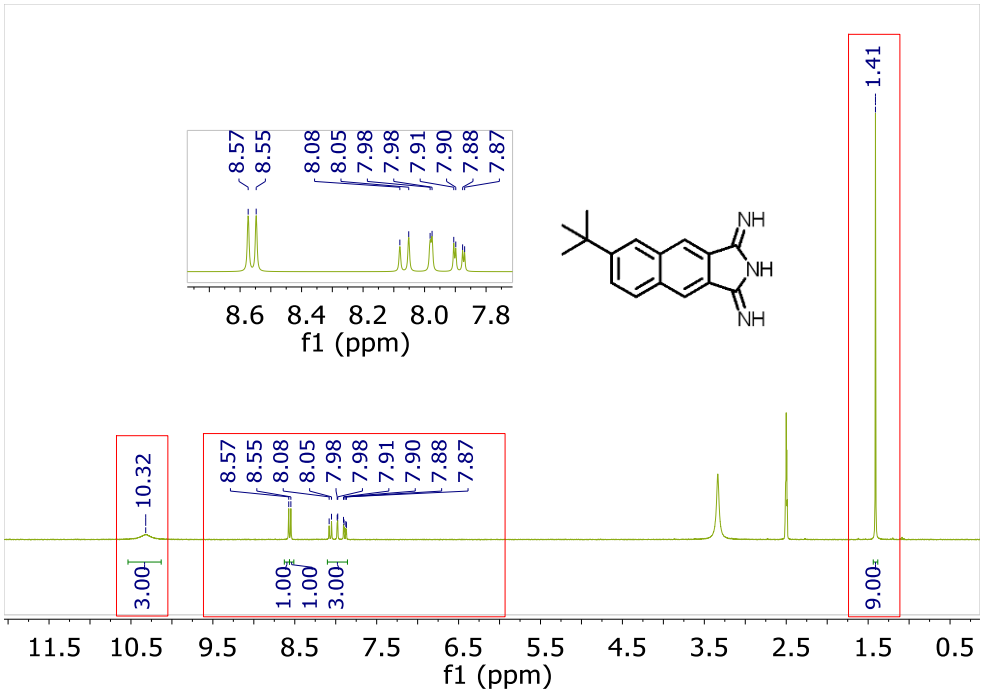

Figure 3.2 ^{1}H NMR spectrum of **^{t}BuNp-DIII** in DMSO-d_6. 10.32 (br, 3H-NH), 8.57 (s, 1H-naphthalene), 8.55 (s, 1H-naphthalene), 7.87 − 8.08 (m, 3H-naphthalene), 1.41 (s, 9H-^{t}Bu).

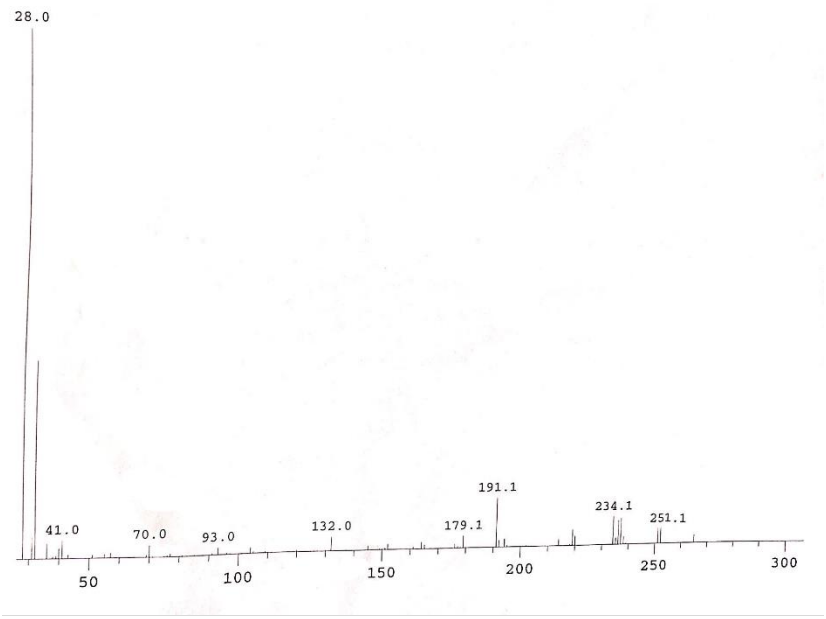

Figure 3.3 The EI-MS spectrum of **^{t}BuNp-DIII**. *m/z* 251.1.

3.2.2 Synthesis of silicon tetra(*tert*-butyl)-2,3-naphthalocyanine dichloride ((^{t}Bu)$_4$SiNPcCl$_2$).

Silicon tetra(*tert*-butyl)-2,3-naphthalocyanine dichloride **(^{t}Bu)$_4$SiNPcCl$_2$** was synthesized *via* the template cyclization reaction as reported in previous studies (Scheme 3.2).[321, 150] A mixture of **^{t}BuNp-DIII** in freshly distilled quinoline was gently heated to 50 °C for 10 min in order to keep the mixture liquid and quite fluid upon $SiCl_4$ addition. After adding $SiCl_4$ dropwise, the reaction mixture quickly turns brown and solidifies after 30 minutes. The resulting green solid residue was washed with toluene and MeOH, then subsequently dissolved in DCM and filtered to remove any insoluble impurities. The DCM was then evaporated by rotary evaporation to afford a lustrous green powder of **(^{t}Bu)$_4$SiNPcCl$_2$**, which was used as prepared for the following axial substitution reactions without further purification. It is also important to note that the position of *tert*-butyl groups was not controlled. Specifically, the cyclization reaction leads to a **(^{t}Bu)$_4$SiNPcCl$_2$** isomeric mixture rather than a single **(^{t}Bu)$_4$SiNPcCl$_2$** isomer as each of the four diiminoisoindoline molecules that enter into the formation of a macrocyclic naphthalocyanine ring can insert in either

one of two ways. Presumably, this mixture and each of the other isomeric mixtures derived from it contain all eight possible isomers.[173]

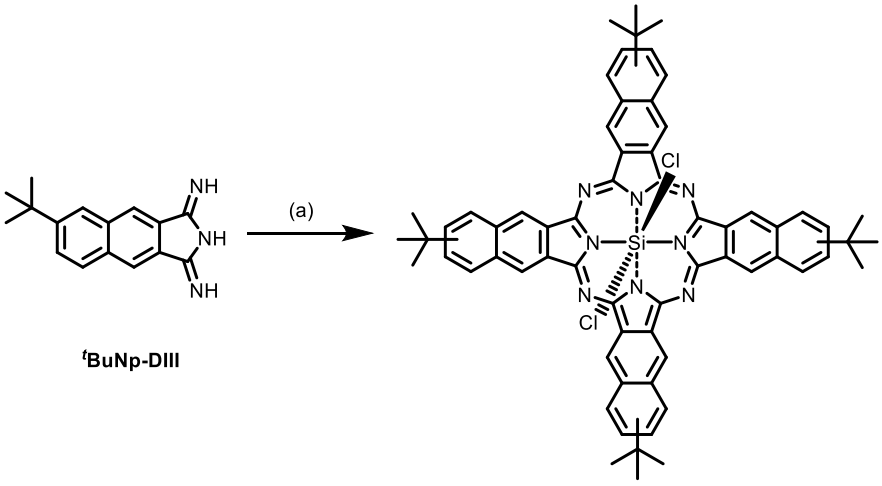

Scheme 3.2 Synthetic route toward the preparation of **(^{t}Bu)$_4$SiNPcCl$_2$**. Reagents and conditions: (a) $SiCl_4$, Quinoline, 200 °C, 30 min.

The identity of the **(^{t}Bu)$_4$SiNPcCl$_2$** was confirmed by IR, ^{1}H NMR and MS. The IR spectrum features a characteristic band at 476 cm^{-1} (Si–Cl stretch), while the ^{1}H NMR spectrum reveals three signals at 9.65, 8.35 and 8.02 ppm, which integrate into a 2:2:1 ratio, representing the five protons in the naphthalene ring, as shown in Figure 3.4. It is necessary to note that the aromatic protons exhibit very broad signals without any fine structure. This can be attributed to the aggregation of molecules in solution, which can be avoided by silylation of the axial groups.[318]

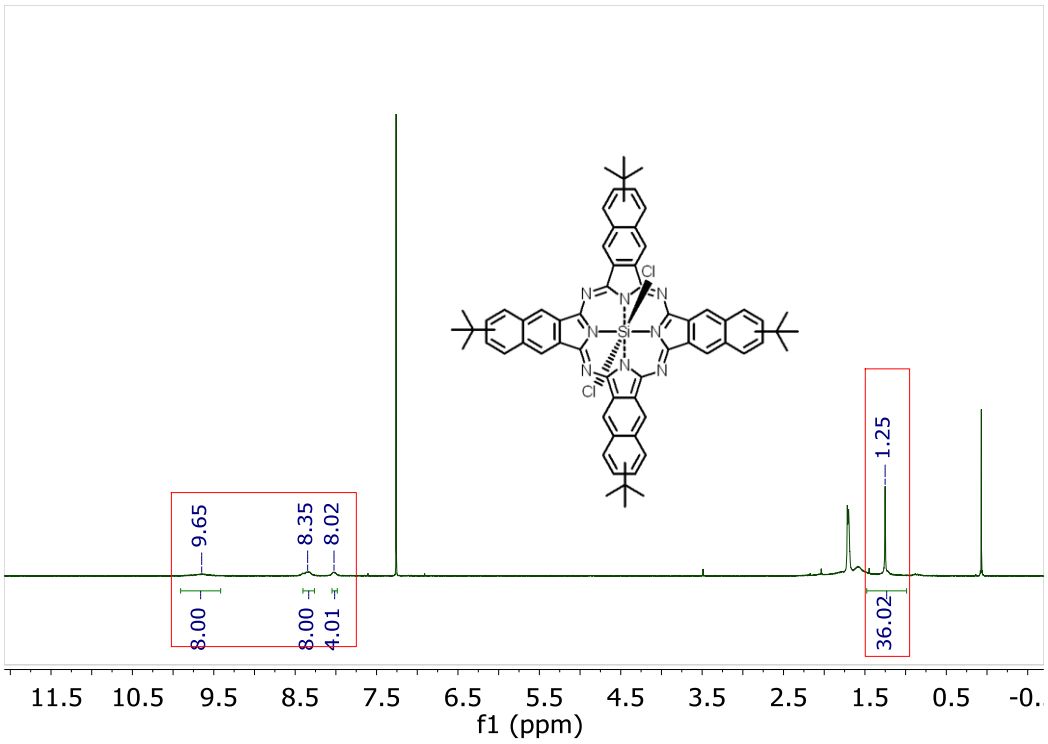

Figure 3.4 ^{1}H NMR spectrum of **(^{t}Bu)$_4$SiNPcCl$_2$** in $CDCl_3$. 9.65 (8H-naphthalene), 8.35 (8H-naphthalene), 8.02 (4H-naphthalene), 1.25 (36H-^{t}Bu).

3.2.3 Synthesis of bis(tri-*n*-propylsiloxy) silicon tetra(*tert*-butyl)-2,3-naphthalocyanine ((^{t}Bu)$_4$SiNPc(Pr$_3$OSi)$_2$).

To prevent the formation of H-aggregates, the axial chlorine atoms in **(^{t}Bu)$_4$SiNPcCl$_2$** were replaced with bulky siloxy groups, which can also reduce interfacial recombination.[326] As shown in Scheme 3.3, the synthesis of **(^{t}Bu)$_4$SiNPc(Pr$_3$OSi)$_2$** followed a two-step route: first of all, **(^{t}Bu)$_4$SiNPcCl$_2$** was hydrolyzed under basic conditions provided by cesium hydroxide.[159] The reaction resulted in a dark green powder with relatively poor solubility, which is sparingly soluble in solvents including MeOH, DCM, chloroform and DMSO. For this reason, NMR spectroscopic analysis was not possible. Nonetheless, the identity of this compound was confirmed by Mass Spectrometry and Infrared Spectroscopy. Using EI-MS analysis, the parent signature $[M]^{+}$ for **(^{t}Bu)$_4$SiNPc(OH)$_2$** was observed at 998.47 m/z; losing one or both OH groups of the compound

leads to fragment signatures at 981.47 m/z and 966.47 m/z, respectively. The EI-MS spectrum is shown in Figure 3.5. The IR spectrum of **(^{t}Bu)$_4$SiNPc(OH)$_2$** features absorption bands at 3444 cm^{-1} (O–H) and 831 cm^{-1} (Si–O).

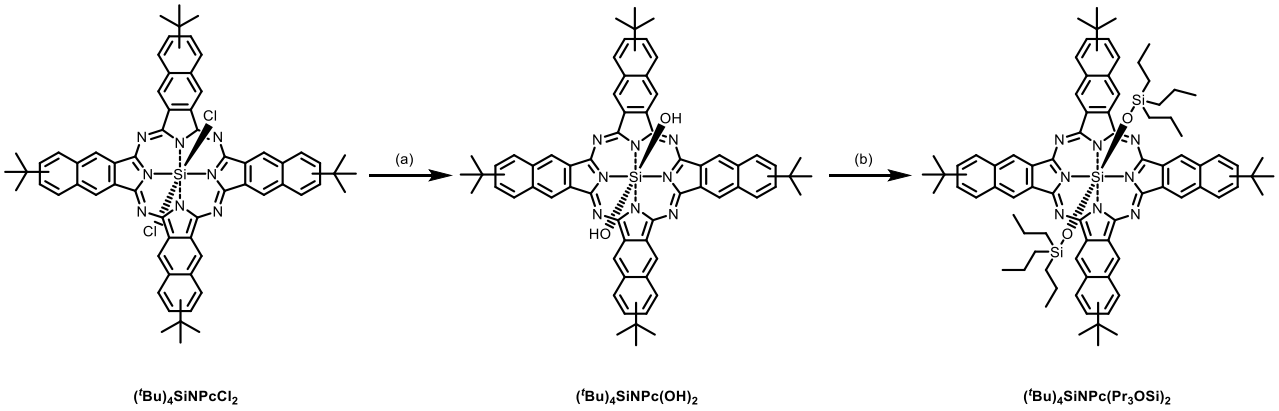

Scheme 3.3 Synthetic routes toward the preparation of **(^{t}Bu)$_4$SiNPc(Pr$_3$OSi)$_2$**. Reagents and conditions: (a) CsOH (50 wt% in water), DMF, 120 °C, 4 h; (b) Chlorotripropylsilane, toluene, 120 °C, 24 h.

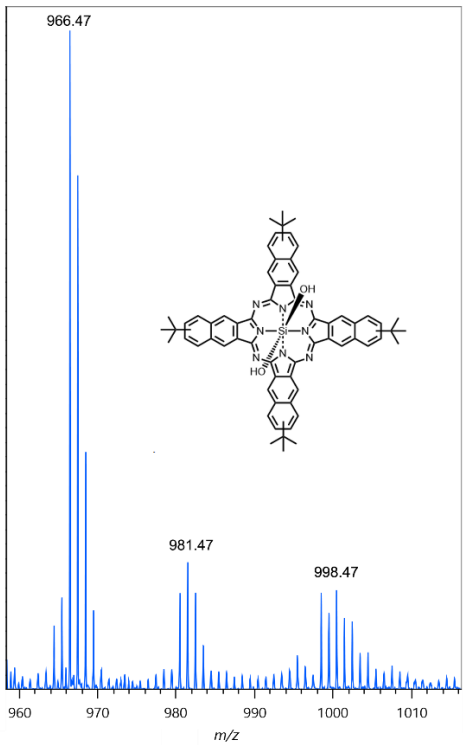

Figure 3.5 EI-MS spectrum of **(^{t}Bu)$_4$SiNPc(OH)$_2$**. *m/z* 998.47.

To form a siloxane bond in the axial position, the precursor **(^{t}Bu)$_4$SiNPc(OH)$_2$** was functionalized with tripropylchlorosilane *via* nucleophilic substitution by refluxing it with an excess of the monosilane in toluene for 24 hours. Following this, **(^{t}Bu)$_4$SiNPc(Pr$_3$OSi)$_2$** was then obtained as a fine green powder with good solubility, which was purified by vacuum sublimation using a three-zone tube furnace, with the zone temperatures at 330−210−120 °C at a pressure of 10^{-5} torr. Both the four *tert*-butyl peripheral substituents and the two bulky alkylsiloxy axial substituents improve solubility in common organic solvents and reduce the likelihood of large-scale aggregation due to weaker intermolecular interactions between the conjugated naphthalocyanine cores of adjacent molecules.[345] ^{1}H NMR analysis (Figure 3.6) shows that the signals of the protons in the axial alkyl groups are found in the upfield region (−0.24, −0.85 and −2.06 ppm), which can be attributed to the magnetic anisotropy of the conjugated NPc macrocycle ring. The IR spectrum of **(^{t}Bu)$_4$SiNPc(Pr$_3$OSi)$_2$** features absorption bands at 1023 cm^{-1} (Si–O–Si) and 1202 cm^{-1} (Si–*n*-propyl), as shown in Figure 3.7.

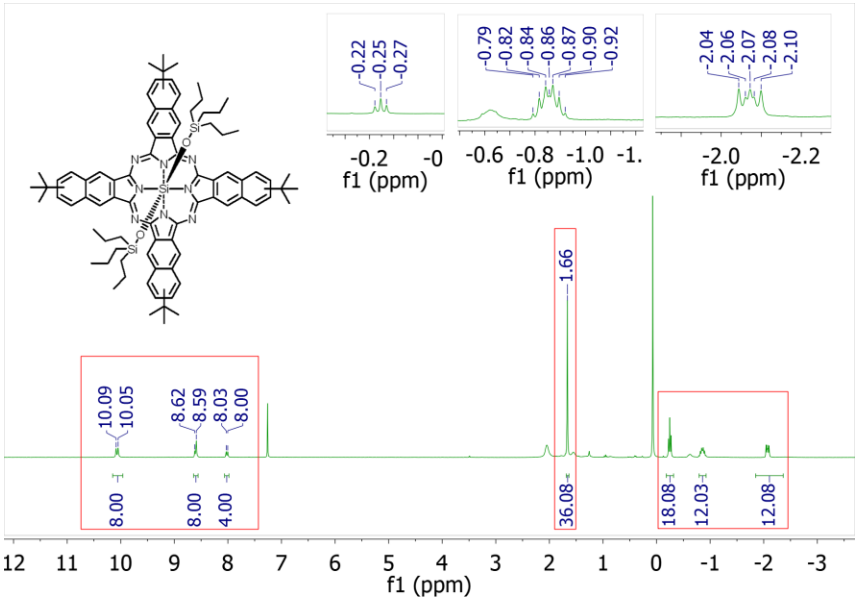

Figure 3.6 ^{1}H NMR spectrum of **(^{t}Bu)$_4$SiNPc(Pr$_3$OSi)$_2$** in $CDCl_3$. 10.07 (d, 8H-ArH), 8.60 (d, 8H-ArH), 8.01 (d, 4H-ArH), 1.67 (s, 36H-^{t}Bu), −0.24 (t, 18H-CH_3), −0.85 (m, 12H-βCH_2), −2.06 (m, 12H-αCH_2).

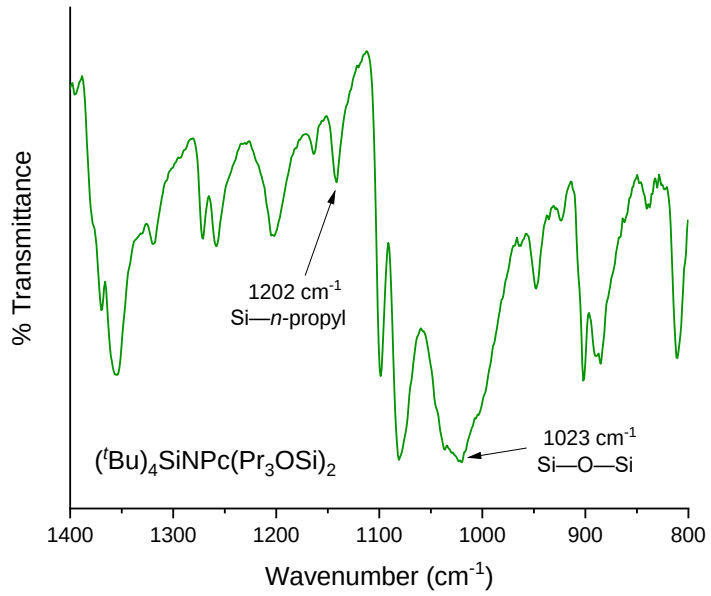

Figure 3.7 FTIR spectrum of **(^{t}Bu)$_4$SiNPc(Pr$_3$OSi)$_2$**.

3.2.4 Optical and electrochemical studies

The absorption characteristics and oxidation/reduction properties of the *tert*-butyl **SiNPc** molecules were measured by UV-vis spectroscopy and cyclic voltammetry. It is known that in going from phthalocyanine to naphthalocyanine compounds, the HOMO level is destabilized and consequently the *Q*-bands become red-shifted, meanwhile the LUMO energy level remains relatively constant.[344] As mentioned in **Chapter 2**, Pcs exhibit typical UV-vis spectra with a sharp *Q*-band at approximately 650 − 750 nm. For naphthalocyanine complexes, *Q*-bands are usually red-shifted by around 100 nm compared to Pcs due to an increase in π-delocalization.[346] As shown in Figure 3.8, the *Q*-band of **(^{t}Bu)$_4$SiNPcCl$_2$** and **(^{t}Bu)$_4$SiNPc(Pr$_3$OSi)$_2$** are 786 and 778, respectively.

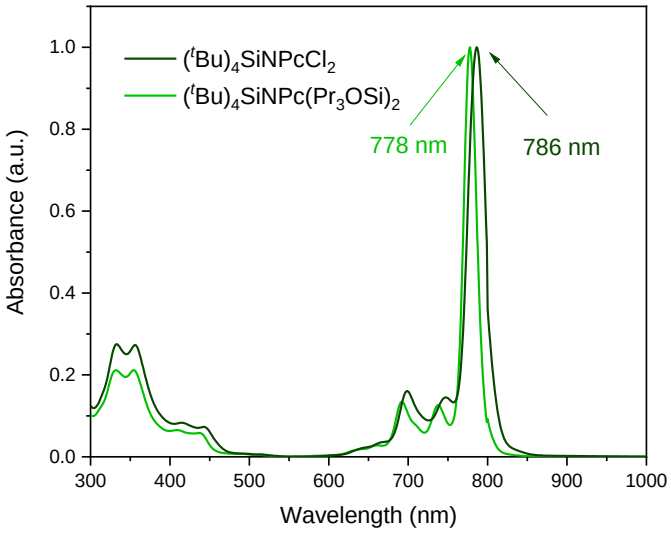

Figure 3.8 Normalized UV-vis spectra of **(^{t}Bu)$_4$SiNPcCl$_2$** and **(^{t}Bu)$_4$SiNPc(Pr$_3$OSi)$_2$** in $CHCl_3$. λ_{max} **(^{t}Bu)$_4$SiNPcCl$_2$** = 786 nm, λ_{max} **(^{t}Bu)$_4$SiNPc(Pr$_3$OSi)$_2$** = 778 nm.

The cyclic voltammogram of **(^{t}Bu)$_4$SiNPc(Pr$_3$OSi)$_2$** is illustrated in Figure 3.9, and its calculated highest occupied molecular orbital (HOMO) and lowest unoccupied molecular orbital (LUMO) energy levels are summarized in Table 3.1. Experiments were carried out in DCM solutions with tetrabutylammonium hexafluorophosphate (NBu_4PF_6) as the supporting electrolyte. The working electrode was a 2 mm glassy carbon disk; the counter electrode was a platinum wire, and the reference electrode was $Ag/AgNO_3$. The potentials were referenced internally to the Fc/Fc^+ redox couple. As shown in Figure 3.9, two quasi-reversible oxidation waves and two quasi-reversible reduction waves were observed for **(^{t}Bu)$_4$SiNPc(Pr$_3$OSi)$_2$** at $E_{1/2,\,red\,1} = -1.46$ V, $E_{1/2,\,red\,2} = -1.98$ V, $E_{1/2,\,ox\,1} = 0.04$ V and $E_{1/2,\,ox\,2} = 0.66$ V versus Fc/Fc^+. The HOMO and LUMO levels of **(^{t}Bu)$_4$SiNPc(Pr$_3$OSi)$_2$** can be calculated from the first oxidation and reduction potential respectively using the following equations:[336]

$$E_{HOMO} = -\,(E_{[onset,\,ox\ vs.\ Fc+/Fc]} + 5.1)\ eV \qquad (3\text{-}1)$$

$$E_{LUMO} = -\,(E_{[onset,\,red\ vs.\ Fc+/Fc]} + 5.1)\ eV \qquad (3\text{-}2)$$

where E_{HOMO} and E_{LUMO} are the energy levels of the HOMO and LUMO, respectively; $E_{[onset, ox vs. Fc^+/Fc]}$ and $E_{[onset, red vs. Fc^+/Fc]}$ are the potentials at which the corresponding redox process is occurring after calibration of the ferrocene signal. The HOMO and LUMO levels of **(^{t}Bu)$_4$SiNPc(Pr$_3$OSi)$_2$** were thus calculated to be −5.09 eV and −3.67 eV *vs.* vacuum, respectively. Compared to normal phthalocyanines, **SiNPc** exhibits a smaller energy band gap due to a larger degree of conjugation of the molecule.

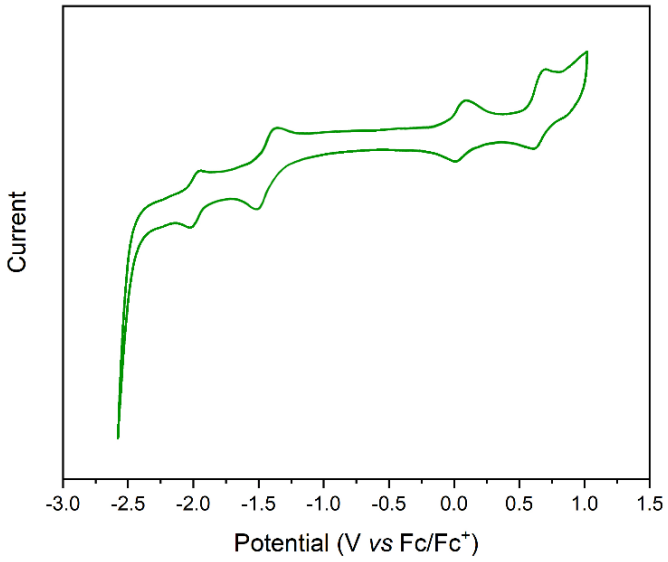

Figure 3.9 Cyclic Voltammagram of **(^{t}Bu)$_4$SiNPc(Pr$_3$OSi)$_2$**.

Table 3.1 Electrochemical results of **(^{t}Bu)$_4$SiNPc(Pr$_3$OSi)$_2$**.

Compound	$E_{1/2, red 1}$ **(V)**	$E_{1/2, red 2}$ **(V)**	$E_{1/2, ox 1}$ **(V)**	$E_{1/2, ox 2}$ **(V)**	
	−1.46	−1.98	0.04	0.66	
(^{t}Bu)$_4$SiNPc(Pr$_3$OSi)$_2$	$E_{onset, ox}$ **(V)**	$E_{onset, red}$ **(V)**	[a]**LUMO (eV)**	[a]**HOMO (eV)**	E_g **(V)**
	−0.01	−1.43	−3.67	−5.09	1.42

a: $E_{HOMO} = -(E_{onset, ox} + 5.1)$ eV, $E_{LUMO} = -(E_{onset, red} + 5.1)$ eV,[336] $E_g = E_{LUMO} - E_{HOMO}$.

3.3 Conclusion

In conclusion, a series of silicon naphthalocyanine molecules containing *tert*-butyl groups on the periphery of the molecule were synthesized, and their optical and electrochemical studies have been described. The important intermediate, **^{t}BuNp-DIII**, was synthesized *via* a new route that eliminates the undesired expenses attributed to the strenuous reaction conditions required and the hazardous reagents employed in the preparation. Compared to normal SiPcs, the extension of π-conjugation leads to obvious bathochromic shifts in the main absorption band (*Q*-band). Both the presence of ^{t}Bu groups and the introduction of the bulky tripropylsilyloxide side groups reduce the tendency of the NPc molecules to aggregate, thereby increase their solubility.

3.4 Future work

Future work for **(^{t}Bu)$_4$SiNPc(Pr$_3$OSi)$_2$** entails investigating its performance in organic electronic devices. Based on its calculated energy levels, **(^{t}Bu)$_4$SiNPc(Pr$_3$OSi)$_2$** might be a promising semiconducting material that can be used in organic photovoltaics (OPVs), organic light-emitting diodes (OLEDs), and organic thin-film transistors (OTFTs). In addition, the ability to tune the axial substituents of Pcs, and thus their properties, is one of the key advantages of using these molecules for semiconductor applications. Therefore, more axial substituted **(^{t}Bu)$_4$SiNPc** derivatives should be further explored.

3.5 Experimental section

Materials and methods.

6-*tert*-Butyl-2,3-naphthalenedicarbonitrile (Sigma-Aldrich), chlorotrimethylsilane (Acros), silicon tetrachloride (Sigma-Aldrich), cesium hydroxide (50 wt% in water, Sigma-Aldrich) and chlorotripropylsilane (Sigma-Aldrich) were obtained commercially and used as received. Lithium bis(trimethylsilylamide) etherate was prepared as outlined in the literature.[337] All solvents were

ACS grade; dry solvents were obtained by passing through activated alumina on a J.C. Meyer solvent purification system. Quinoline (Oakwood) was distilled over zinc dust.

All reactions were performed under an atmosphere of dry nitrogen. Melting points were taken using a Mel-Temp apparatus and are uncorrected. NMR spectra were run in either DMSO-d_6 or $CDCl_3$ solutions at room temperature on Bruker Avance 300 or 400 MHz spectrometers (Billerica, MA, USA). Spin multiplicities are designated by the following abbreviations: s (singlet), d (doublet), t (triplet), q (quartet), m (multiplet), and br (broad). Infrared spectra of solid samples were recorded either on an Agilent Technologies Cary 630 FT-IR spectrometer using Attenuated Total Reflection, or in KBr pellets on BOMEM MB100 FT-IR spectrometer. UV-vis absorption spectra were measured using an Agilent Cary 5000 UV-Vis-NIR spectrophotometer in the range 300 – 1000 nm. Solution absorption measurements were completed using $CHCl_3$ solutions with standard 10 mm pathlength cuvettes. Cyclic voltammetry was carried out using a Bioanalytical Systems C3 electrochemical workstation. The working electrode was a 2 mm glassy carbon disk; the counter electrode was a platinum wire, and the reference electrode was $Ag/AgNO_3$. Spec-grade dichloromethane was purged with N_2 gas at room temperature prior to its use. Two cycles from +1.3 to −2.3 V at a scan rate of 100 mV/s were measured for the sample. Tetrabutylammonium hexafluorophosphate (0.1 M) was used as the supporting electrolyte, and decamethylferrocene was used as an internal reference. Mass spectroscopy was acquired on an AccuTOF GCx plus mass spectrometer (JEOL USA Inc., Peabody, Massachusetts, USA) equipped with an Electron Ionization (EI) ion source, or on a Kratos Concept - Magnetic sector Electron impact mass spectrometer, or on a Micromass Q-TOF I - Time of flight Electrospray Ionization mass spectrometer.

Synthesis of 6-(*tert*-butyl)-1*H*-benzo[*f*]isoindole-1,3(2*H*)-diimine (^{t}BuNp-DIII). To a solution of 6-*tert*-butyl-2,3-naphthalenedicarbonitrile (5.00 g, 21.34 mmol) in anhydrous toluene (60 mL) was added lithium bis(trimethylsilyl)amide etherate (6.18 g, 25.61 mmol) in one portion under a nitrogen atmosphere. After stirring the reaction mixture for 3 hours at room temperature, chlorotrimethylsilane (2.98 mL, 23.47 mmol) was added *via* a syringe in one portion and the reaction mixture was kept stirring overnight at room temperature. Lithium chloride was removed through filtration of the mixture. The solvent of the filtrate was then partially removed by rotary evaporation to about one-third of the initial volume and the crude was poured onto a silica gel plug. The latter was flushed with DCM (2 x 100 mL), EtOAc (2 x 100 mL) and MeOH until the dark green color fades. The MeOH fraction was concentrated under vacuum and the product was isolated from the residue by precipitation from the ether. The solids were collected by filtration, washed with ether and dried in air to afford a greenish-yellow fine powder. Yield: 3.33 g (62%). MS (EI) calcd for 251.14, found 251.15. ^{1}H NMR (δ, DMSO-d_6, RT, 300 MHz): 10.32 (br, 3H-NH), 8.57 (s, 1H-naphthalene), 8.55 (s, 1H-naphthalene), 7.87─8.08 (m, 3H-naphthalene), 1.41 (s, 9H-^{t}Bu). ^{13}C NMR (δ, DMSO-d_6, RT, 400 MHz): 175.36, 152.29, 150.95, 134.04, 132.10, 130.19, 130.01, 129.60, 128.26, 125.28, 124.70, 124.12, 34.92, 30.75. IR ν_{max} (cm^{-1}): 3006, 2954, 2905, 2868, 1655, 1543, 1509, 1459, 1365, 1341, 1309, 1263, 1280, 1262, 1152, 1130, 1048, 919, 817, 728.

Synthesis of silicon tetra(*tert*-butyl)-2,3-naphthalocyanine dichloride ((^{t}Bu)$_4$SiNPcCl$_2$). **^{t}BuNp-DIII** (1.00 g, 3.98 mmol) was placed into a flame-dried two-necked round-bottom flask under a nitrogen atmosphere. Freshly distilled quinoline (15 mL) was added *via* a syringe and the mixture was gently heated to 50°C for 10 minutes. Silicon tetrachloride (0.69 mL, 5.97 mmol) was added dropwise, and the reaction mixture was quickly heated to 200°C for 30 minutes under N_2.

After cooling to room temperature, the reaction mixture was poured into 150 mL MeOH and filtered over a Buchner funnel. The brown solids were washed with a small portion of toluene and then MeOH until the solvent became colorless. The resulting solid was then dissolved in DCM and filtered to remove insoluble impurities, the DCM in the filtrate was then removed by rotary evaporation, giving a lustrous green powder. Yield: 0.26 g (25%). MS (ESI) calcd for 1034.38, found 1034.63. ^{1}H NMR (δ, $CDCl_3$, RT, 300 MHz): 9.65 (8H-naphthalene), 8.35 (8H-naphthalene), 8.02 (4H-naphthalene), 1.25 (36H-^{t}Bu). IR ν_{max} (KBr, cm^{-1}): 2955, 2905, 2864, 1766, 1714, 1616, 1504, 1462, 1408, 1370, 1355, 1319, 1272, 1257, 1207, 1098, 1077, 945, 901, 887, 811, 749, 728, 644, 476.

Synthesis of bis(hydroxy) silicon tetra(*tert*-butyl)-2,3-naphthalocyanine ((^{t}Bu)$_4$SiNPc(OH)$_2$).[159] To an oven-dried two-necked round-bottom flask was added **(^{t}Bu)$_4$SiNPcCl$_2$** (0.20 g, 0.19 mmol), cesium hydroxide (50 wt% in water, 0.08 mL, 0.48 mmol), and DMF (2 mL) in one portion under a nitrogen atmosphere. The reaction mixture was heated to 120 °C for 4 hours. The crude product was precipitated into MeOH and filtered to give a dark green powder which was used for the subsequent axial substitution reaction without further purification. Yield: 0.26 g (85 %). MS (EI) calcd for 998.44, found 998.47. IR ν_{max} (cm^{-1}): 3444, 2953, 2904, 2862, 1618, 1458, 1370, 1358, 1319, 1271, 1257, 1207, 1070, 946, 902, 890, 831, 811, 751, 728.

Synthesis of bis(tri-*n*-propylsiloxy) silicon tetra(*tert*-butyl)-2,3-naphthalocyanine ((^{t}Bu)$_4$SiNPc(Pr$_3$OSi)$_2$). (^{t}Bu)$_4$SiNPc(OH)$_2$ (0.10 g, 0.10 mmol), chlorotripropylsilane (0.21 mL, 0.96 mmol) and toluene (5 mL) was placed into an oven-dried two-necked round-bottom flask under a nitrogen atmosphere. The reaction mixture was heated to 120 °C for 24 hours. After cooling to room temperature, the reaction mixture was poured into 100 mL MeOH and filtered

over a Buchner funnel. The solid was washed thoroughly with MeOH, and dried to afford a green powder. Yield: 0.08 g (61%). The crude solid was sublimed using a three-zone tube furnace (330–210–120 °C) to afford a green powder at a pressure of 10^{-5} torr (Yield: 66%). m.p. = 382 °C. MS (ESI) calcd for 1310.71, found 1310.71. ^{1}H NMR (δ, $CDCl_3$, RT, 300 MHz): 10.07 (d, 8H-ArH), 8.60 (d, 8H-ArH), 8.01 (d, 4H-ArH), 1.67 (s, 36H-^{t}Bu), −0.24 (t, 18H-CH_3), −0.85(m, 12H-βCH_2), −2.06(m, 12H-αCH_2). IR ν_{max} (cm^{-1}): 2950, 2906, 2863, 1619, 1508, 1459, 1370, 1356, 1321, 1271, 1258, 1202, 1098, 1081, 1023, 948, 901, 885, 811, 751, 728, 709.

Chapter 4 Metal-containing Tetra-2,3-pyrazinoporphyrazine (MPz)

4.1 Introduction

To date, most of the transition metals in the periodic table have been successfully incorporated into the center of the phthalocyanine molecule, as discussed in Section 1.6. Having said that, zinc phthalocyanines (ZnPcs) and cobalt phthalocyanines (CoPcs) present special interests with respect to this thesis due to their potential photoelectronic properties. Furthermore, they can be easily prepared and are non-toxic to the environment. For example, both ZnPc and CoPc are promising candidates for solar-cell applications[347,348] and organic thin-film transistors.[349–353] Here, we aim to tailor the Pc backbone (*i.e.*, enhance the electronegativity fo the Pc framework by replacing it with tetrapyrazinoporphyrazine) to obtain a series of MPzs, which may be effective as active materials in OFETs. Tetrapyrazinoporphyrazine is a phthalocyanine analog with nitrogen atoms replacing -CH- groups at position 1,4,10,13,22,28,31, as shown in Figure 4.1.[354] In this chapter, zinc tetra-2,3-pyrazinoporphyrazines (**ZnPzs**) and cobalt tetra-2,3-pyrazinoporphyrazines (**CoPzs**) were synthesized, and characterized by Nuclear magnetic resonance spectroscopy (NMR), Infrared spectroscopy (IR), UV-vis Spectroscopy (UV-vis), and Mass Spectroscopy (MS).

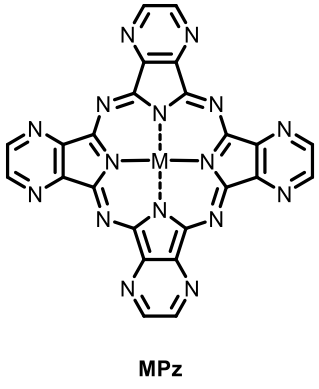

Figure 4.1 Structure of metal-containing tetra-2,3-pyrazinoporphyrazine.

4.2 Result and discussion

4.2.1 Synthesis of cobalt tetra-2,3-pyrazinoporphyrazine (CoPz) and zinc tetra-2,3-pyrazinoporphyrazine (ZnPz).

MPz complexes are easier to prepare compared to their Si counterparts since they can be directly synthesized in the single-step template reaction from 2,3-dicyanopyrazine and the metal precursor as outlined in Scheme 4.1, thus DIII is no longer required as was the case for Si-based materials.[355] The reactions were carried out under an inert atmosphere, not only to prevent the hydrolysis of the nitrile groups but also to avoid unwanted oxidation of the metal cation.[355] Dissolving the 2,3-dicyanopyrazine in *n*-pentanol afforded a brown solution, which turned green upon the addition of $CoCl_2 \cdot 6H_2O$ and blue with the addition of $ZnCl_2$. To complete the reaction, 1,8-diazabicyclo(5.4.0)undec-7-ene (DBU) was added, which effectively catalyzes the cyclotetramerization of 2,3-dicyanopyrazine in solution. After refluxing for two hours, the reaction mixture turned darker in color. The solid was then isolated by filtration and washed with water and ethanol as described in the experimental section. The solubility of the as-produced complexes were tested, the results of which are summarized in Table 4.1. The products exhibit poor solubility in most organic solvents, with slight solubility in polar aprotic solvents such as DMSO, DMF and NMP. In addition, tetra-2,3-pyrazinoporphyrazine cannot be sublimed.[325] More specifically, sublimation either at a pressure of 10^{-5} torr or with carbon dioxide as the carrier gas was insufficient to sublime the material even at temperatures up to 400 °C. Both factors led to difficulty in the purification of MPzs.

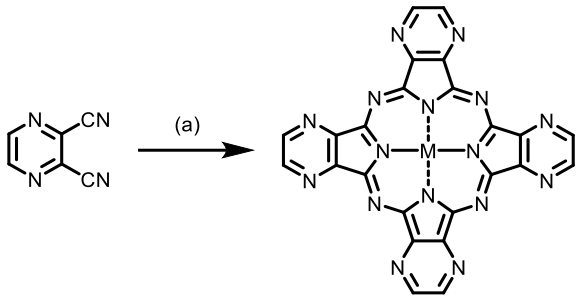

Scheme 4.1 Synthetic routes toward the preparation of MPz, M = Co or Zn. Reagents and conditions: (a) $CoCl_2 \cdot 6H_2O$ or $ZnCl_2$, DBU, *n*-pentanol, 140 °C, 2 h.

Table 4.1 Solubility test of **CoPz** and **ZnPz**.

Solvent	CoPz		ZnPz	
	RT	**Heating**	**RT**	**Heating**
DCM	++[a]	+++	+	+
$CHCl_3$	++	+++	−	−
MeOH	+	+	−	−
EtOH	++	+++	+	+
Isopropanol	−	−	+	+
Acetone	−	−	+	++
Toluene	−	−	+	+
Chlorobenzene	+	++	−	−
Dichlorobenzene	+	++	+	++
DMF	++++		++++	
DMSO	++++		++++	
Acetonitrile	+	+++	+	++
Ether	−	−	−	−

Hexane	−	−	−	−
EtOAc	−	−	−	+
Dioxane	+	++	+	++
NMP	++++		++++	

a. Cannot dissolve (−) > Silghtly dissolve (+) > Partially dissolve (++) > Mostly dissolve (+++) > Totally dissolve (++++).

The FTIR spectra of **CoPz** and **ZnPz** are shown in Figure 4.2. In the case of **CoPz**, the peak at ca. 758 cm^{-1} shows the in-plane C–N–C bend. The spectrum also indicates the C–H bend at ca. 1155 cm^{-1}, a strong C–C stretch peak at ca. 1366 cm^{-1}, and the C=N stretch at 1548 cm^{-1}. The spectrum of **ZnPz** indicates the in-plane C–N–C bend at ca. 753 cm^{-1}, the C–H bend at ca. 1189 cm^{-1}, a C–C stretch peak at ca. 1361 cm^{-1}, and the C=N stretch at 1537 cm^{-1}. The peaks of Co–N and Zn–N are at ca. 934 cm^{-1} and 904 cm^{-1}, respectively. Small shifts between the Pzs are expected due to the different metals.

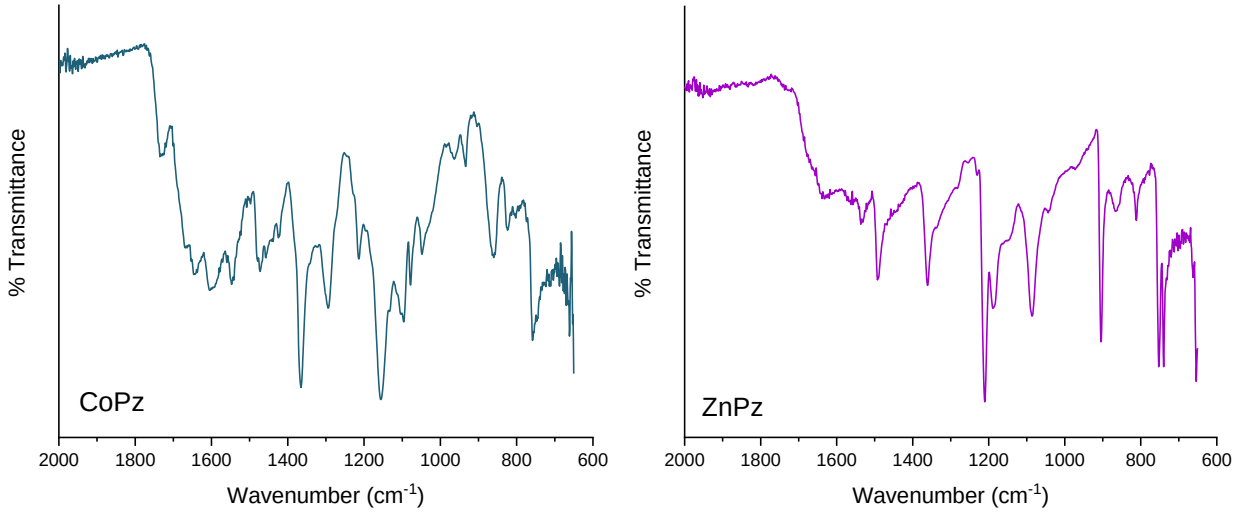

Figure 4.2 FTIR spectrum of **CoPz** and **ZnPz**.

The structures of MPzs were also confirmed by ^{1}H NMR, shown in Figure 4.3. The NMR clearly indicates the formation of the highly symmetric complex, with only one type of chemically different hydrogen atom which shows a chemical shift at approximately 9.5 ppm. Attempts to perform ^{13}C NMR were unfortunately unsuccessful due to aggregation. The EI-MS data also confirmed the mass peaks of **CoPz** and **ZnPz** at *m/z* 579.25 and 584.04, respectively (Figure 4.4). Attempts to recrystallize or sublime were unsuccessful.

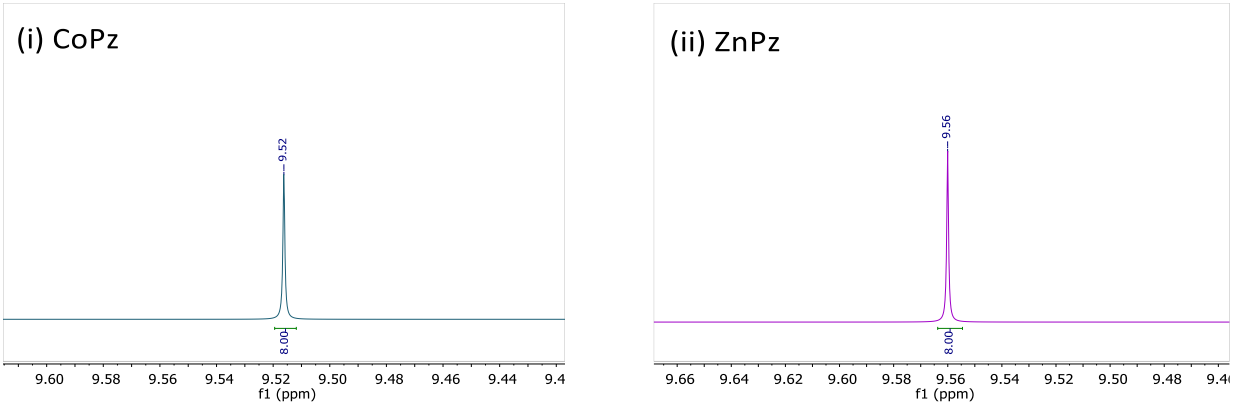

Figure 4.3 ^{1}H NMR spectrum of (i) **CoPz** and (ii) **ZnPz** in DMSO-d_6. (i) 9.52 (s, 8H-pyrazino), (ii) 9.56 (s, 8H-pyrazino).

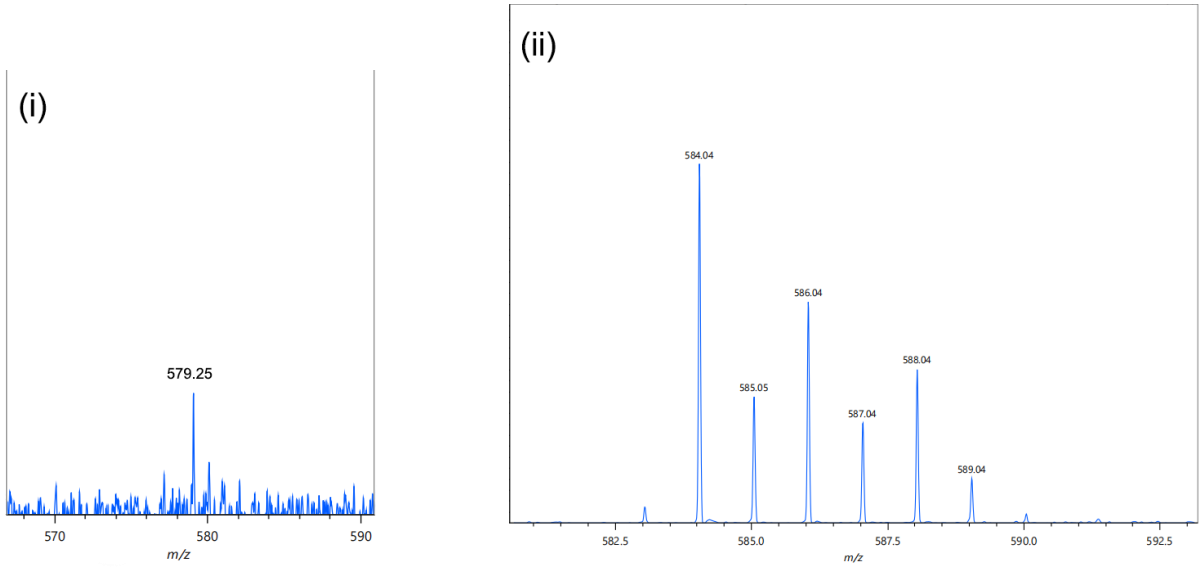

Figure 4.4 EI-MS spectrum of (i) **CoPz** (*m/z* 579.25) and (ii) **ZnPz** (*m/z* 584.04).

4.2.2 Optical studies

UV-vis spectroscopy was utilized to study the absorptive behavior of MPzs. As mentioned in Section 2.2.3, the central atom will influence the *Q*-band position. With the decrease in electronegativity of the central metal, the *Q*-band usually shifts to red. In this case, the transition from Co → Zn results in a redshift of the lowest energy π-π* excitation (Figure 4.5). Such trends are explicable in terms of decreasing electronegativity of metal ion, which shifts charge onto the ring and raises the energy of the $a_{2u}(\pi)$ HOMO.[150, 356] In addition, the extreme red emission of **ZnPz** and **CoPz** under visible light in DMSO was observed, as shown in Figure 4.6. Cyclic voltammograms of the compounds were not obtained due to their very poor solubility.

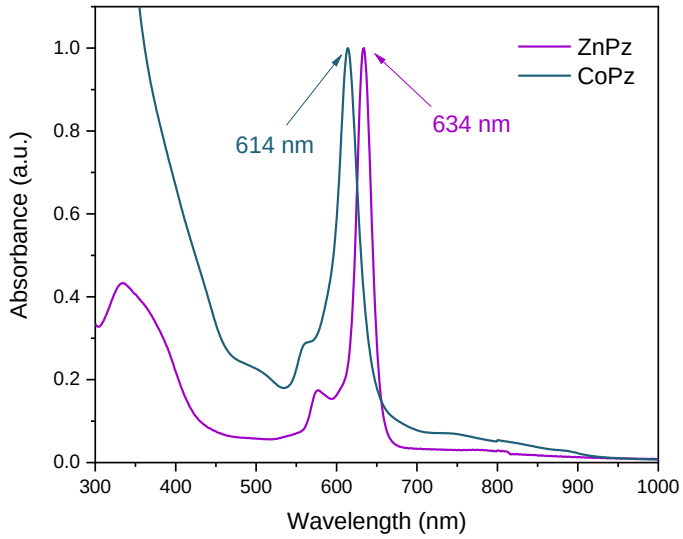

Figure 4.5 Normalized UV-vis spectra of **CoPz** and **ZnPz** in DMSO solutions. λ_{max}**CoPz** = 614 nm, λ_{max}**ZnPz** = 634 nm.

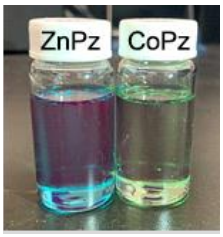

Figure 4.6 Solution of **ZnPz** (left) and **CoPz** (right) in DMSO.

4.3 Conclusion

In conclusion, two types of metal-containing tetra-2,3-pyrazinoporphyrazines **CoPz** and **ZnPz** were synthesized and characterized. Compared to normal Pcs, the substitution of CH groups in the Pc macrocycle for nitrogen atoms leads to an obvious hypsochromic shift of the *Q*-band position. However, their applications are limited due to challenges with purification.

4.4 Future work

Since unsubstituted MPzs cannot be either sublimed or purified by recrystallization or chromatographic methods due to their poor solubility in most organic solvents, their characterization proved difficult, limiting their applicability. Future work may focus on growing MPz crystals. Apart from this, the investigation of MPzs substituted with various peripheral patterns which can effectively improve their solubility will be worthwhile to try. In addition, different metals, such as lanthanides, may be introduced into the center of the Pzs to form sandwich complexes.

4.5 Experimental section

Materials and methods.

$CoCl_2 \cdot 6H_2O$ (Sigma-Aldrich), $ZnCl_2$ (Sigma-Aldrich), DBU (Sigma-Aldrich) and *n*-pentanol (Aldrich) were obtained commercially and used as received. 2,3-Dicyanopyrazine was prepared by published methods.[338]

All reactions were performed under an atmosphere of dry nitrogen. NMR spectra were run in DMSO-d_6 solution at room temperature on a Bruker Avance 400 MHz spectrometer (Billerica, MA, USA). IR spectra of solid samples were recorded on an Agilent Technologies Cary 630 FT-IR spectrometer using Attenuated Total Reflection. UV-vis absorption spectra were measured

using an Agilent Cary 5000 UV-Vis-NIR spectrophotometer in the range 300 – 1000 nm. Solution absorption measurements were completed using DMSO solutions with standard 10 mm pathlength cuvettes. Mass spectroscopy was acquired on an AccuTOF GCx plus mass spectrometer (JEOL USA Inc., Peabody, Massachusetts, USA) equipped with an Electron Ionization (EI) ion source.

Synthesis of cobalt tetra-2,3-pyrazinoporphyrazine (CoPz).[355] 2,3-Dicyanopyrazine (0.51 g, 3.90 mmol) and $CoCl_2 \cdot 6H_2O$ (0.24 g, 1.00 mmol) were dissolved in *n*-pentanol (2.00 mL). DBU (0.10 mL, 0.70 mmol) was added, and the mixture was heated for 2 hours at 140 °C, forming a dark green solution. The reaction was cooled down to ambient temperature, filtered under vacuum and washed with water (5 x 10 mL) and then with EtOH (5 x 10 mL). This gave a dark green powder. Yield: 0.54 g (93%). ^{1}H NMR (δ, DMSO-d_6, RT, 400 MHz): 9.52 (s, 8H-pyrazino). MS (EI) calcd for 579.04, found 579.25. IR ν_{max} (cm^{-1}): 1735, 1644, 1604, 1548, 1473, 1424, 1366, 1294, 1214, 1155, 1096, 1078, 1048, 963, 934, 860, 824, 758.

Synthesis of zinc tetra-2,3-pyrazinoporphyrazine (ZnPz).[355] The synthesis of **ZnPz** was performed under similar conditions to that of **CoPz**, except for using $ZnCl_2$ as the source of Zn. Yield: 0.54 g (94%). MS (EI) calcd for 584.04, found 584.04. ^{1}H NMR (δ, DMSO-d_6, RT, 400 MHz): 9.56 (s, 8H-pyrazino). IR ν_{max} (cm^{-1}): 1638, 1537, 1493, 1361, 1210, 1189, 1086, 973, 904, 866, 812, 753, 740.

Chapter 5 Conclusions and future directions

5.1 Conclusions

This thesis describes the synthesis and study of a family of novel phthalocyanine derivatives. Silicon phthalocyanines (SiPcs) are of particular interest as they have two axial substituents that enable modification, thereby providing a facile avenue for functionalization.[152] To that end, a series of axially substituted silicon tetra-2,3-pyrazinoporphyrazine (**SiPz**) and silicon tetra(*tert*-butyl)-2,3-naphthalocyanine complexes (**(^{t}Bu)$_4$SiNPc**) were prepared and characterized.

Chapter 2 describes the synthesis and characterization of silicon tetra-2,3-pyrazinoporphyrazine derivatives (**SiPzs**). In order to make **SiPzCl$_2$**, two synthetic routes were explored using phthalonitrile as the starting material. The poor solubility of **SiPzCl$_2$** can be overcome by introducing alkylsiloxy chains to the axial position of Pzs. The two synthesized bissilyloxy derivatives, **SiPz(^{t}BuMe$_2$OSi)$_2$** and **SiPz(Et$_3$OSi)$_2$**, exhibit hypsochromic shifts in their main absorption band (*Q*-band) and possess lower HOMO and LUMO energy levels compared to SiPcs, due to the isosteric substitution of CH groups in Pc macrocycle for nitrogen atoms. In addition, the solubility of **SiPz(^{t}BuMe$_2$OSi)$_2$** and **SiPz(Et$_3$OSi)$_2$** was improved, since the two alkylsiloxy substituents bring very good inhibition of aggregation. For those reasons, **SiPz** might be a promising air-stable *n*-type semiconducting material in OFETs. Although this thesis presents the synthesis and characterization of **SiPz(^{t}BuMe$_2$OSi)$_2$** and **SiPz(Et$_3$OSi)$_2$**, pure material remains elusive. Having said that, purification *via* different crystallization techniques may be achievable. For example, vapor diffusion crystallization was tried to purify **SiPz(Et$_3$OSi)$_2$** as mentioned in **Chpater 2**; however, due to time constraints, further attempts will be completed in the future.

The synthesis and characterization of axial substituted silicon tetra(*tert*-butyl)-2,3-naphthalocyanine complexes (**(^{t}Bu)$_4$SiNPc**) was studied in **Chapter 3**. Those complexes are soluble in most of the organic solvents, due to the reduced tendency of aggregation resulting from the presence of ^{t}Bu groups and the introduction of the bulky tripropylsilyloxide side groups. Compared to normal SiPcs, the extension of π-conjugation leads to obvious bathochromic shifts in their main absorption band (*Q*-band). Due to time constraints, there is only one axial substituted derivative **(^{t}Bu)$_4$SiNPc(Pr$_3$OSi)$_2$** that was synthesized and characterized; more derivatives will be investigated in the future.

In **Chapter 4**, two types of transition-metal tetra-2,3-pyrazinoporphyrazines were prepared, which are **CoPz** and **ZnPz**. However, their very poor solubility leads to purification difficulty, thereby restricting their applications. Overall, this thesis detailed a series of novel phthalocyanine complexes, providing more possibilities of potential semiconducting materials for OFETs.

5.2 Future work

Exploring various novel phthalocyanine materials to be employed as the semiconducting active layer in organic field-effect transistors (OFETs) has been a long-standing goal of this project. Future investigation for silicon tetra-2,3-pyrazinoporphyrazine complexes (**SiPzs**) that were discussed in **Chapter 2** will focus on obtaining analytical pure compounds and exploring their application in OFETs. Diverse axial substituted derivatives are also expected to be studied. In addition, efforts to improve the solubility of **SiPz** compounds have been made by our group by attaching alkyl chains into the peripheral positions of the Pz molecule. Similarly, more axial substituted silicon tetra(*tert*-butyl)-2,3-naphthalocyanine complexes (**(^{t}Bu)$_4$SiNPcs**, **Chapter 3**) derivatives should be further explored. Bis(tri-*n*-propylsiloxy) silicon tetra(*tert*-butyl)-2,3-naphthalocyanine (**(^{t}Bu)$_4$SiNPc(Pr$_3$OSi)$_2$**) still remain to be tested for its OFET applicability.

Device testing should provide valuable feedback toward further refining the molecular structure. Metal-containing tetra-2,3-pyrazinoporphyrazine complexes (**MPz**, **Chapter 4**) also demand further research attention. Lanthanides in general are a very interesting topic, thus our group is currently exploring introducing lanthanides into the center of Pz molecule to form sandwich complexes.

Appendix A: Tables from Chapter 1

Table A.1 Field-effect performances for Group 13 main-group phthalocyanines in organic thin-tape transistors. Reproduced from Ref. 35 with permission from the Royal Society of Chemistry.

Organic Semiconductor	Gate/Insulator	Inducing Layer	S/D Contact	Structure	Deposit Temp. (°C)	Type (n/p)	V_T[a] (V)	μ[a] ($cm^2/V{\cdot}s$)	I_{on}/I_{off}[a]	Ref.
Cl-BSubPc[b]	Au/ Parylene-C	None	Ca/Ag	TC/BG	N/A	*n*	11	5.4×10^{-5}	N/A	62
Cl-BSubPc[b]	Au/ Parylene-C	None	Au	TC/BG	N/A	*n*	45	1.2×10^{-5}	N/A	62
Cl-BSubPc[b,d]	Au/ Parylene-C	None	Au	TC/BG	N/A	*p*	N/A	7.5×10^{-7}	N/A	62
Cl-AlPc[b]	Si/SiO_2	None	N/A	TC/BG	25	*p*	N/A	1×10^{-4}	N/A	55
Cl-AlPc[b]	Si/SiO_2	None	N/A	TC/BG	120	*p*	N/A	1×10^{-6}	N/A	55
Cl-AlPc[b]	Si/SiO_2	OTS	N/A	TC/BG	120	*p*	N/A	6×10^{-2}	N/A	55
Cl-AlPc[b]	Si/SiO_2	OTS	Au	BC/BG	120	*p*	−13	1×10^{-3}	10^4	33
Cl-AlPc[b,d]	Si/SiO_2	OTS	Au	BC/BG	120	*p*	2	4×10^{-2}	10^4	33
Cl-Al(F_{16})Pc[c]	Grid/Ta_2O_5 or SiO_2 or Al_2O_3	OTS	Al	TC/BG	25-250	*n*	N/A	1.2×10^{-2}	10^5	56
Cl-Al(F_{16})Pc[c]	Grid/Ta_2O_5 or SiO_2 or Al_2O_3	*p*-6p	Al	TC/BG	25-250	*n*	N/A	2.3×10^{-2}	10^5	56
Cl-Al(F_{16})Pc[c]	Grid/Ta_2O_5 or SiO_2 or Al_2O_3	OTS	Au	TC/BG	25-250	*n*	N/A	1.0×10^{-2}	10^5	56
Cl-Al(F_{16})Pc[c]	Grid/Ta_2O_5 or SiO_2 or Al_2O_3	*p*-6p	Au	TC/BG	25-250	*n*	N/A	1.7×10^{-2}	10^5	56
Cl-Al(Cl_{16})Pc[c]	Grid/Ta_2O_5 or SiO_2 or Al_2O_3	OTS	Al	TC/BG	25-250	*n*	N/A	1.4×10^{-2}	10^5	56
Cl-Al(Cl_{16})Pc[c]	Grid/Ta_2O_5 or SiO_2 or Al_2O_3	*p*-6p	Al	TC/BG	25-250	*n*	N/A	2.2×10^{-2}	10^5	56
Cl-Al(Cl_{16})Pc[c]	Grid/Ta_2O_5 or SiO_2 or Al_2O_3	OTS	Au	TC/BG	25-250	*n*	N/A	1.3×10^{-2}	10^5	56
Cl-Al(Cl_{16})Pc[c]	Grid/Ta_2O_5 or SiO_2 or Al_2O_3	*p*-6p	Au	TC/BG	25-250	*n*	N/A	1.7×10^{-2}	10^5	56
HO-Al($SO_3Na)_{1.5}$ Pc[c]	Si/SiO_2	None	Cr/Au	N/A	–	*p*	−1.4	2×10^{-2}	10^3	194

HO-Al(SO_3Na)$_{1.5}$ Pc[c]	Al/SiO_2	None	Cr/Au	N/A	–	*p*	−1.4	2×10^{-2}	10^3	195
Cl-GaPc[b]	Grid/Ta_2O_5 or SiO_2 or Al_2O_3/PMMA	None	Au	TC/BG	25-250	*p*	N/A	1×10^{-2}	10^5	56
Cl-InPc[b]	PET with ITO/ nylon 11 and Al_2O_3	None	Ag	TC/BG	24	*p*	0.59	36.2	N/A	196
Cl-InPc[b]	Grid/Ta_2O_5 or SiO_2 or Al_2O_3/PMMA	None	Au	TC/BG	25-250	*p*	N/A	2.5×10^{-2}	10^5	56
F-InPc[c]	Grid/Ta_2O_5 or SiO_2 or Al_2O_3	OTS	Al	TC/BG	25-250	*n*	N/A	1×10^{-2}	10^5	56
F-InPc[c]	Grid/Ta_2O_5 or SiO_2 or Al_2O_3	*p*-6p	Al	TC/BG	25-250	*n*	N/A	1.8×10^{-2}	10^5	56
F-InPc[c]	Grid/Ta_2O_5 or SiO_2 or Al_2O_3	OTS	Au	TC/BG	25-250	*n*	N/A	5.1×10^{-2}	10^5	56
F-InPc[c]	Grid/Ta_2O_5 or SiO_2 or Al_2O_3	*p*-6p	Au	TC/BG	25-250	*n*	N/A	7.4×10^{-2}	10^5	56
Cl-In(F_{16})Pc[c]	Grid/Ta_2O_5 or SiO_2 or Al_2O_3	OTS	Al	TC/BG	25-250	*n*	N/A	1.5×10^{-2}	10^5	56
Cl-In(F_{16})Pc[c]	Grid/Ta_2O_5 or SiO_2 or Al_2O_3	*p*-6p	Al	TC/BG	25-250	*n*	N/A	2.1×10^{-1}	10^5	56
Cl-In(F_{16})Pc[c]	Grid/Ta_2O_5 or SiO_2 or Al_2O_3	OTS	Au	TC/BG	25-250	*n*	N/A	1.2×10^{-2}	10^5	56
Cl-In(F_{16})Pc[c]	Grid/Ta_2O_5 or SiO_2 or Al_2O_3	*p*-6p	Au	TC/BG	25-250	*n*	N/A	2.7×10^{-1}	10^5	56
Cl-In(Cl_{16})Pc[c]	Grid/Ta_2O_5 or SiO_2 or Al_2O_3	OTS	Al	TC/BG	25-250	*n*	N/A	1.5×10^{-2}	10^5	56
Cl-In(Cl_{16})Pc[c]	Grid/Ta_2O_5 or SiO_2 or Al_2O_3	*p*-6p	Al	TC/BG	25-250	*n*	N/A	1.9×10^{-2}	10^5	56
Cl-In(Cl_{16})Pc[c]	Grid/Ta_2O_5 or SiO_2 or Al_2O_3	OTS	Au	TC/BG	25-250	*n*	N/A	1.6×10^{-1}	10^5	56
Cl-In(Cl_{16})Pc[c]	Grid/Ta_2O_5 or SiO_2 or Al_2O_3	*p*-6p	Au	TC/BG	25-250	*n*	N/A	2.1×10^{-1}	10^5	56

[a] S/D: Source and drain electrodes; μ: best reported carrier (hole for p-channel, electron for n-channel) mobility; V_T: best reported threshold voltage; I_{on}/I_{off}: on/off current ratio. [b] Commercially available. [c] Prepared in the lab. [d] Performed in air

Table A.2 Field-effect performances for Group 14 main-group phthalocyanines in organic thin-film transistors. Reproduced from Ref. 35 with permission from the Royal Society of Chemistry.

Organic Semiconductor	Gate/Insulator	Inducing Layer	Structure	Deposit Temp. (°C)	S/D Contact [a]	Type (*n*/*p*)	V_T [a] (V)	μ [a] ($cm^2/V{\cdot}s$)	I_{on}/I_{off} [a]	Ref.
$(PhCOO)_2$-SiPc [c]	Si/SiO_2	Plasma	BC/BG	200	Au	*n*	26.3±3.2	5.55×10^{-4}	10^2-10^3	32
$(PhCOO)_2$-SiPc [c]	Si/SiO_2	OTS	BC/BG	200	Au	*n*	26.9±2.9	1.07×10^{-2}	10^4-10^5	32
$(PhCOO)_2$-SiPc [c]	Si/SiO_2	ODTS	BC/BG	200	Au	*n*	21.3±2.1	1.35×10^{-2}	10^3-10^5	32
$(PhCOO)_2$-SiPc [c]	Si/SiO_2	FOTS	BC/BG	200	Au	*n*	22.2±1.7	8.56×10^{-5}	10^2-10^4	32
$(1\text{-NpCOO})_2$-SiPc [c]	Si/SiO_2	Plasma	BC/BG	100	Au	*n*	17.5±2.7	3.28×10^{-4}	10^2-10^3	32
$(9\text{-AnCOO})_2$-SiPc [c]	Si/SiO_2	Plasma	BC/BG	100	Au	*n*	15.0±0.6	5.56×10^{-5}	10^1-10^2	32
Cl_2-SiPc [b]	Si/SiO_2	OTS	BC/BG	140	Au/ITO	*n*	37.2±14.1	9.73×10^{-2}	10^5	38
$(2,4,6\text{-}F_3PhO)_2$-SiPc [c]	Si/SiO_2	OTS	BC/BG	140	Au/ITO	*n*	35.2±3.4	4.31×10^{-2}	10^4-10^5	38
$(3,4,5\text{-}F_5PhO)_2$-SiPc [c]	Si/SiO_2	OTS	BC/BG	140	Au/ITO	*n*	17.1±7.5	3.14×10^{-2}	10^4-10^5	38
$(F_5PhO)_2$-SiPc [c]	Si/SiO_2	OTS	BC/BG	140	Au/ITO	*n*	12.0±4.8	5.37×10^{-1}	10^4-10^5	38
$(F_5PhO)_2$-SiPc [c]	Si/SiO_2	OTS	TC/BG	25	Au	*n*	23.5±0.4	2.7×10^{-1}	N/A	34
$(F_5PhO)_2$-SiPc [c]	Si/SiO_2	OTS	TC/BG	25	Au/Cr	*n*	13.4±1.4	1.5×10^{-1}	N/A	34
$(F_5PhO)_2$-SiPc [c]	Si/SiO_2	OTS	TC/BG	25	Au/Mn	*n*	10.0±2.1	1.9×10^{-1}	N/A	34
$(F_5PhO)_2$-SiPc [c]	Si/SiO_2	OTS	TC/BG	25	Au/BCP	*n*	12.4±1.3	1.8×10^{-1}	N/A	34
$(F_5PhO)_2$-SiPc [c]	Si/SiO_2	OTS	TC/BG	25	Ag	*n*	28.7±1.7	1.7×10^{-1}	N/A	34
$(F_5PhO)_2$-SiPc [c]	Si/SiO_2	OTS	TC/BG	25	Ag/Cr	*n*	20.8±2.1	9.0×10^{-2}	N/A	34
$(F_5PhO)_2$-SiPc [c]	Si/SiO_2	OTS	TC/BG	25	Ag/Mn	*n*	7.8±1.4	1.7×10^{-1}	N/A	34
$(F_5PhO)_2$-SiPc [c]	Si/SiO_2	OTS	TC/BG	25	Ag/BCP	*n*	23.9±1.6	2.1×10^{-1}	N/A	34
$((Bu)_3SiO)_2SiPc$	Si/SiO_2	OTS	BC/BG	100	Au/ITO	*n*	21.8±1.8	14.4×10^{-5}	10^2-10^3	179
$((Bu)_3SiO)_2SiPc$	Si/SiO_2	OTS	BC/BG	150	Au/ITO	*n*	21.8±0.69	159×10^{-5}	10^2-10^3	179
$((Hx)_3SiO)_2SiPc$	Si/SiO_2	OTS	BC/BG	100	Au/ITO	*n*	22.4±1.0	2.66×10^{-5}	10-10^4	179
$((Hx)_3SiO)_2SiPc$	Si/SiO_2	OTS	BC/BG	150	Au/ITO	*n*	25.4±1.1	1.62×10^{-5}	10-10^3	179
Cl_2-GePc [b]	Grid/Ta_2O_5 [d]	OTS	TC/BG	25-250	Au	*p*	N/A	6.1×10^{-2}	10^5	56
Cl_2-GePc [b]	Grid/Ta_2O_5 [d]	*p*-6P	TC/BG	25-250	Au	*p*	N/A	9.0×10^{-1}	10^5	56
SnPc [b]	Au/SiO_2	None	BC/BG	30	Au	*p*	N/A	7.3×10^{-5}	N/A	357
SnPc [b]	Au/SiO_2	None	BC/BG	125	Au	*p*	N/A	3.4×10^{-5}	N/A	357
SnPc [b]	Au/SiO_2	None	BC/BG	200	Au	*p*	N/A	No field effect	N/A	357
Cl_2-SnPc [b]	Al/SiO_2	None	TC/BG	60	Ag	*n*	4	1.0×10^{-2}	10^4	52

Cl_2-SnPc [b]	Si/SiO_2	*p*-6P	TC/BG	180	Au	*n*	27	3.0×10^{-1}	10^6	53
O-SnPc [b]	Si/SiO_2	*p*-6P	TC/BG	180	Au	*n*	37	4.4×10^{-1}	10^3	57
$((Bu)_3SiO)_2SiPc$	Si/SiO_2	OTS	BC/BG	100	Au/ITO	*n*	0.21±0.68	44.0×10^{-5}	10	179
$((Bu)_3SiO)_2SiPc$	Si/SiO_2	OTS	BC/BG	150	Au/ITO	*n*	−2.90±1.2	9.16×10^{-5}	1-10	179
$((Hx)_3SiO)_2SiPc$	Si/SiO_2	OTS	BC/BG	100	Au/ITO	*n*	9.26±1.1	12.6×10^{-5}	$10\text{-}10^2$	179
$((Hx)_3SiO)_2SiPc$	Si/SiO_2	OTS	BC/BG	150	Au/ITO	*n*	6.79±0.97	17.6×10^{-5}	$10\text{-}10^2$	179
Cl_2-Sn(F_{16})Pc [c]	Si/SiO_2	*p*-6P	TC/BG	180	Au	*n*	7.62	8.5×10^{-4}	N/A	358
Cl_2-Sn(F_{16})Pc [c]	Grid/Ta_2O_5 [d]	OTS	TC/BG	25-250	Al	*n*	N/A	1.0×10^{-2}	10^5	56
Cl_2-Sn(F_{16})Pc [c]	Grid/Ta_2O_5 [d]	*p*-6P	TC/BG	25-250	Al	*n*	N/A	1.1×10^{-1}	10^5	56
Cl_2-Sn(F_{16})Pc [c]	Grid/Ta_2O_5 [d]	OTS	TC/BG	25-250	Au	*n*	N/A	1.3×10^{-2}	10^5	56
Cl_2-Sn(F_{16})Pc [c]	Grid/Ta_2O_5 [d]	*p*-6P	TC/BG	25-250	Au	*n*	N/A	2.4×10^{-1}	10^5	56
Cl_2-Sn(F_{16})Pc [c]	Grid/Ta_2O_5 [d]	OTS	TC/BG	25-250	Al	*n*	N/A	1.2×10^{-2}	10^5	56
Cl_2-Sn(F_{16})Pc [c]	Grid/Ta_2O_5 [d]	*p*-6P	TC/BG	25-250	Al	*n*	N/A	1.7×10^{-2}	10^5	56
Cl_2-Sn(F_{16})Pc [c]	Grid/Ta_2O_5 [d]	OTS	TC/BG	25-250	Au	*n*	N/A	2.3×10^{-2}	10^5	56
Cl_2-Sn(F_{16})Pc [c]	Grid/Ta_2O_5 [d]	*p*-6P	TC/BG	25-250	Au	*n*	N/A	1.7×10^{-1}	10^5	56
PbPc [b]	Si/SiO_2	None	TC/BG	N/A	Au	*p* [e]	−82 [e]	1.4×10^{-5} [e]	N/A	199
						p [f]	N/A [f]	3.0×10^{-5} [f]	N/A [f]	
						n [f]	N/A [f]	1.8×10^{-5} [f]	N/A [f]	
PbPc [b]	Au/Parylene-C	None	TC/BG	N/A	Au	*n*	45	1.3×10^{-3}	N/A	51
						p	−27	4.2×10^{-3}	N/A	
PbPc [b]	Au/Parylene-C	None	TC/BG	N/A	Ca	*n*	31	2.0×10^{-3}	N/A	51
						p	−22	1.8×10^{-3}	N/A	
Pb (C_6H_{13})$_8$Pc [c]	ITO/PVA [a]	None	TC/BG	–	Au	*p*	N/A	N/A	N/A	200

[a] S/D: Source and drain electrodes; μ: best reported carrier (hole for *p*-channel, electron for *n*-channel) mobility; V_T: best reported threshold voltage; I_{on}/I_{off}: on/off current ratio; PVA: Polyvinyl alcohol. [b] Commercially available. [c] Prepared in the lab. [d] or SiO_2 or Al_2O_3. [e] Performed in dark. [f] Performed in light.

Table A.3 Mean field-effect mobility (μ) and threshold voltage (V_T) of OTFTs using X_2-SiPc as semiconductors deposited at 140 °C characterized in both vacuum (P < 0.1 Pa) and in air. Results were obtained both in hole accumulation (V_{GS}, V_{DS} < 0 V) and electron accumulation (V_{GS}, V_{DS} > 0 V) regions under both environmental conditions. Reproduced from Ref. 35 with permission from the Royal Society of Chemistry.

Organic semiconductor		*n*-type (V_{GS}, V_{DS} > 0 V)		*p*-type (V_{GS}, V_{DS} < 0 V)	
		Vacuum	Air	Vacuum	Air
Cl_2-SiPc[a]	μ[b]	1.55×10^{-2}	5.18×10^{-5}	N/A	N/A
	V_T[c]	35.3	39.9	N/A	N/A
$(F_5PhO)_2$-SiPc[d]	μ[b]	4.87×10^{-2}	6.40×10^{-3}	4.92×10^{-5}	4.16×10^{-3}
	V_T[c]	15.1	29.3	−60.5	−30.7
$(2,4,6\text{-}F_3PhO)_2$-SiPc[d]	μ[b]	2.90×10^{-2}	2.47×10^{-5}	1.51×10^{-3}	1.93×10^{-2}
	V_T[c]	32.6	45.4	−45.6	−26.0
$(3,4,5\text{-}F_3PhO)_2$-SiPc [d]	μ[b]	1.72×10^{-2}	2.95×10^{-4}	2.17×10^{-5}	2.37×10^{-3}
	V_T[c]	23.3	35.1	−58.4	−30.3

[a] Commercially available. [b] In units of $cm^2/V{\cdot}s$. [c] In units of V. [d] Prepared in the lab.

Appendix B: Copyright Permission

The copyright permission for the reproduction of material from the articles “From chemical curiosity to versatile building blocks: unmasking the hidden potential of main-group phthalocyanines in organic field-effect transistors”[35] can be seeing bellow.

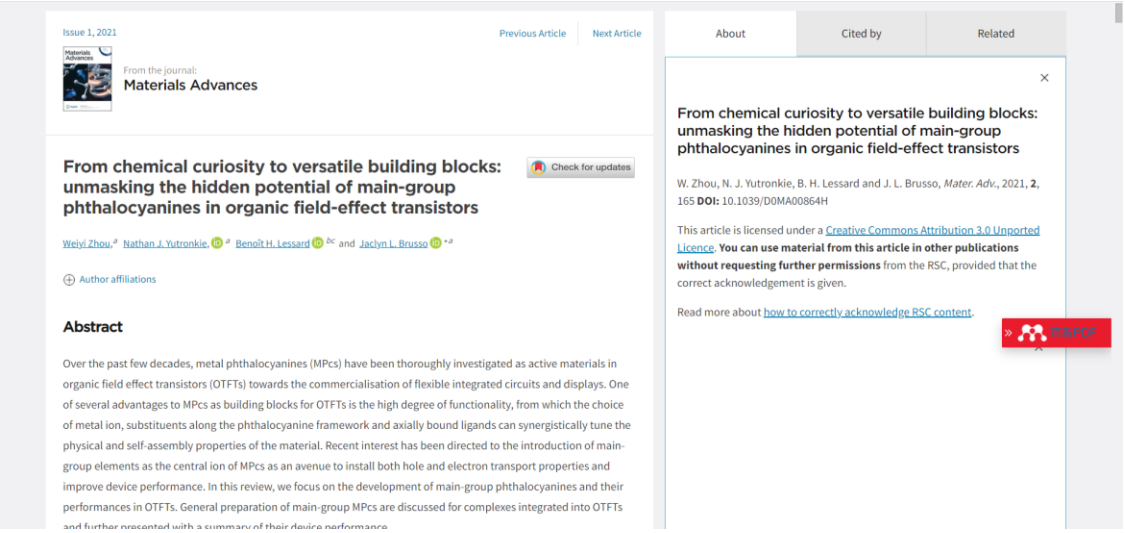

The copyright permission for the reproduction of material from the articles “Regiospecific synthesis of tetrasubstituted phthalocyanines and their liquid crystalline order”[333] can be seeing bellow.

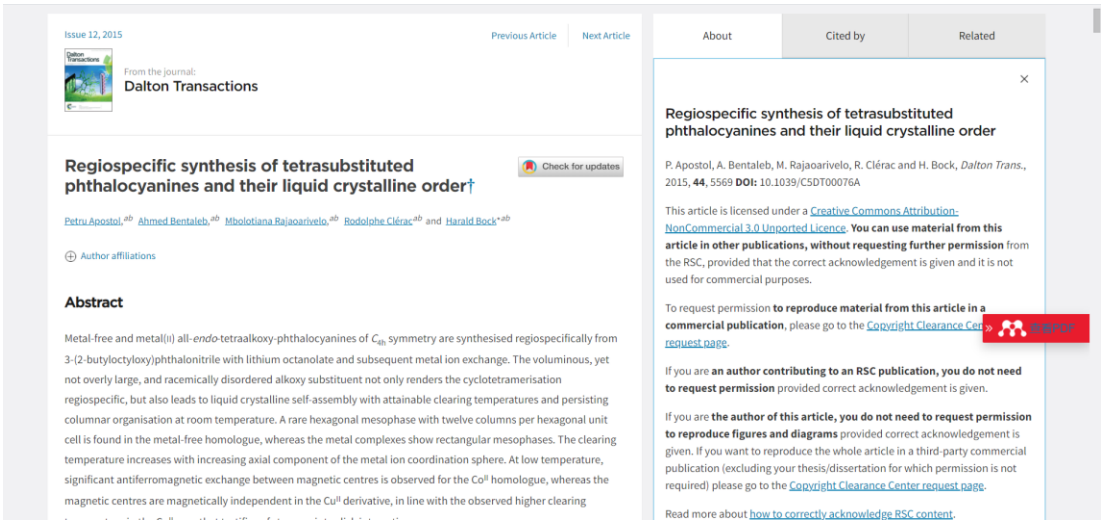

Reference

(1) Gregory, P. *J. Porphyr. Phthalocyanines* **2000**, *04* (04), 432–437.

(2) Linstead, R. P. *J. Chem. Soc.* **1934**, 1016–1017.

(3) Robertson, J. M. *J. Chem. Soc.* **1935**, 615–621.

(4) *Phthalocyanines, Properties and Applications, Volumes 1-4*; Leznoff, C. C., Lever, A. B. P., Eds.; VCH: Weinheim, Germany, 1996.

(5) Ishii, K.; Kobayaski, N. In *The Porphyrin Handbook, Volume 16*; Kadish, K. M., Smith, K. M., Guilard, R., Eds.; Academic Press: New York, 2003; Vol. 16, pp 1–42.

(6) Mack, J.; Stillman, M. J. In *The Porphyrin Handbook*; Kadish, K. M., Smith, K. M., Guilard, R., Eds.; Academic Press: New York, 2003; Vol. 16, pp 43–116.

(7) L'Her, M.; Pondaven, A. In *The Porphyrin Handbook*; Kardish, K. M., Smith, K. M., Guilard, R., Eds.; Academic Press: New York, 2003; Vol. 16, pp 117–170.

(8) Sorokin, A. B. *Chem. Rev.* **2013**, *113* (10), 8152–8191.

(9) de la Torre, G.; Nicolau, M.; Torres, T. In *Supramolecular Photosensitive and Electroactive Materials*; Elsevier, 2001; pp 1–111.

(10) Li, X.; De Zheng, B.; Peng, X. H.; Li, S. Z.; Ying, J. W.; Zhao, Y.; Huang, J. D.; Yoon, J. *Coordination Chemistry Reviews*. Elsevier B.V. January 2019, pp 147–160.

(11) Wong, E. W. Y.; Walsby, C. J.; Storr, T.; Leznoff, D. B. *Inorg. Chem.* **2010**, *49* (7), 3343–3350.

(12) Zhou, W.; Leznoff, D. B. *Chem. Commun.* **2018**, *54* (15), 1829–1832.

(13) McKearney, D.; Zhou, W.; Zellman, C.; Williams, V. E.; Leznoff, D. B. *Chem. Commun.* **2019**, *55* (47), 6696–6699.

(14) Zhou, W.; McKearney, D.; Leznoff, D. B. *Chem. – A Eur. J.* **2020**, *26* (5), 1027–1031.

(15) Bartolomé, J.; Monton, C.; Schuller, I. K. *Magnetism of Metal Phthalocyanines*; Bartolomé, J., Luis, F., Fernández, J. F., Eds.; Springer, Berlin, Heidelberg, 2014; pp 221–245.

(16) Bouvet, M.; Gaudillat, P.; Suisse, J. M. *J. Porphyr. Phthalocyanines* **2013**, *17* (10), 913–919.

(17) de la Torre, G.; Vázquez, P.; Agulló-López, F.; Torres, T. *Chem. Rev.* **2004**, *104* (9), 3723–3750.

(18) Claessens, C. G.; Hahn, U.; Torres, T. *Chem. Rec.* **2008**, *8* (2), 75–97.

(19) *Functional Phthalocyanine Molecular Materials*; Jiang, J., Ed.; Structure and Bonding; Springer Berlin Heidelberg: Berlin, Heidelberg, 2010; Vol. 135.

(20) Morse, G. E.; Bender, T. P. *ACS Appl. Mater. Interfaces* **2012**, *4* (10), 5055–5068.

(21) Melville, O. A.; Lessard, B. H.; Bender, T. P. *ACS Appl. Mater. Interfaces* **2015**, *7* (24), 13105–13118.

(22) Grant, T. M.; Josey, D. S.; Sampson, K. L.; Mudigonda, T.; Bender, T. P.; Lessard, B. H. *Chem. Rec.* **2019**, *19* (6), 1093–1112.

(23) Verreet, B.; Schols, S.; Cheyns, D.; Rand, B. P.; Gommans, H.; Aernouts, T.; Heremans, P.; Genoe, J. *J. Mater. Chem.* **2009**, *19* (30), 5295–5297.

(24) Chauhan, K. V.; Sullivan, P.; Yang, J. L.; Jones, T. S. *J. Phys. Chem. C* **2010**, *114* (7),

3304–3308.

(25) Lessard, B. H.; White, R. T.; Al-Amar, M.; Plint, T.; Castrucci, J. S.; Josey, D. S.; Lu, Z. H.; Bender, T. P. *ACS Appl. Mater. Interfaces* **2015**, *7* (9), 5076–5088.

(26) Josey, D. S.; Nyikos, S. R.; Garner, R. K.; Dovijarski, A.; Castrucci, J. S.; Wang, J. M.; Evans, G. J.; Bender, T. P. *ACS Energy Lett.* **2017**, *2* (3), 726–732.

(27) Helander, M. G.; Morse, G. E.; Qiu, J.; Castrucci, J. S.; Bender, T. P.; Lu, Z. H. *ACS Appl. Mater. Interfaces* **2010**, *2* (11), 3147–3152.

(28) Plint, T.; Lessard, B. H.; Bender, T. P. *J. Appl. Phys.* **2016**, *119* (14).

(29) Zysman-Colman, E.; Ghosh, S. S.; Xie, G.; Varghese, S.; Chowdhury, M.; Sharma, N.; Cordes, D. B.; Slawin, A. M. Z.; Samuel, I. D. W. *ACS Appl. Mater. Interfaces* **2016**, *8* (14), 9247–9253.

(30) Pearson, A. J.; Plint, T.; Jones, S. T. E.; Lessard, B. H.; Credgington, D.; Bender, T. P.; Greenham, N. C. *J. Mater. Chem. C* **2017**, *5* (48), 12688–12698.

(31) Li, Q.; Tang, Q.; Li, H.; Hu, W.; Yang, X.; Shuai, Z.; Liu, Y.; Zhu, D. *Pure Appl. Chem.* **2008**, *80* (11), 2231–2240.

(32) Melville, O. A.; Grant, T. M.; Lessard, B. H. *J. Mater. Chem. C* **2018**, *6* (20), 5482–5488.

(33) Boileau, N. T.; Cranston, R.; Mirka, B.; Melville, O. A.; Lessard, B. H. *RSC Adv.* **2019**, *9* (37), 21478–21485.

(34) Melville, O. A.; Grant, T. M.; Lochhead, K.; King, B.; Ambrose, R.; Rice, N. A.; Boileau, N. T.; Peltekoff, A. J.; Tousignant, M.; Hill, I. G.; Lessard, B. H. *ACS Appl. Electron. Mater.* **2020**.

(35) Zhou, W.; Yutronkie, N. J.; Lessard, B. H.; Brusso, J. L. *Mater. Adv.* **2021**, *2* (1), 165–185.

(36) De La Torre, G.; Claessens, C. G.; Torres, T. *Chem. Commun.* **2007**, No. 20, 2000–2015.

(37) Claessens, C. G.; Martínez-Díaz, M. V.; Torres, T. In *Supramolecular Chemistry*; John Wiley & Sons, Ltd: Chichester, UK, 2012.

(38) Melville, O. A.; Grant, T. M.; Mirka, B.; Boileau, N. T.; Park, J.; Lessard, B. H. *Adv. Electron. Mater.* **2019**, *5* (8), 1900087.

(39) Mack, J.; Kobayashi, N. *Chem. Rev.* **2011**, *111* (2), 281–321.

(40) Kobayashi, N.; Nakajima, S.; Ogata, H.; Fukuda, T. *Chem. - A Eur. J.* **2004**, *10* (24), 6294–6312.

(41) Kobayashi, N.; Furuyama, T.; Satoh, K. *J. Am. Chem. Soc.* **2011**, *133* (49), 19642–19645.

(42) Furuyama, T.; Satoh, K.; Kushiya, T.; Kobayashi, N. *J. Am. Chem. Soc.* **2014**, *136* (2), 765–776.

(43) Forrest, S. R. *Nature* **2004**, *428* (6986), 911–918.

(44) Newman, C. R.; Frisbie, C. D.; Da Silva Filho, D. A.; Brédas, J. L.; Ewbank, P. C.; Mann, K. R. *Chem. Mater.* **2004**, *16* (23), 4436–4451.

(45) Veres, J.; Ogier, S.; Lloyd, G.; De Leeuw, D. *Chem. Mater.* **2004**, *16* (23), 4543–4555.

(46) Dimitrakopoulos, C. D.; Malenfant, P. R. L. *Adv. Mater.* **2002**, *14* (2), 99–117.

(47) Zaumseil, J.; Sirringhaus, H. *Chem. Rev.* **2007**, *107* (4), 1296–1323.

(48) Roncali, J.; Leriche, P.; Cravino, A. *Adv. Mater.* **2007**, *19* (16), 2045–2060.

(49) Mascaro, D. J. **2001**, *45* (1), 11–27.

(50) Zhang, Y., Cai X., Bian Y., and J. J. In *Functional Phthalocyanine Molecular Materials*; Jiang, J., Ed.; Springer-Verlag Berlin Heidelberg, 2010; pp 275–322.

(51) Yasuda, T.; Tsutsui, T. *Japanese J. Appl. Physics, Part 2 Lett.* **2006**, *45* (20–23).

(52) Md. Obaidulla, S.; Goswami, D. K.; Giri, P. K. *Appl. Phys. Lett.* **2014**, *104* (21), 213302.

(53) Song, D.; Wang, H.; Zhu, F.; Yang, J.; Tian, H.; Geng, Y.; Yan, D. *Adv. Mater.* **2008**, *20* (11), 2142–2144.

(54) Cricenti, A.; Riele, L.; Buick, B.; Speiser, E.; Fimland, B.-O.; Vogt, P.; Richter, W. *Epioptics-11* **2012**, 1–15.

(55) Li, L.; Hu, W.; Fuchs, H.; Chi, L. *Adv. Energy Mater.* **2011**, *1* (2), 188–193.

(56) Yan, D.; Song, D.; Zhu, F.; Yu, B. US 7,871,855 B2, 2011.

(57) Song, D.; Zhu, F.; Yu, B.; Huang, L.; Geng, Y.; Yan, D. *Appl. Phys. Lett.* **2008**, *92* (14), 90–93.

(58) Ling, M. M.; Bao, Z.; Erk, P. *Appl. Phys. Lett.* **2006**, *89* (16), 4–7.

(59) Bao, Z.; Lovinger, A. J.; Dodabalapur, A. *Appl. Phys. Lett.* **1996**, *69* (20), 3066–3068.

(60) Takahashi, T.; Takenobu, T.; Takeya, J.; Iwasa, Y. *Appl. Phys. Lett.* **2006**, *88* (3), 1–3.

(61) Peng, Y.; Lv, W.; Yao, B.; Xie, J.; Yang, T.; Fan, G.; Chen, D.; Gao, P.; Zhou, M.; Wang, Y. *IEEE Trans. Electron Devices* **2013**, *60* (3), 1208–1212.

(62) Yasuda, T.; Tsutsui, T. *Mol. Cryst. Liq. Cryst.* **2006**, *462* (1), 3–9.

(63) Schmechel, R.; Ahles, M.; Von Seggern, H. *J. Appl. Phys.* **2005**, *98* (8).

(64) Chen, X. K.; Zou, L. Y.; Guo, J. F.; Ren, A. M. *J. Mater. Chem.* **2012**, *22* (13), 6471–6484.

(65) Facchetti, A. *Chem. Mater.* **2011**, *23* (3), 733–758.

(66) Sancho-García, J. C.; Pérez-Jiménez, A. J.; Olivier, Y.; Cornil, J. *Phys. Chem. Chem. Phys.* **2010**, *12* (32), 9381–9388.

(67) Sakamoto, Y.; Suzuki, T.; Kobayashi, M.; Gao, Y.; Fukai, Y.; Inoue, Y.; Sato, F.; Tokito, S. *J. Am. Chem. Soc.* **2004**, *126* (26), 8138–8140.

(68) Geng, H.; Niu, Y.; Peng, Q.; Shuai, Z.; Coropceanu, V.; Brédas, J. L. *J. Chem. Phys.* **2011**, *135* (10).

(69) Bao, Z.; Lovinger, A. J.; Brown, J. *J. Am. Chem. Soc.* **1998**, *120* (1), 207–208.

(70) Wang, Z.; Kim, C.; Facchetti, A.; Marks, T. J. *J. Am. Chem. Soc.* **2007**, *129* (44), 13362–13363.

(71) Kuo, M. Y.; Chen, H. Y.; Chao, I. *Chem. - A Eur. J.* **2007**, *13* (17), 4750–4758.

(72) Jones, B. A.; Ahrens, M. J.; Yoon, M. H.; Facchetti, A.; Marks, T. J.; Wasielewski, M. R. *Angew. Chemie - Int. Ed.* **2004**, *43* (46), 6363–6366.

(73) Hutchison, G. R.; Ratner, M. A.; Marks, T. J. *J. Am. Chem. Soc.* **2005**, *127* (7), 2339–2350.

(74) Chen, X. K.; Guo, J. F.; Zou, L. Y.; Ren, A. M.; Fan, J. X. *J. Phys. Chem. C* **2011**, *115* (43), 21416–21428.

(75) McKeown, N. B. *Phthalocyanine Materials: Synthesis, Structure, and Function*; McKeown, N. B., Ed.; Cambridge University Press: Cambridge, U.K., 1998.

(76) Rodríguez-Morgade, M. S.; Stuzhin, P. A. *J. Porphyr. Phthalocyanines* **2004**, *08* (09), 1129–1165.

(77) Claessens, C. G.; González-Rodríguez, D.; Rodríguez-Morgade, M. S.; Medina, A.; Torres, T. *Chem. Rev.* **2014**, *114* (4), 2192–2277.

(78) Zdravkovski, D.; Milletti, M. C. *J. Mol. Struct. THEOCHEM* **2005**, *717* (1–3), 85–89.

(79) Beaumont, N.; Castrucci, J. S.; Sullivan, P.; Morse, G. E.; Paton, A. S.; Lu, Z. H.; Bender, T. P.; Jones, T. S. *J. Phys. Chem. C* **2014**, *118* (27), 14813–14823.

(80) Verreet, B.; Cnops, K.; Cheyns, D.; Heremans, P.; Stesmans, A.; Zango, G.; Claessens, C. G.; Torres, T.; Rand, B. P. *Adv. Energy Mater.* **2014**, *4* (8), 1–8.

(81) Mutolo, K. L.; Mayo, E. I.; Rand, B. P.; Forrest, S. R.; Thompson, M. E. *J. Am. Chem. Soc.* **2006**, *128* (25), 8108–8109.

(82) Morse, G. E.; Gantz, J. L.; Steirer, K. X.; Armstrong, N. R.; Bender, T. P. *ACS Appl. Mater. Interfaces* **2014**, *6* (3), 1515–1524.

(83) Mauldin, C. E.; Piliego, C.; Poulsen, D.; Unruh, D. A.; Woo, C.; Ma, B.; Mynar, J. L.; Fréchet, J. M. J. *ACS Appl. Mater. Interfaces* **2010**, *2* (10), 2833–2838.

(84) Virdo, J. D.; Lough, A. J.; Bender, T. P. *Acta Crystallogr. Sect. C Struct. Chem.* **2016**, *72* (4), 297–307.

(85) Claessens, C. G.; González-Rodríguez, D.; Torres, T. *Chem. Rev.* **2002**, *102* (3), 835–853.

(86) Meller, A.; Ossko, A. *Monatshefte für Chemie* **1972**, *103* (1), 150–155.

(87) Giribabu, L.; Kumar, C. V.; Surendar, A.; Reddy, V. G.; Chandrasekharam, M.; Reddy, P.

Y. *Synth. Commun.* **2007**, *37* (23), 4141–4147.

(88) Claessens, C. G.; González-Rodríguez, D.; Del Rey, B.; Torres, T.; Mark, G.; Schuchmann, H. P.; Von Sonntag, C.; MacDonald, J. G.; Nohr, R. S. *European J. Org. Chem.* **2003**, No. 14, 2547–2551.

(89) Stuzhin, P. A.; Skvortsov, I. A.; Zhabanov, Y. A.; Somov, N. V.; Razgonyaev, O. V.; Nikitin, I. A.; Koifman, O. I. *Dye. Pigment.* **2019**, *162*, 888–897.

(90) Gotfredsen, H.; Storm, F. E.; Muñoz, A. V.; Santella, M.; Kadziola, A.; Hammerich, O.; Mikkelsen, K. V.; Nielsen, M. B. *Chem. - A Eur. J.* **2017**, *23* (64), 16194–16198.

(91) Hamdoush, M.; Ivanova, S. S.; Pakhomov, G. L.; Stuzhin, P. A. *Macroheterocycles* **2016**, *9* (3), 230–233.

(92) Hamdoush, M.; Skvortsov, I. A.; Mikhailov, M. S.; Pakhomov, G.; Stuzhin, P. A. *J. Fluor. Chem.* **2017**, *204*, 31–36.

(93) Hamdoush, M.; Nikitin, K.; Skvortsov, I.; Somov, N.; Zhabanov, Y.; Stuzhin, P. A. *Dye. Pigment.* **2019**, *170*, 107584.

(94) Zyskowski, C. D.; Kennedy, V. O. *J. Porphyr. Phthalocyanines* **2000**, *4* (8), 707–712.

(95) Shimizu, S.; Nakano, S.; Hosoya, T.; Kobayashi, N. *Chem. Commun.* **2011**, *47* (1), 316–318.

(96) Shimizu, S.; Miura, A.; Khene, S.; Nyokong, T.; Kobayashi, N. *J. Am. Chem. Soc.* **2011**, *133* (43), 17322–17328.

(97) Kamino, B. A.; Bender, T. P. *Dalt. Trans.* **2013**, *42* (36), 13145.

(98) Shang, H.; Zhao, L.; Qi, D.; Chen, C.; Jiang, J. *Chem. - A Eur. J.* **2014**, *20* (49), 16266–16272.

(99) Nečedová, M. M.; Magdolen, P.; Fülöpová, A.; Cigáň, M.; Zahradník, P.; Filo, J. *Dye. Pigment.* **2016**, *130*, 24–36.

(100) Wang, Y.; Uchihara, K.; Mori, S.; Furuta, H.; Shimizu, S. *Org. Lett.* **2019**, *21* (9), 3103–3107.

(101) Tejerina, L.; Martínez-Díaz, M. V.; Torres, T. *Org. Lett.* **2019**, *21* (8), 2908–2912.

(102) Kobayashi, N. *J. Chem. Soc. Chem. Commun.* **1991**, No. 17, 1203.

(103) Fukuda, T.; Stork, J. R.; Potucek, R. J.; Olmstead, M. M.; Noll, B. C.; Kobayashi, N.; Durfee, W. S. *Angew. Chemie Int. Ed.* **2002**, *41* (14), 2565–2568.

(104) Nakano, S.; Kage, Y.; Furuta, H.; Kobayashi, N.; Shimizu, S. *Chem. - A Eur. J.* **2016**, *22* (23), 7706–7710.

(105) Zhang, Y.; Oh, J.; Wang, K.; Shin, D.; Zhan, X.; Zheng, Y.; Kim, D.; Jiang, J. *Chem. Commun.* **2016**, *52* (69), 10517–10520.

(106) Hanack, M.; Geyer, M. *J. Chem. Soc. Chem. Commun.* **1994**, No. 19, 2253.

(107) Rauschnabel, J.; Hanack, M. *Tetrahedron Lett.* **1995**, *36* (10), 1629–1632.

(108) Geyer, M.; Plenzig, F.; Rauschnabel, J.; Hanack, M.; Del Rey, B.; Sastre, A.; Torres, T. *Synthesis (Stuttg).* **1996**, *1996* (9), 1139–1151.

(109) Goto, K.; Kubo, T.; Yamamoto, K.; Nakasuji, K.; Sato, K.; Shiomi, D.; Takui, T.; Kubota, M.; Kobayashi, T.; Yakusi, K.; Ouyang, J. *J. Am. Chem. Soc.* **1999**, *121* (7), 1619–1620.

(110) Martínez-Díaz, M. V.; del Rey, B.; Torres, T.; Agricole, B.; Mingotaud, C.; Cuvillier, N.; Rojo, G.; Agulló-López, F. *J. Mater. Chem.* **1999**, *9* (7), 1521–1526.

(111) González-Rodríguez, D.; Torres, T.; Denardin, E. L. G.; Samios, D.; Stefani, V.; Corrêa, D. S. *J. Organomet. Chem.* **2009**, *694* (11), 1617–1622.

(112) González-Rodríguez, D.; Torres, T.; Guldi, D. M.; Rivera, J.; Herranz, M. Á.; Echegoyen, L. *J. Am. Chem. Soc.* **2004**, *126* (20), 6301–6313.

(113) Solntsev, P. V.; Spurgin, K. L.; Sabin, J. R.; Heikal, A. A.; Nemykin, V. N. *Inorg. Chem.* **2012**, *51* (12), 6537–6547.

(114) Shibata, N.; Das, B.; Tokunaga, E.; Shiro, M.; Kobayashi, N. *Chem. - A Eur. J.* **2010**, *16* (25), 7554–7562.

(115) Adachi, K.; Watarai, H. *Anal. Chem.* **2006**, *78* (19), 6840–6846.

(116) Morse, G. E.; Castrucci, J. S.; Helander, M. G.; Lu, Z. H.; Bender, T. P. *ACS Appl. Mater. Interfaces* **2011**, *3* (9), 3538–3544.

(117) Barrett, P. A.; Frye, D. A.; Linstead, R. P. *J. Chem. Soc.* **1938**, *0* (0), 1157.

(118) Colaïtis, D. *R. Hebd. Seances Acad. Sci.* **1956**, *242*, 1026.

(119) Wynne, K. J. *Inorg. Chem.* **1984**, *23* (26), 4658–4663.

(120) Janczak, J.; Kubiak, R. *Inorganica Chim. Acta* **1999**, *288* (2), 174–180.

(121) Hasegawa, M.; Sato, N. *Mol. Cryst. Liq. Cryst. Sci. Technol. Sect. A Mol. Cryst. Liq. Cryst.* **1997**, *296*, 409–426.

(122) Yanik, H.; Aydin, D.; Durmuş, M.; Ahsen, V. *J. Photochem. Photobiol. A Chem.* **2009**, *206*

(1), 18–26.

(123) Masilela, N.; Nyokong, T. *J. Lumin.* **2010**, *130* (10), 1787–1793.

(124) Durmuş, M.; Nyokong, T. *Polyhedron* **2007**, *26* (13), 3323–3335.

(125) Chen, Y.; Hanack, M.; Araki, Y.; Ito, O. *Chem. Soc. Rev.* **2005**, *34* (6), 517–529.

(126) Masilela, N.; Nyokong, T. *Dye. Pigment.* **2010**, *84* (3), 242–248.

(127) Hanack, M.; Schneider, T.; Barthel, M.; Shirk, J. S.; Flom, S. R.; Pong, R. G. S. *Coord. Chem. Rev.* **2001**, *219–221*, 235–258.

(128) Chen, Y.; Hanack, M.; Blau, W. J.; Dini, D.; Liu, Y.; Lin, Y.; Bai, J. *J. Mater. Sci.* **2006**, *41* (8), 2169–2185.

(129) Plater, M. J.; Jeremiah, A.; Bourhill, G. *J. Chem. Soc. Perkin 1* **2002**, *2* (1), 91–96.

(130) Owen, J. E.; Kenney, M. E. *Inorg. Chem.* **1962**, *1* (2), 331–333.

(131) Schneider, T.; Heckmann, H.; Barthel, M.; Hanack, M. *European J. Org. Chem.* **2001**, No. 16, 3055–3065.

(132) Peng, Y.; Huang, F.; Wen, J.; Huang, B.; Ma, X.; Wang, Q. *J. Coord. Chem.* **2008**, *61* (10), 1503–1512.

(133) Peng, Y.; Lin, P.; Lin, J.; Xu, G.; Zhang, H.; Shi, J. *Mater. Lett.* **2009**, *63* (11), 914–916.

(134) Guay, D.; Dodelet, J. P.; Côté, R.; Langford, C. H.; Gravel, D. *J. Electrochem. Soc.* **1989**, *136* (8), 2272–2280.

(135) Yamasaki, K.; Okada, O.; Inami, K.; Oka, K.; Kotani, M.; Yamada, H. *J. Phys. Chem. B* **1997**, *101* (1), 13–19.

(136) Linsky, J. P.; Paul, T. R.; Nohr, R. S.; Kenney, M. E. *Inorg. Chem.* **1980**, *19* (10), 3131–3135.

(137) Lessard, B. H.; Al-Amar, M.; Grant, T. M.; White, R.; Lu, Z. H.; Bender, T. P. *J. Mater. Chem. A* **2015**, *3* (9), 5047–5053.

(138) Grant, T. M.; McIntyre, V.; Vestfrid, J.; Raboui, H.; White, R. T.; Lu, Z. H.; Lessard, B. H.; Bender, T. P. *ACS Omega* **2019**, *4* (3), 5317–5326.

(139) Kraus, G. A.; Vander Louw, S. J. *Synlett*. 1996, p 726.

(140) Raboui, H.; Al-Amar, M.; Abdelrahman, A. I.; Bender, T. P. *RSC Adv.* **2015**, *5* (57), 45731–45739.

(141) Chen, Y.; Hanack, M.; O'Flaherty, S.; Bernd, G.; Zeug, A.; Roeder, B.; Blau, W. J. *Macromolecules* **2003**, *36* (11), 3786–3788.

(142) Sakai, Y.; Ueda, M.; Yahagi, A.; Tanno, N. *Polymer (Guildf).* **2002**, *43* (12), 3497–3503.

(143) Li, Y. X.; Zhu, J.; Chen, Y.; Zhang, J.; Wang, J.; Zhang, B.; He, Y.; Blau, W. J. *Nanotechnology* **2011**, *22* (20).

(144) Kojima, Y.; Osano, Y. T.; Ohashi, T. *Bull. Chem. Soc. Jpn.* **2000**, *73* (11), 2469–2475.

(145) Barrett, P. A.; Dent, C. E.; Linstead, R. P. *J. Chem. Soc.* **1936**, 1719.

(146) Dent, C. E.; Linstead, R. P. **1934**, 1719–1736.

(147) Joyher R. D. , JR. Cekada, J., Linck R.G., K. M. E. *J. Inorg. Nucl. Chem.* **1960**, *15* (3–4), 387–388.

(148) Joyner, R. D.; Kenney, M. E. *Inorg. Chem.* **1962**, *1* (2), 236–238.

(149) Lowery, M. K.; Starshak, A. J.; Esposito, J. N.; Krueger, P. C.; Kenney, M. E. *Inorg. Chem.* **1965**, *4* (1), 128–128.

(150) Dirk, C. W.; Inabe, T.; Schoch, K. F.; Marks, T. J. *J. Am. Chem. Soc.* **1983**, *105* (6), 1539–1550.

(151) Noboru Sasa, Kenji Okada, Kazuo Nakamura, S. O. *J. Mol. Struct.* **1998**, *446* (3), 163–178.

(152) Yutronkie, N. J.; Grant, T. M.; Melville, O. A.; Lessard, B. H.; Brusso, J. L. *Materials (Basel).* **2019**, *12* (8), 5–10.

(153) Joyner, R. D.; Kenney, M. E. *J. Am. Chem. Soc.* **1960**, *82* (22), 5790–5791.

(154) Janczak, J.; Kubiak, R. *Acta Crystallogr. Sect. C Cryst. Struct. Commun.* **2003**, *59* (6), 237–240.

(155) Slodeka, A.; Schnurpfeilb, G.; Wöhrle, D. *J. Porphyr. Phthalocyanines* **2017**, *21* (12), 811–823.

(156) Stover, R. L.; Thrall, C. L.; Joyner, R. D. *Inorg. Chem.* **1971**, *10* (10), 2335–2337.

(157) Sayer, P.; Gouterman, M.; Connell, C. R. *Acc. Chem. Res.* **1982**, *15* (3), 73–79.

(158) Davison, J. B.; Wynne, K. J. *Macromolecules* **1978**, *11* (1), 186–191.

(159) Lessard, B. H.; Dang, J. D.; Grant, T. M.; Gao, D.; Seferos, D. S.; Bender, T. P. *ACS Appl. Mater. Interfaces* **2014**, *6* (17), 15040–15051.

(160) Barker, C. A.; Findlay, K. S.; Bettington, S.; Batsanov, A. S.; Perepichka, I. F.; Bryce, M. R.; Beeby, A. *Tetrahedron* **2006**, *62* (40), 9433–9439.

(161) Esposito, J. N.; Sutton, L. E.; Kenney, M. E. *Inorg. Chem.* **1967**, *6* (6), 1116–1120.

(162) Bandera, Y.; Burdette, M. K.; Shetzline, J. A.; Jenkins, R.; Creager, S. E.; Foulger, S. H. *Dye. Pigment.* **2016**, *125*, 72–79.

(163) Biyiklioğlu, Z. *Dye. Pigment.* **2013**, *99* (1), 59–66.

(164) Saka, E. T.; Yalazan, H.; Bıyıklıoglu, Z.; Kantekin, H.; Tekintas, K. *J. Mol. Struct.* **2020**, *1199*.

(165) Xiao, B.; Zhu, M.; Li, X.; Yang, P.; Qiu, L.; Lu, C. *Int. J. Hydrogen Energy* **2016**, *41* (27), 11537–11546.

(166) Ma, D.; Chen, X.; Wang, Y.; Guo, Q.; Ye, Q.; Guo, R.; Xiao, S.; Ye, Q.; Huang, Y.; Peng, Y. *J. Lumin.* **2019**, *207*, 597–601.

(167) Kim, K. N.; Choi, C. S.; Kay, K. Y. *Tetrahedron Lett.* **2005**, *46* (40), 6791–6795.

(168) Biyiklioglu, Z.; Alp, H. *Dye. Pigment.* **2016**, *132*, 213–222.

(169) Hanack, M.; Mitulla, K.; Pawlowshi, G.; Subramanian, L. R. *J. Organiometalllic Chem.* **1981**, *204*, 315–325.

(170) Kroenke, W. J.; Kenney, M. E. *Inorg. Chem.* **1964**, *3* (2), 251–254.

(171) Seoudi, R.; El-Bahy, G. S.; El Sayed, Z. A. *J. Mol. Struct.* **2005**, *753* (1–3), 119–126.

(172) Eneva, I.; Aliosman, M.; Angelov, I.; Popov, K.; Mantareva, V. *Bulg. Chem. Commun.* **2017**, *49* (D), 246–252.

(173) Ford, W. E.; Rodgers, M. A. J.; Schechtman, L. A.; Sounik, J. R.; Rihter, B. D.; Kenney, M. *Inorg. Chem.* **1992**, *31* (16), 3371–3377.

(174) Kašpar, J.; Emmer, I.; Collins, R. A. *Int. J. Electron.* **1994**, *76* (5), 793–796.

(175) Yamana, M.; Kashiwazaki, N. *Sensors Actuators, B Chem.* **1997**, *40* (2–3), 237–241.

(176) Kuprikova, N. M.; Klyamer, D. D.; Sukhikh, A. S.; Krasnov, P. O.; Mrsic, I.; Basova, T. V. *Dye. Pigment.* **2020**, *173*, 107939.

(177) Maree, S.; Phillips, D.; Nyokong, T. *J. Porphyr. Phthalocyanines* **2002**, *6* (1), 17–25.

(178) Rafaeloff, R.; Kohl, F. J.; Krueger, P. C.; Kenney, M. E. *J. Inorg. Nucl. Chem.* **1966**, *28* (3), 899–902.

(179) Grant, T. M.; Rice, N. A.; Muccioli, L.; Castet, F.; Lessard, B. H. *ACS Appl. Electron. Mater.* **2019**, *1* (4), 494–504.

(180) Gouterman, M.; Sayer, P.; Shankland, E.; Smith, J. P. *Inorg. Chem.* **1981**, *20* (1), 87–92.

(181) Breusova, M. O.; Pushkarev, V. E.; Tomilova, L. G. *Russ. Chem. Bull.* **2007**, *56* (7), 1456–1460.

(182) Antunes, E. M.; Nyokong, T. *J. Porphyr. Phthalocyanines* **2009**, *13* (1), 153–160.

(183) Isago, H.; Kagaya, Y. *Inorg. Chem.* **2012**, *51* (15), 8447–8454.

(184) Isago, H. *Chem. Commun.* **2003**, *9* (15), 1864–1865.

(185) Isago, H.; Kagaya, Y. **2009**, No. V, 382–389.

(186) Janczak, J.; Perpétuo, G. J. *Acta Crystallogr. Sect. C Cryst. Struct. Commun.* **2006**, *62* (2), 45–47.

(187) Janczak, J.; Kubiak, R.; Jezierski, A. *Inorg. Chem.* **1999**, *38* (9), 2043–2049.

(188) Kubiak, R.; Razik, M. *Acta Crystallogr. Sect. C Cryst. Struct. Commun.* **1998**, *54* (4), 483–485.

(189) Yutaka KAGAYA, H. I. *Chem. Lett.* **1994**, *23* (10), 1957–1960.

(190) Knör, G. *Inorg. Chem.* **1996**, *35*, 7916–7918.

(191) Kubiak, R.; Ejsmont, K. *J. Mol. Struct.* **1999**, *474* (1–3), 275–281.

(192) Isago, H.; Kagaya, Y. *Bull. Chem. Soc. Jpn.* 1994, pp 383–389.

(193) Castrucci, J. S.; Helander, M. G.; Morse, G. E.; Lu, Z. H.; Yip, C. M.; Bender, T. P. *Cryst. Growth Des.* **2012**, *12* (3), 1095–1100.

(194) Chaidogiannos, G.; Petraki, F.; Glezos, N.; Kennou, S.; Nešpůrek, S. *Mater. Sci. Eng. B Solid-State Mater. Adv. Technol.* **2008**, *152* (1–3), 105–108.

(195) Chaidogiannos, G.; Petraki, F.; Glezos, N.; Kennou, S.; Nešpůrek, S. *Appl. Phys. A Mater. Sci. Process.* **2009**, *96* (3), 763–767.

(196) Sánchez-Vergara, M. E.; Hamui, L.; Habib, S. G. *Materials (Basel).* **2019**, *12* (10).

(197) Grant, T. M.; Kaller, K. L. C.; Coathup, T. J.; Rice, N. A.; Hinzer, K.; Lessard, B. H. *Org. Electron.* **2020**, *87*, 105976.

(198) Dang, M. T.; Grant, T. M.; Yan, H.; Seferos, D. S.; Lessard, B. H.; Bender, T. P. *J. Mater. Chem. A* **2017**, *5* (24), 12168–12182.

(199) Peng, Y.; Gao, P.; Lv, W.; Yao, B.; Fan, G.; Chen, D.; Xie, J.; Zhou, M.; Li, Y.; Wang, Y. *IEEE Photonics Technol. Lett.* **2013**, *25* (22), 2149–2152.

(200) Mukherjee, B.; Mukherjee, M. *Org. Electron.* **2009**, *10* (7), 1282–1287.

(201) Platel, R. H.; Teixeira Tasso, T.; Zhou, W.; Furuyama, T.; Kobayashi, N.; Leznoff, D. B. *Chem. Commun.* **2015**, *51* (27), 5986–5989.

(202) Arokiyanathan, A. L.; Lakshmipathi, S. *Inorganica Chim. Acta* **2018**, *483* (July), 203–210.

(203) Ganga-Sah, Y.; Tajbakhsh, E.; Platel, R. H.; Zhou, W.; Leznoff, D. B. *J. Porphyr. Phthalocyanines* **2019**, *23* (11–12), 1592–1602.

(204) Ou, C.; Lv, W.; Chen, J.; Yu, T.; Song, Y.; Wang, Y.; Wang, S.; Yang, G. *Dye. Pigment.* **2021**, *184* (September 2020), 108862.

(205) Ishikawa, N.; Iino, T.; Kaizu, Y. *J. Phys. Chem. A* **2002**, *106* (41), 9543–9550.

(206) Kasuga, K.; Ando, M.; Morimoto, H.; Isa, M. *Chem. Lett.* **1986**, *15* (7), 1095–1098.

(207) Galanin, N. E.; Yakubov, L. A.; Shaposhnikov, G. P. *Russ. J. Org. Chem.* **2008**, *44* (6), 921–926.

(208) Galanin, N. E.; Shaposhnikov, G. P. *Russ. J. Gen. Chem.* **2012**, *82* (4), 764–769.

(209) Lu, G.; Wang, K.; Kong, X.; Pan, H.; Zhang, J.; Chen, Y.; Jiang, J. *ChemElectroChem* **2018**, *5* (4), 605–609.

(210) Jiang, J.; Xie, J.; Choi, M. T. M.; Yan, Y.; Sun, S.; Ng, D. K. P. *J. Porphyr. Phthalocyanines* **1999**, *3* (4), 322–328.

(211) Zhang, Y.; Cai, X.; Qi, D.; Yao, P.; Bian, Y.; Jiang, J. *ChemPhysChem* **2008**, *9* (5), 781–792.

(212) Paillaud, J. L.; Drillon, M.; De Cian, A.; Fischer, J.; Weiss, R.; Villeneuve, G. *Phys. Rev. Lett.* **1991**, *67* (2), 244–247.

(213) Bairamukov, V. Y.; Kuklin, A. I.; Orlova, D. N.; Lebedev, V. T. *J. Surf. Investig.* **2019**, *13* (5), 793–801.

(214) Gorbunova, Y. G.; Lapkina, L. A.; Golubeva, S. V.; Larchenko, V. E.; Tsivadze, A. Y. *Mendeleev Commun.* **2001**, *11* (6), 214–215.

(215) Barthel, M.; Dini, D.; Vagin, S.; Hanack, M. *European J. Org. Chem.* **2002**, No. 22, 3756–3762.

(216) Muranaka, A.; Okuda, M.; Kobayashi, N.; Somers, K.; Ceulemans, A. *J. Am. Chem. Soc.* **2004**, *126* (14), 4596–4604.

(217) Palomares, E.; Martínez-Díaz, M. V.; Haque, S. A.; Torres, T.; Durrant, J. R. *Chem. Commun.* **2004**, No. 18, 2112–2113.

(218) Ballesteros, B.; De La Torre, G.; Torres, T.; Hug, G. L.; Rahman, G. M. A.; Guldi, D. M. *Tetrahedron* **2006**, *62* (9), 2097–2101.

(219) Sevim, A. M.; Yenilmez, H. Y.; Aydemir, M.; Koca, A.; Bayir, Z. A. *Electrochim. Acta* **2014**, *137*, 602–615.

(220) Aktaş, A.; Acar, I.; Biyiklioğlu, Z.; Saka, E. T.; Kantekin, H. *Synth. Met.* **2014**, *198*, 212–220.

(221) Erdomu, A.; Durmu, M.; Uur, A. L.; Avciata, O.; Avciata, U.; Nyokong, T. *Synth. Met.* **2010**, *160* (17–18), 1868–1876.

(222) Mbambisa, G.; Tau, P.; Antunes, E.; Nyokong, T. *Polyhedron* **2007**, *26* (18), 5355–5364.

(223) Tomachynski, L. A.; Chernii, V. Y.; Gorbenko, H. N.; Filonenko, V. V.; Volkov, S. V. *Chem. Biodivers.* **2004**, *1* (6), 862–867.

(224) Zhou, W.; Platel, R. H.; Teixeira Tasso, T.; Furuyama, T.; Kobayashi, N.; Leznoff, D. B. *Dalt. Trans.* **2015**, *44* (31), 13955–13961.

(225) Tomachynski, L. A.; Chernii, V. Y.; Volkov, S. V. *J. Porphyr. Phthalocyanines* **2001**, *5* (10), 731–734.

(226) Tomachynski, L. A.; Tretyakova, I. N.; Chernii, V. Y.; Volkov, S. V.; Kowalska, M.; Legendziewicz, J.; Gerasymchuk, Y. S.; Radzki, S. *Inorganica Chim. Acta* **2008**, *361* (9–10), 2569–2581.

(227) Gerasymchuk, Y. S.; Volkov, S. V.; Chernii, V. Y.; Tomachynski, L. A.; Radzki, S. *J. Alloys Compd.* **2004**, *380* (1-2 SPEC. ISS.), 186–190.

(228) Tomachynski, L. A.; Chernii, V. Y.; Volkov, S. V. **2002**, 114–121.

(229) Tretyakova, I. N.; Chernii, V. Y.; Tomachynski, L. A.; Volkov, S. V. *Dye. Pigment.* **2007**, *75* (1), 67–72.

(230) Chernii, V. Y.; Bon, V. V.; Tretyakova, I. N.; Severinovskaya, O. V.; Volkov, S. V. *Dye. Pigment.* **2012**, *94* (2), 187–194.

(231) Silver, J.; Lukes, P. J.; Hey, P. K.; Park, W. **1989**, *8* (13), 1631–1635.

(232) Jiang, Z.; Ou, Z.; Chen, N.; Wang, J.; Huang, J.; Shao, J.; Kadish, K. M. *J. Porphyr. Phthalocyanines* **2005**, *9* (5), 352–360.

(233) Safaiee, M.; Zolfigol, M. A.; Afsharnadery, F.; Baghery, S. *RSC Adv.* **2015**, *5* (124), 102340–102349.

(234) Mbambisa, G.; Nyokong, T. *Polyhedron* **2008**, *27* (13), 2799–2804.

(235) Eguchi, K.; Nakagawa, T.; Takagi, Y.; Yokoyama, T. *J. Phys. Chem. C* **2015**, *119* (18), 9805–9815.

(236) Kobayashi, N.; Narita, F.; Ishii, K.; Muranaka, A. *Chem. - A Eur. J.* **2009**, *15* (39), 10173–10181.

(237) Donzello, M. P.; Ercolani, C.; Lukes, P. J. *Inorganica Chim. Acta* **1997**, *256* (2), 171–172.

(238) Maria Pia Donzello, Claudio Ercolani, Angiola Chiesi-Villa, and C. R. *Inorg. Chem.* **1998**, *37* (6), 1347–1351.

(239) Cellucci, L.; Ercolani, C.; Lukes, P. J.; Chiesi-villa, A.; Rizzoli, C. *J. Porphyr. Phthalocyanines* **1998**, *2*, 9–19.

(240) Chauke, V.; Nyokong, T. *Inorganica Chim. Acta* **2010**, *363* (14), 3662–3669.

(241) Tau, P.; Nyokong, T. *J. Porphyr. Phthalocyanines* **2006**, *10* (2), 69–75.

(242) Myers, J. F.; Canham, G. W. R.; Lever, A. B. P. *Inorg. Chem.* **1975**, *14* (3), 461–468.

(243) Elvidge, J. A.; Lever, A. B. P. *J. Chem. Soc.* **1961**, No. 127, 1257–1265.

(244) Ercolani, C.; Neri, C.; Porta, P. *Inorganica Chim. Acta* **1967**, *1* (C), 415–418.

(245) Zhou, W.; Thompson, J. R.; Leznoff, C. C.; Leznoff, D. B. *Chem. - A Eur. J.* **2017**, *23* (10), 2323–2331.

(246) Frick, K.; Verma, S.; Sundermeyer, J.; Hanack, M. *Eur. J. Inorg. Chem.* **2000**, No. 5, 1025–1030.

(247) Darwish, W.; Seikel, E.; Harms, K.; Burghaus, O.; Sundermeyer, J. *Dalt. Trans.* **2011**, *40* (5), 1183–1188.

(248) Edmondson, S. J.; Mitchell, P. C. H. *Polyhedron* **1986**, *5* (1–2), 315–317.

(249) Hill, H. A. O.; Norgett, M. M. *J. Chem. Soc. A Inorganic, Phys. Theor.* **1966**, 1476–1478.

(250) Nyokong, T. *Polyhedron* **1994**, *13* (2), 215–220.

(251) Mafatle, T. J.; Nyokong, T. *J. Electroanal. Chem.* **1996**, *408* (1–2), 213–218.

(252) Quinton, D.; Antunes, E.; Griveau, S.; Nyokong, T.; Bedioui, F. *Inorg. Chem. Commun.* **2011**, *14* (1), 330–332.

(253) Piantek, M.; Serrate, D.; Moro-Lagares, M.; Algarabel, P.; Pascual, J. I.; Ibarra, M. R. *J. Phys. Chem. C* **2014**, *118* (31), 17895–17899.

(254) Agboola, B.; Ozoemena, K. I.; Westbroek, P.; Nyokong, T. *Electrochim. Acta* **2007**, *52* (7), 2520–2526.

(255) Erdomu, A.; Akinbulu, I. A.; Nyokong, T. *Polyhedron* **2010**, *29* (11), 2352–2363.

(256) Sehlotho, N.; Durmuş, M.; Ahsen, V.; Nyokong, T. *Inorg. Chem. Commun.* **2008**, *11* (5), 479–483.

(257) Obirai, J.; Rodrigues, N. P.; Bedioui, F.; Nyokong, T. *J. Porphyr. Phthalocyanines* **2003**, *7* (7), 508–520.

(258) Yoshihara, K.; Wolf, G. K.; Baumgärtner, F. *Radiochim. Acta* **1974**, *21* (1–2), 96–100.

(259) Murata, K.; Koike, Y.; Ishii, K. *Chem. Commun.* **2020**, *56* (89), 13760–13763.

(260) Li, J.; Hu, J.; Wang, H.; Wu, R. Q. *Appl. Phys. Lett.* **2015**, *107* (3).

(261) Goedken, V. L.; Ercolani, C. *J. Chem. Soc. Chem. Commun.* **1984**, No. 6, 378–379.

(262) Eberhardt, W.; Hanack, M. *Synthesis (Stuttg).* **1997**, *1997* (1), 95–100.

(263) Guo, J.; Yan, X.; Liu, Q.; Li, Q.; Xu, X.; Kang, L.; Cao, Z.; Chai, G.; Chen, J.; Wang, Y.; Yao, J. *Nano Energy* **2018**, *46*, 347–355.

(264) Fischer, M. K. R.; López-Duarte, I.; Wienk, M. M.; Martínez-Díaz, M. V.; Janssen, R. A. J.; Bäuerle, P.; Torres, T. *J. Am. Chem. Soc.* **2009**, *131* (24), 8669–8676.

(265) Rawling, T.; McDonagh, A. *Coord. Chem. Rev.* **2007**, *251* (9–10), 1128–1157.

(266) Farrell, N. P.; Murray, A. J.; Thornback, J. R.; Dolphin, D. H.; James, B. R. *Inorganica Chim. Acta* **1978**, *28* (C), 144–146.

(267) Rodríguez-Morgade, M. S.; Plonska-Brzezinska, M. E.; Athans, A. J.; Carbonell, E.; De Miguel, G.; Guldi, D. M.; Echegoyen, L.; Torres, T. *J. Am. Chem. Soc.* **2009**, *131* (30), 10484–10496.

(268) Vermehren, M. H. and P. *Inorg. Chem.* **1990**, *29* (14), 134–136.

(269) Sekota, M.; Nyokong, T. *Polyhedron* **1996**, *15* (17), 2901–2908.

(270) Caminiti, R.; Donzello, M. P.; Ercolani, C.; Sadun, C. *Inorg. Chem.* **1998**, *37* (17), 4210–4213.

(271) Sakamoto, K.; Ohno, E. *Dye. Pigment.* **1998**, *37* (4), 291–306.

(272) Pan, Y.; Chen, W.; Lu, S.; Zhang, Y. *Dye. Pigment.* **2005**, *66* (2), 115–121.

(273) Sakamoto, K.; Ohno, E. *Dye. Pigment.* **1997**, *35* (4), 375–386.

(274) Nevin, W. A.; Liu, W.; Greenberg, S.; Hempstead, M. R.; Marcuccio, S. M.; Melník, M.; Leznoff, C. C.; Lever, A. B. P. *Inorg. Chem.* **1987**, *26* (6), 891–899.

(275) Menzel, E. R.; Rieckhoff, K. E.; Voigt, E. M. *J. Chem. Phys.* **1973**, *58* (12), 5726–5734.

(276) Murata, K.; Ishii, K. *Eur. J. Inorg. Chem.* **2017**, *2017* (44), 5103–5107.

(277) Youssef, T. E.; Mohamed, H. H. *Polyhedron* **2011**, *30* (12), 2045–2050.

(278) Praveen Kumar, N. Y.; Mounesh, M.; Sharanakumar, T. M.; Venugopala Reddy, K. R. *Chem. Pap.* **2021**, *75* (6), 2683–2694.

(279) Timoumi, A.; Wederni, M. A.; Bouguila, N.; Jamoussi, B.; AL Turkestani, M. K.; Chakroun, R.; Al-Mur, B. *Synth. Met.* **2021**, *272*, 116659.

(280) Lokesh, K. S.; Adriaens, A. *Dye. Pigment.* **2013**, *96* (1), 269–277.

(281) Zorlu, Y.; Dumoulin, F.; Durmuş, M.; Ahsen, V. *Tetrahedron* **2010**, *66* (17), 3248–3258.

(282) Volov, A. N.; Burtsev, I. D. *J. Organomet. Chem.* **2020**, *922*, 121372.

(283) Vacus, J.; Doppelt, P.; Simon, J.; Memetzidis, G. *J. Mater. Chem.* **1992**, *2* (10), 1065–1068.

(284) Keen, I. M. *Platin. Met. Rev.* **1964**, *8* (4), 143–144.

(285) Mo, X.; Chen, H. Z.; Wang, Y.; Shi, M. M.; Wang, M. *J. Phys. Chem. B* **2005**, *109* (16), 7659–7663.

(286) Topuz, B. B.; Gündüz, G.; Mavis, B.; Çolak, Ü. *Dye. Pigment.* **2013**, *96* (1), 31–37.

(287) Fournier, M.; Pépin, C.; Houde, D.; Ouellet, R.; van Lier, J. E. *Photochem. Photobiol. Sci.* **2004**, *3* (1), 120–126.

(288) Breloy, L.; Alcay, Y.; Yilmaz, I.; Breza, M.; Bourgon, J.; Brezová, V.; Yagci, Y.; Versace, D. L. *Polym. Chem.* **2021**, *12* (9), 1273–1285.

(289) Van Der Pol, A.; Reijerse, E. J.; de Boer, E.; Wasowicz, T.; Michalik, J. *Mol. Phys.* **1963**, *75* (1), 37–42.

(290) MacCragh, A.; Koski, W. S. *J. Am. Chem. Soc.* **1965**, *87* (11), 2496–2497.

(291) Chidawanyika, W.; Ogunsipe, A.; Nyokong, T. *New J. Chem.* **2007**, *31* (3), 377–384.

(292) Tackley, D. R.; Dent, G.; Smith, W. E. *Phys. Chem. Chem. Phys.* **2000**, *2* (18), 3949–3955.

(293) Bueno, C.; Encinas, M. V. *Helv. Chim. Acta* **2003**, *86* (10), 3363–3375.

(294) Iwatsu, F.; Kobayashi, T.; Uyeda, N. *J. Phys. Chem.* **1980**, *84* (24), 3223–3230.

(295) Ogunsipe, A.; Maree, D.; Nyokong, T. *J. Mol. Struct.* **2003**, *650* (1–3), 131–140.

(296) Guo, Z.; Shao, C.; Mu, J.; Zhang, M.; Zhang, Z.; Zhang, P.; Chen, B.; Liu, Y. *Catal. Commun.* **2011**, *12* (10), 880–885.

(297) Chidawanyika, W.; Nyokong, T. *J. Photochem. Photobiol. A Chem.* **2009**, *202* (2–3), 99–106.

(298) Chambrier, I.; White, G. F.; Cook, M. J. *Chem. - A Eur. J.* **2007**, *13* (27), 7608–7618.

(299) George, R. D.; Snow, A. W.; Mcmillan, P. F.; Burrows, V. A. *J. Am. Chem. Soc.* **1992**, *114*, 8286–8287.

(300) Gu, W.; Hu, Y.; Zhu, Z.; Liu, N.; Zhang, J.; Wang, J. *Solid. State. Electron.* **2013**, *89*, 101–104.

(301) Wang, H.; Zhu, F.; Yang, J.; Geng, Y.; Yan, D. *Adv. Mater.* **2007**, *19* (16), 2168–2171.

(302) Li, L.; Tang, Q.; Li, H.; Yang, X.; Hu, W.; Song, Y.; Shuai, Z.; Xu, W.; Liu, Y.; Zhu, D. *Adv. Mater.* **2007**, *19* (18), 2613–2617.

(303) Pan, F.; Tian, H.; Qian, X.; Huang, L.; Geng, Y.; Yan, D. *Org. Electron.* **2011**, *12* (8), 1358–1363.

(304) Yoon, S. M.; Song, H. J.; Hwang, I. C.; Kim, K. S.; Choi, H. C. *Chem. Commun.* **2010**, *46* (2), 231–233.

(305) Takabayashi, Y.; Prassides, K. *50 Years of Structure and Bonding – The Anniversary Volume - Google Livros*; 2016.

(306) LINSTEAD, R. P.; NOBLE, E. G.; WRIGH, J. M. *J. Chem. Soc.* **1937**, 911–921.

(307) Donzello, M. P.; Viola, E.; Bergami, C.; Dini, D.; Ercolani, C.; Giustini, M.; Kadish, K. M.; Meneghetti, M.; Monacelli, F.; Rosa, A.; Ricciardi, G. *Inorg. Chem.* **2008**, *47* (19), 8757–8766.

(308) De Mori, G.; Fu, Z.; Viola, E.; Cai, X.; Ercolani, C.; Pia Donzello, M.; Kadish, K. M. *Inorg. Chem.* **2011**, *50* (17), 8225–8237.

(309) Machacek, M.; Cidlina, A.; Novakova, V.; Svec, J.; Rudolf, E.; Miletin, M.; Kučera, R.; Simunek, T.; Zimcik, P. *J. Med. Chem.* **2015**, *58* (4), 1736–1749.

(310) Zimcik, P.; Miletin, M.; Ponec, J.; Kostka, M.; Fiedler, Z. *J. Photochem. Photobiol. A Chem.* **2003**, *155* (1–3), 127–131.

(311) Manet, I.; Manoli, F.; Donzello, M. P.; Viola, E.; Masi, A.; Andreano, G.; Ricciardi, G.; Rosa, A.; Cellai, L.; Ercolani, C.; Monti, S. *Inorg. Chem.* **2013**, *52* (1), 321–328.

(312) Donzello, M. P.; Viola, E.; Ercolani, C.; Fu, Z.; Futur, D.; Kadish, K. M. *Inorg. Chem.* **2012**, *51* (22), 12548–12559.

(313) Manet, I.; Manoli, F.; Donzello, M. P.; Ercolani, C.; Vittori, D.; Cellai, L.; Masi, A.; Monti, S. *Inorg. Chem.* **2011**, *50* (16), 7403–7411.

(314) Donzello, M. P.; Vittori, D.; Viola, E.; Manet, I.; Mannina, L.; Cellai, L.; Monti, S.; Ercolani, C. *Inorg. Chem.* **2011**, *50* (16), 7391–7402.

(315) Bohrer, F. I. *Univ. CALIFORNIA, SAN DIEGO* **2008**.

(316) Evgeny V. Kudrik, Alexander Theodoridis, R. van E. and S. V. M. *Dalt. Trans.* **2005**, 1117–1122.

(317) Shishkin, V. N.; Kudrik, E. V.; Makarov, S. V.; Shaposhnikov, G. P. *Kinet. Catal.* **2007**, *48* (5), 660–663.

(318) Kleinwachter, J.; Subramanian, L. R.; Hanack, M. *J. Porphyr. Phthalocyanines* **2000**, *4* (5), 498–504.

(319) Jung, C. Y.; Park, J. M.; Song, C. J.; Jaung, J. Y. *J. Lumin.* **2016**, *170*, 305–311.

(320) Frisch, M. J.; Trucks, G. W.; Schlegel, H. B.; Scuseria, G. E.; Robb, M. A.; Cheeseman, J. R.; Scalmani, G.; Barone, V.; Mennucci, B.; Petersson, G. A.; Nakatsuji, H.; Caricato, M.; Li, X.; Hratchian, H. P.; Izmaylov, A. F.; Bloino, J.; Zheng, G.; Sonnenberg, J. L.; Hada, M.; Ehara, M.; Toyota, K.; Fukuda, R.; Hasegawa, J.; Ishida, M.; Nakajima, T.; Honda, Y.; Kitao, O.; Nakai, H.; Vreven, T.; Montgomery, J. A., J.; Peralta, J. E.; Ogliaro, F.; Bearpark, M.; Heyd, J. J.; Brothers, E.; Kudin, K. N.; Staroverov, V. N.; Kobayashi, R.; Normand, J.; Raghavachari, K.; Rendell, A.; Burant, J. C.; Iyengar, S. S.; Tomasi, J.; Cossi, M.; Rega, N.; Millam, N. J.; Klene, M.; Knox, J. E.; Cross, J. B.; Bakken, V.; Adamo, C.; Jaramillo, J.; Gomperts, R.; Stratmann, R. E.; Yazyev, O.; Austin, A. J.; Cammi, R.; Pomelli, C.; Ochterski, J. W.; Martin, R. W.; Morokuma, K.; Zakrzewski, V. G.; Voth, G. A.; Salvador, P.; Dannenberg, J. J.; Dapprich, S.; Daniels, A. D.; Farkas, O.; Foresman, J. B.; Ortiz, J. V.; Cioslowski, J.; Fox, D. J. Gaussian 09, Revision D.01. Gaussian 09, Revision D.01. Gaussian Inc.: Wallingford CT 2009.

(321) Michael K.Lowery, Albert J. Starshak, John N. Esposito, Paul C. Krueger, and M. E. K. *Inorg. Chem.* **1965**, *4* (1), 128.

(322) Dirk, C. W.; Inabe, T.; Schoch, K. F.; Marks, T. J. *J. Am. Chem. Soc.* **1983**, *105* (6), 1539–1550.

(323) Biitseva, A. V.; Rudenko, I. V.; Hordiyenko, O. V.; Omelchenko, I. V.; Arrault, A. *Synth.* **2015**, *47* (23), 3733–3740.

(324) P. A. Barrett, C .E. Dent, R. P. L. *J. Chem. Soc.* **1934**, 1719–1736.

(325) Kudrevich, S. V; Lier, J. E. Van. *Can. J. Chem.* **1996**, *74*, 1718–1723.

(326) Lim, B.; Margulis, G. Y.; Yum, J. H.; Unger, E. L.; Hardin, B. E.; Grätzel, M.; McGehee, M. D.; Sellinger, A. *Org. Lett.* **2013**, *15* (4), 784–787.

(327) Mooney, J. R.; Choy, C. K.; Knox, K.; Kenney, M. E. *J. Am. Chem. Soc.* **1975**, *97* (11), 3033–3038.

(328) Kleinwächter, J.; Hanack, M. *J. Am. Chem. Soc.* **1997**, *119* (44), 10684–10695.

(329) Fukuda, T.; Kobayashi, N. In *Handbook of Porphyrin Science With Applications to Chemistry, Physics, Materials Science, Engineering, Biology and Medicine*; 2010; Vol. 9, pp 1–644.

(330) Davidson, A. T. *J. Chem. Phys.* **1982**, *77* (1), 168–172.

(331) Bayrak, R.; Demirbaş, Ü.; Bıyıklıoğlu, Z.; Akçay, H. T.; Kantekin, H. **2018**, 1–5.

(332) Lever, A. B. P. *Adv. Inorg. Chem. Radiochem.* **1965**, *7* (C), 27–114.

(333) Apostol, P.; Bentaleb, A.; Rajaoarivelo, M.; Clérac, R.; Bock, H. *Dalt. Trans.* **2015**, *44* (12), 5569–5576.

(334) Kostka, M.; Zimcik, P.; Miletin, M.; Klemera, P.; Kopecky, K.; Musil, Z. *J. Photochem.*

Photobiol. A Chem. **2006**, *178* (1), 16–25.

(335) Zimcik, P.; Novakova, V.; Miletin, M.; Kopecky, K. *Macroheterocycles* **2008**, *1* (1), 21–29.

(336) Cardona, C. M.; Li, W.; Kaifer, A. E.; Stockdale, D.; Bazan, G. C. *Adv. Mater.* **2011**, *23* (20), 2367–2371.

(337) Boeré, R. T.; Oakley, R. T.; Reed, R. W. *J. Organomet. Chem.* **1987**, *331* (2), 161–167.

(338) Hordiyenko, O. V.; Rudenko, I. V.; Zamkova, I. A.; Denisenko, O. V.; Biitseva, A. V.; Arrault, A.; Tolmachev, A. A. *Synth.* **2013**, *45* (24), 3375–3382.

(339) Hirao, A.; Akiyama, T.; Okujima, T.; Yamada, H.; Uno, H.; Sakai, Y.; Aramaki, S.; Ono, N. *Chem. Commun.* **2008**, No. 39, 4714–4716.

(340) Royer, J. E.; Zhang, C.; Kummel, A. C.; Trogler, W. C. *Langmuir* **2012**, *28* (14), 6192–6200.

(341) Shopova, M.; Woehrle, D.; Mantareva, V.; Mueller, S. *J. Biomed. Opt.* **2017**, *4* (3), 276–285.

(342) Taratula, O.; Doddapaneni, B. S.; Schumann, C.; Li, X.; Bracha, S.; Milovancev, M.; Alani, A. W. G.; Taratula, O. *Chem. Mater.* **2015**, *27* (17), 6155–6165.

(343) Bézière, N.; Ntziachristos, V. *J. Nucl. Med.* **2015**, *56* (2), 323–328.

(344) MacOr, L.; Fungo, F.; Tempesti, T.; Durantini, E. N.; Otero, L.; Barea, E. M.; Fabregat-Santiago, F.; Bisquert, J. *Energy Environ. Sci.* **2009**, *2* (5), 529–534.

(345) Lim, B.; Bloking, J. T.; Ponec, A.; Mcgehee, M. D.; Sellinger, A. *ACS Appl. Mater.*

Interfaces **2014**, *6*, 6905–6913.

(346) Mitra, K.; Hartman, M. C. T. *Org. Biomol. Chem.* **2021**, *19* (6), 1168–1190.

(347) Senthilarasu, S.; Velumani, S.; Sathyamoorthy, R.; Subbarayan, A.; Ascencio, J. A.; Canizal, G.; Sebastian, P. J.; Chavez, J. A.; Perez, R. *Appl. Phys. A Mater. Sci. Process.* **2003**, *77* (3–4), 383–389.

(348) Silva Sousa, D. F.; Rosso Dotto, M. E.; Eccher, J.; Bock, H.; Bechtold, I. H. *Synth. Met.* **2020**, *263*, 116367.

(349) Zhang, Y. S.; Wang, D. X.; Wang, Z. Y.; Wang, Y. Y. *Opt. Quantum Electron.* **2016**, *48* (1), 1–7.

(350) Jiménez Tejada, J. A.; Awawdeh, K. M.; Villanueva, J. A. L.; Carceller, J. E.; Deen, M. J.; Chaure, N. B.; Basova, T.; Ray, A. K. *Org. Electron.* **2011**, *12* (5), 832–842.

(351) Nar, I.; Atsay, A.; Pekbelgin Karaoğlu, H.; Altındal, A.; Hamuryudan, E. *Dalt. Trans.* **2018**, *47* (42), 15017–15023.

(352) Bilgiçli, A. T.; Yaraşir, M. N.; Kandaz, M.; Ilik, C.; Demir, A.; Baɬci, S. *Synth. Met.* **2015**, *206*, 33–41.

(353) Golmar, F.; Stoliar, P.; Monton, C.; Valmianski, I.; Schuller, I. K.; Hueso, L. E.; Casanova, F. *Phys. Status Solidi Appl. Mater. Sci.* **2015**, *212* (3), 607–611.

(354) Ohta, K.; Watanabe, T.; Hasebe, H.; Morizumi, Y.; Fujimoto, T.; Yamamoto, I.; Lelièvre, D.; Simon, J. *Mol. Cryst. Liq. Cryst.* **1991**, *196* (1), 13–26.

(355) Denekamp, I. M.; Veenstra, F. L. P.; Jungbacker, P.; Rothenberg, G. *Appl. Organomet. Chem.* **2019**, *33* (5), 1–7.

(356) Gouterman, M. *J. Chem. Phys.* **1959**, *30* (5), 1139–1161.

(357) Bao, Z.; Lovinger, A. J.; Dodabalapur, A. *Adv. Mater.* **1997**, *9* (1), 42–44.

(358) Song, S.; Ma, F.; Wang, S.; Li, X.; Yin, X.; Liu, F. *Dig. J. Nanomater. Biostructures* **2017**, *12* (1), 119–126.